CONTROL METHODOLOGIES FOR POWERED PROSTHETIC INTERVENTIONS IN UNILATERAL AND BILATERAL TRANSFEMORAL AMPUTEES

By

Brian Edward Lawson

Dissertation

Submitted to the Faculty of the

Graduate School of Vanderbilt University

in partial fulfillment of the requirements

for the degree of

DOCTOR OF PHILOSOPHY

in

Mechanical Engineering

August, 2014

Nashville, Tennessee

Approved:

Professor Michael Goldfarb

Professor Nilanjan Sarkar

Professor Eric J. Barth

Professor Robert J. Webster III

Professor George E. Cook

For my inadequately named dog.

Here's to many more happy years, Pupdog.

ACKNOWLEDGMENTS

This dissertation, along with all of my work in the Center for Intelligent Mechatronics, is a contribution towards a research effort that is much larger than a single graduate student. Michael Goldfarb was developing a new generation of prostheses long before I started, and the effort will continue after I am gone. Consequently, with regard to this work specifically, I must first acknowledge Michael Goldfarb as the source, drive, and inspiration for all that has been accomplished. Had I attended a different university, or joined a different lab, my training in the field may have been just as sufficient, but the nature of my work would have necessarily been different. In the end, I am glad this was not the case, and I am truly grateful that Michael Goldfarb invited me to play a role in his legacy.

My work has received funding from multiple sources. I would like to recognize the National Institutes of Health (R01 EB005684, R21 HD076124), the Rehabilitation Institute of Chicago and the Department of Defense (W81XWH-09-2-0020), and the discretionary funds from the endowment of the H. Fort Flowers family.

I would like to thank Drs. Sarkar, Barth, Webster, and Cook for serving as members of my committee. In my time at Vanderbilt I have seen the department grow substantially, and I have been proud to be part of a program that is developing such depth in the fields of rehabilitation and medical robotics.

A number of other researchers have played significant roles in both this work and in my graduate experience. As a postdoc, Tom Withrow was instrumental in welcoming me to the lab and getting me up to speed on the culture of academia and graduate school. As a professor, he has continued to serve as my friend and advisor throughout my time at Vanderbilt.

Drs. Frank Sup and Atakan Varol were incredibly gracious and welcomed me into their project. Their partnership rivaled the best found in literature, and Atakan's role in my career was equally dramatic. The two years we worked together was an

entirely different experience from the three that followed. Despite his best efforts at scolding, challenging, and insulting me, never once did I feel that I did not have his respect. Atakan cared deeply about the quality of work we produced, and he infected others with that dedication as well.

It is common to retain a certain level of awe and respect for those that came before you, and I can only imagine that Amanda Shultz and Elissa Ledoux hold me in such high regard. In all seriousness, however, I am truly grateful that I was fortunate enough to have such students join the lab after me. Both have been a pleasure to work with, and, for the near term, I look forward to our continued collaboration.

In my time at Vanderbilt, Jason Mitchell and Don Truex have firmly secured their legacies as pillars of the Center for Intelligent Mechatronics. Their combined expertise in mechanical and electrical design has taken the prototypes produced by this lab to a level that I believe is unprecedented in an academic research environment. Furthermore, both have maintained a consistent, patient attitude towards the other members of the lab, including an unending tolerance for interruption, preemption, and redirection.

All remaining members of the Center for Intelligent Mechatronics, past and present, know that you have not been selected for named recognition in this acknowledgment. If it should come to pass that you find yourself reading this, I can only assume it is because you are copying the format for your own dissertation. Should that be the case, please do not avoid specifically acknowledging my contribution to your work simply because I didn't acknowledge your role in mine.

My parents, Brandt and Christine, my wife, Katie, my brother, Ben, and his wife, Devon, have all played significant roles in both my life and in supporting me throughout this program. To a lesser extent my nephew, Gus, has also been helpful. As he was only born last year, however, his contribution was notably lacking for the first four years of my program...

TABLE OF CONTENTS

LIST OF FIGURES

LIST OF TABLES

CHAPTER I

INTRODUCTION

This document serves to summarize the research I have completed at the Center for Intelligent Mechatronics (CIM) as part of my graduate study in mechanical engineering. My work at the CIM has been part of a larger effort by Dr. Goldfarb and other researchers to improve lower limb prosthetic technology. There are a number of other publications including journal articles, doctoral dissertations, and master's theses that have preceded this manuscript [1–6]. A brief overview of the relevant literature pertaining to lower limb amputee demographics and current developments in lower limb prosthetic technology has been included to give context to the work presented. The remainder of this chapter provides some history of the Vanderbilt powered prosthesis, along with a section describing the philosophical control framework that has been the basis of the control design.

The remaining chapters consist of both published works and supplementary material covering the implementation of specific algorithms for control on a variety of hardware configurations. When necessary, manuscript-based chapters include an addendum to supplement the published material. Chapter II describes several approaches for active stumble recovery leveraging inertial measurement for stumble detection and classification. The manuscript in this chapter was presented at the 32nd Annual International Conference of the IEEE Engineering in Medicine and Biology Society in Buenos Aires, Argentina. Chapter III describes control systems for stair ascent and

descent that utilize the finite state-based impedance control framework described in this chapter. The manuscript in this chapter was published in the 3rd issue of the 21st volume of the IEEE Transactions on Neural Systems and Rehabilitation. Chapter IV introduces a modification to the finite state-based impedance control framework that reduces the parameterization of the control system and achieves real time, continuously variable cadence. The manuscript in this chapter has been submitted to the IEEE Robotics and Automation Magazine for a Special Issue on Wearable Robotics. Chapter V further extends both pure finite-state based impedance control, and subsequently a hybrid scheme similar to that presented in Chapter IV, for a bilateral, transfemoral prosthetic intervention. This chapter also describes a communication approach for sharing data between bilateral prostheses. The manuscript in this chapter has been recommended for acceptance to the IEEE Transactions on Biomedical Engineering with minor revisions. Chapter VI presents an algorithm for the estimation of a bicycle's crank angle using only measurements internal to the powered prosthesis. Such a scheme could be used to develop a control system to supply supplemental knee torque for an amputee while cycling. The manuscript in this chapter has been submitted to the 36th Annual International Conference of the IEEE Engineering in Medicine and Biology Society in Chicago, Illinois, USA. In Chapter VII, several conclusions are drawn, and a description of possible future directions is included for this work.

1. Lower Limb Amputee Demographics

In 2008, Ziegler-Graham *et al.* published an article in the Archives of Physical Medicine and Rehabilitation that provided current estimates of limb loss in the United States, along with projections of limb loss rates through the year 2050 [7]. Starting with work from 1996 claiming an amputation rate of approximately 185,000 persons

per year [8] and a total of 1.2 million persons living with limb loss [9], Ziegler-Graham *et al.* constructed a probabilistic model that accounts for new incidents of limb loss and mortality. From this model, it was estimated that 1.6 million persons were living in the United States with limb loss in 2005, and, by 2050, this number will more than double. For the 2005 estimate, approximately 623,000 of the 1.6 million amputees had suffered a major lower limb amputation, which was defined as an amputation more proximal than the toes.

The preceding article does not distinguish between transfemoral and transtibial amputations. In a recent survey of lower limb amputees, 42.4% of the 396 respondents had transfemoral amputations [10]. This survey was intended to determine factors that influence the use of prosthetic devices by lower limb amputees. 85% of the respondents did use prostheses, with over half using the devices in outdoor settings. Furthermore, another study shows that lower limb amputees of Medicare Functional Classification Level (MFCL)-2 and -3 benefit from more technologically advanced prostheses (in this case, prosthetic legs with microprocessor-controlled damping at the knee) [11]. Specific benefits included improvements in hill and stair gait, speed, and multitasking abilities. Additionally, a significant percentage of participants increased their MFCL over the course of the study, implying that enhanced prosthetic functionality can lead to increased activity levels.

2. An Overview of Prosthetic Technology for Transfemoral Amputees

A transfemoral prosthesis is a customized device assembled and adjusted by a licensed prosthetist to meet the individual needs of the amputee. A variety of companies manufacture and sell the various components of a prosthesis, and inter-compatibility varies depending upon the nature of each particular prosthetic component.

Figure 1.1 labels the major components of a typical transfemoral prosthesis. The

interface between the prosthesis and the amputee is known as the socket and is generally constructed from carbon-fiber and shaped specifically for the amputee's residual limb by a prosthetist. The socket is held to the residual limb by a suspension system. Simple suspension systems can consist of external straps that attach to a higher point on the user's body, while more sophisticated systems may include silicone liners and suction valves to create an air-tight seal between the residual limb and the socket.

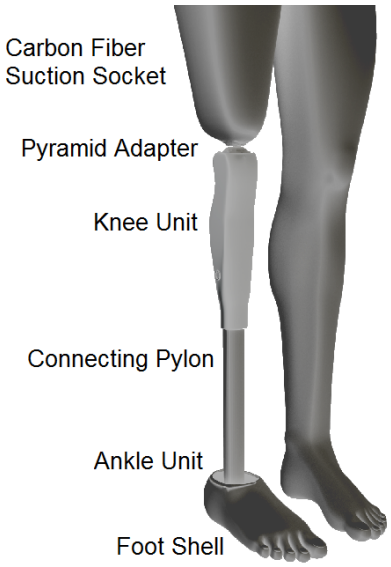

Figure 1.1: The major components of a typical transfemoral prosthesis.

The distal end of the socket typically contains a pyramid adapter, which is a standardized piece of mounting hardware that allows general prosthetic components to be attached and adjusted for tilt in the sagittal and coronal planes. This mounting point represents the division between the custom-formed portions of the prosthesis that are unique to the amputee (i.e. the socket/liner system) and the mass-produced prosthetic components such as knee and ankle units.

In a transfemoral prosthesis, a knee unit is connected to the socket. A variety of knee mechanisms have been designed, and a complete review of all the passive devices currently available is beyond the scope of this manuscript. The general families of

devices, however, include:

- Polycentric knees - These knees utilize a four-bar mechanism that provides enhanced stability in stance by moving the center of rotation when the knee is straight.
- Hydraulic knees - These knees provide a damping-like resistance by resisting the flow of a hydraulic fluid through an orifice.
- Pneumatic knees - These knees are similar to hydraulic knees though they use a gas instead of a hydraulic fluid.
- Microprocessor-controlled knees - These knees provide resistance (usually hydraulic or pneumatic), but the amount of resistance is modulated by a microprocessor depending on the state of various sensors integrated into the prosthesis.

In order to attain the proper prosthetic shank length, a connecting pylon is cut to a custom length to join the knee unit to the ankle unit. Ankle units are typically non-articulated and form an ankle-foot complex. Often this complex is constructed from carbon fiber composite and acts as a stiff spring around a virtual ankle joint. The primary benefits of this style of prosthetic ankle include shock absorption at heel strike and energy storage and return from middle stance to late stance.

The final component in a transfemoral prosthesis is a cosmesis. The purpose of the cosmesis is to cover the mechanical portions of the prosthesis and make the limb appear more life-like. The relative degree of importance of this component varies according to user preference, but at the very least, the majority of transfemoral prostheses include a cosmetic foot shell that is anthropomorphic in shape. In addition to its cosmetic qualities, the foot shell protects the carbon fiber ankle-foot complex and facilitates the wearing of a shoe with the prosthesis. Some amputees choose to use more complete cosmeses that include life-like silicone shanks, including leg hair and proper skin colors.

3. Current Research in Lower Limb Prosthetics

Traditionally, lower limb prostheses were passive by necessity; the technology required to construct a powered device comparable in size and weight to the anatomical limb has only been developed in the last five to ten years. Now that the supporting technology has arrived (power-dense motors/batteries and efficient microprocessors), the field of prosthetics is struggling to understand and accept this paradigm shift. A number of research groups have published preliminary results on a variety of powered lower limb devices, but, as of the writing of this manuscript, only two powered joints have reached the commercial market. A brief review of these two devices is now provided, along with the major efforts in the research community.

3.1 Ossur Power Knee

The prosthetics and orthotics company Ossur has released two versions of a powered knee joint called the Power Knee. This knee prosthesis is designed to be used in conjunction with an off-the-shelf passive prosthetic ankle/foot. Because the Power Knee has only existed as a commercial product, no literature is publicly available concerning its design. Additionally, the author knows of no peer-reviewed studies demonstrating its advantages over traditional passive prostheses. Video footage of Power Knee users ascending stairs in a step-over manner (i.e. using both their sound side and their affected side to lift themselves up the step) is available, however, suggesting an improved biomechanical performance for this activity.

3.2 iWalk BiOM

The prosthetics start-up iWalk grew out of a research effort led by Dr. Hugh Herr at MIT. The company's first commercially available prosthesis is a powered ankle based

upon a number of publications by Dr. Herr and his students [12–16]. This ankle uses passive components to both shield the motor and transmission from impacts, and to enhance the power delivery of the system. In order to estimate the output torque of such a system, feed-forward models converting the displacements of series and parallel springs to torques are needed, along with, depending upon the relative compliances in the system, a model of the carbon fiber foot. However, for a system that largely supplies a linear, spring-like behavior for most of the gait cycle (with the addition of an impulse of torque at push off) the accuracy of such models is not likely to be critical with regards to the performance of the device.

One manifestation of the control system for this ankle is partitioned into two tiers, the higher of which is implemented as a finite state machine that switches state based upon the estimated phase of gait [12]. The lower tier contains an impedance controller (based upon torque control of the series-elastic actuator) and a standard PD position controller. It will be shown later that these two approaches are mathematically similar but philosophically distinct. The finite state machine selects between these two controllers as it cycles through the phases of gait. More complicated control techniques have been published for this powered ankle, though they differ mainly through the implementation of a non-linear impedance based upon a Hill-type muscle model [16].

In a study on 3 transtibial amputees comparing the use of a passive ankle and a precursor to the BiOM, it was shown that the powered ankle was able to reduce the energetic cost of transport (reported in Joules) by 7-20% [12]. In addition, the control approach demonstrated in [16] incorporates intrinsic speed adaptation, allowing an efficient gait across a range of walking speeds.

3.3 SPARKy Powered Ankle

Another group led by Sugar has presented a two degree of freedom ankle named SPARKy 3, which stands for Spring Ankle with Regenerative Kinetics [17, 18]. Currently available literature covers the mechanical design in detail, and much of this technology has transitioned to a start-up company known as Spring Active, which now has several active projects targeting both walking and running performance.

3.4 Other Research Efforts

The previous three projects are the most well-developed and longest lasting efforts in powered prostheses known to the author. A number of other groups, however, have proposed designs and started to show preliminary data for both powered knees and powered ankles [19–28]. With the exception of this effort, no other integrated powered knee and ankle prostheses have been reported in the literature to date.

4. History of the Vanderbilt Powered Prosthesis

Although many doctoral students, masters students, and postdoctoral researchers contributed to this effort, notable early contributions were made by Kevin Fite, Amit Bohara, and Frank Sup. Their work produced what is referred to as Generation 0 of the Vanderbilt powered prosthesis. Generation 0 devices were tethered legs that had power and computation provided remotely to facilitate rapid development and initial testing [29]. This work laid the foundation for both the impedance-based control framework, and also for the mechanical design of the Generation 1 series of prototypes (pneumatic actuators were replaced with motors and ballscrew assemblies).

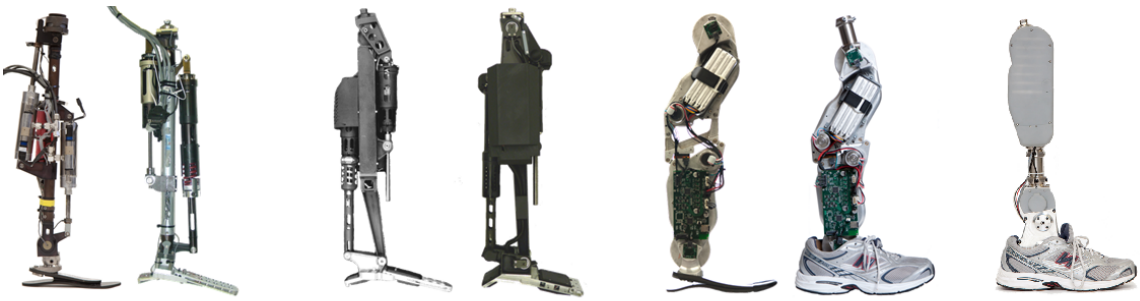

Figure 1.2: The evolution of the Vanderbilt powered prosthesis.

Generation 1 culminated in the doctoral work of Frank Sup and Atakan Varol [30, 31]. This generation was the first self-contained powered knee and ankle prosthesis to be developed. It was fully functional for variable cadence walking on level ground, up slope [4] and down slope walking, and sit-to-stand and stand-to-sit transitions [32], all of which were integrated with an intent recognition algorithm based upon Gaussian mixture models [6]. Generation 1 was also subsequently used for stumble detection and recovery [33], a unified ground adaptive standing controller [3], and preliminary stair ascent and descent development [34]. Furthermore, volitional knee control through the use of electromyography was demonstrated first by Kevin Ha [2], and later by collaborators at the Rehabilitation Institute of Chicago (RIC) [35].

Generation 2 preserved the fundamental control framework of its predecessors and deviated mainly in mechanical design. The transmission was changed from a slider-crank mechanism (carried over from the original pneumatic design) to a more robust and easily contained multi-stage belt and chain transmission. Furthermore, the load sensing was changed from independent strain gage bridges on an aluminum prosthetic foot to a uniaxial load cell in the shank. With this generation fully functional stair ascent and descent was implemented [34] (RIC also demonstrated stair ascent with EMG control [36]), a biomechanically appropriate running controller was developed, and a coordinated bilateral control system was developed. Furthermore, the hybrid control system present herein was initially prototyped on a Generation 2 prosthesis.

Finally, Generation 3 contains further refinement of the mechanical design. Although this generation contained minor revisions to the embedded system, it was primarily aimed at improving the packaging and commercial viability of Generation 2. An improved mass distribution gave the device more favorable inertial properties, and the knee and ankle units were separated to make a modular system interconnected by off-the-shelf prosthetic components.

5. Control Approach

The theoretical framework that underlies the design of the original finite state-based impedance control system will now be developed and examined. The form of this controller is largely unchanged from [30]. Conclusions drawn from this analysis, along with empirical evidence from the controller's implementation, will be used as justification for the hybrid controller presented subsequently.

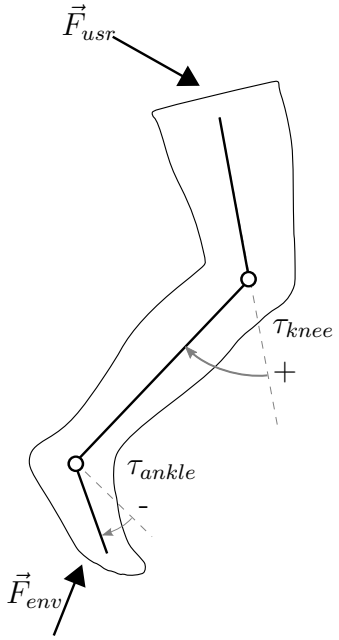

Figure 1.3: Angle conventions and generalized interactions with the lower limb.

With respect to the control problem for a powered knee and ankle prosthesis, first several working definitions are established. There are three dynamic systems involved: the prosthesis, the user, and the environment. The prosthesis consists of the robotic manipulator itself. The user's thigh and prosthetic socket are considered its base and the prosthetic foot is considered its end effector. The user is considered distinct from the prosthesis for an intrinsic control system (i.e. the user is not directly supplying torque commands to the prosthetic joints). Instead, the user introduces forces on the prosthesis from the thigh. On the other end, the environment exerts forces on the prosthetic foot. Therefore the prosthesis has two mechanical ports through which it interacts with other systems. The prosthesis is assumed to consist of three rigid bodies connected with two coplanar pin joints. The joints are considered to be actuated by backdrivable and lossless torque generators. The convention for measuring the knee angle and the ankle angle is depicted in Fig. 1.3. The shank being colinear with the thigh denotes zero knee angle and knee flexion is considered a positive displacement. The sole being perpendicular to the shank denotes zero ankle angle and dorsiflexion is considered a positive displacement.

5.1 Impedance Control

At the heart of the design of the control system for this prosthesis is notion of impedance control as described by Neville Hogan in his seminal 3-part paper entitled "Impedance Control: An Approach to Manipulation" [37–39]. Traditional robotics research has tended to focus on well-defined and easily modeled environments. Under these conditions, extremely high performance controllers can be designed by dictating the kinematics of the manipulator through closed-loop position/trajectory control. This degree of performance (as measured by trajectory-tracking at high bandwidths) is accomplished by specifying the highest possible impedances for the

actuators. When the environment is known and well-modeled, interaction forces between the manipulator and its environment can be controlled by carefully selecting trajectories, or by implementing closed-loop force control during contact conditions. In both of these cases the work exchanged between the manipulator and the environment is considered negligible. Since one of the main functions of a powered lower limb prosthesis is to propel the user in gait, the work exchanged between the prosthesis and the environment is most assuredly *not* negligible. In fact, the amount of work exchanged is a useful performance metric, as one of the goals of this work is to reduce the metabolic cost of transport for amputees.

Since a prosthesis fundamentally exchanges work with its environment, it is desirable to account for this energy exchange explicitly in the control system. As a result, we must consider both force and position in the controller, and modulate the dynamic relation between the two, as opposed to specifying one as a target and modulating the other without restraint in order to achieve this goal. Consider the power bond between the prosthesis and the environment:

$$Prosthesis \xrightarrow[v]{F} Environment$$

Figure 1.4: The exchange of power between a prosthesis and its environment.

If the prosthesis were implemented as an ideal position controller, then the causal stroke would fall on the left, the prosthesis would impart flow and the environment would impart a corresponding effort. In nature, however, position (or, more precisely, momentum) is never actually specified, instead it is force that is specified, and momentum follows. As a result, in a position control scenario, the prosthesis is actually imparting an effort, and then modulating that effort with negative feedback in order to achieve a flow. Force control, on the other hand, can be implemented without negative feedback or a model of the environment, although certain assumptions about

the environment are necessary (i.e. a contact condition) in order to ensure that the resulting system will be stable.

In the case of either force control or position control we can see that the prosthesis is still imparting a force on the environment. When we model the prosthesis as an effort source, we can correctly place the causal stroke on the right. Now the motion (or flow) of the prosthetic joint is determined by the environment. In other words, the dynamics of the environment provide a mapping from the interaction force, specified by the prosthesis (or manipulator), to the state (i.e. position/velocity). Since this mapping takes the general form of

$$v(s) = Y(s)\, F(s) \tag{1.1}$$

where s is the Laplace variable, $v(s)$ is the velocity (or flow), $F(s)$ is the force (or effort), and $Y(s)$ is the operator that maps $F(s)$ to $v(s)$, then we can view the behavior of the environment as that of an admittance. The dual nature of impedance and admittance often encourages us to invert this relationship when convenient, casting a system behavior that is admittance-like as an impedance (see eq. (1.2)).

$$Z(s) = \frac{F(s)}{\omega(s)} \Longleftrightarrow Y(s) = \frac{\omega(s)}{F(s)} \tag{1.2}$$

In general, however, this relationship is not invertible. Consider, for example, the constitutive behavior of an inertial entity with a position-level constraint. In the constrained degree of freedom, the system's admittance can be described trivially: $(x = x_0 \,\forall F)$. However, this behavior cannot be modeled as an impedance since it is not invertible. Since the environment of a prosthesis inevitably contains inertias, and since, generally speaking, the prosthesis should not act with such conviction as to violate the constraints of those inertias, we will consider the environment to be admittance-like and enforce a specific impedance for the prosthesis. Therefore, we

will use state feedback to calculate a torque according to an impedance control law:

$$\tau(s) = Z(s)\,\omega(s) \tag{1.3}$$

where $\tau(s)$ is the prosthetic joint torque, $\omega(s)$ is the angular velocity of the joint, and $Z(s)$ is the emulated joint impedance. In addition to this behavior, we may still want to specify a position or velocity level reference for the prosthetic joint. In this case, we can model the prosthetic joint controller as a flow source in conjunction with an impedance, which can be represented by the bond graph presented by Hogan in [37]:

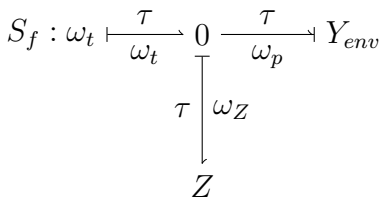

Figure 1.5: Hogan's bond graph representation of impedance control [37].

We will use a linear spring and damper to represent Z, but let the coefficients (k for the stiffness and b for the damping) be functions of our choosing (namely, functions of state), such that we have no loss of generality. This control system can be represented as follows:

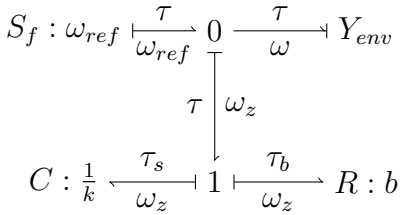

Figure 1.6: A linear impedance controller

We will now derive an expression for the torque control law from this bond graph. The goal is to generate an expression for τ, the torque imposed by the prosthesis on the

environment, in terms of the impedance parameters (stiffness k and damping b) and the kinematic reference represented by the flow source. The constitutive equations for each lumped parameter element in this model are as follows:

$$(0:\tau) \quad \omega_{env} = \omega_{ref} - \omega_z \tag{1.4}$$

$$(1:\omega_z) \quad \tau_b = \tau - \tau_s \tag{1.5}$$

$$(C:k) \quad \frac{d\tau_s}{dt} = k\,\omega_z \tag{1.6}$$

$$(R:b) \quad \tau_b = b\,\omega_z \tag{1.7}$$

Integrating (1.6) provides a more familiar expression for spring behavior:

$$\tau_s = k\,\theta_z + c_1 \tag{1.8}$$

We are free to select the equilibrium position of this virtual spring through the constant of integration, $c_1 = k\,\theta_{eq}$. Because of our flow source will accomplish this, however, we will simply set the equilibrium position to zero and drop this term. From (1.4) we can see that τ is simply the sum of the spring torque (τ_s) and the damper torque (τ_b), which are defined by (1.8) and (1.7), respectively. Therefore,

$$\tau = k\,\theta_z + b\,\omega_z \tag{1.9}$$

Eq. (1.9) is easily recognized as the linear spring and damper system when k and b are constants. However, its torque is generated with respect to ω_z and not the physical state ω_{env}. The flow source injected at the zero junction provides this transformation by adding offsets in both position and velocity. Rearranging (1.4) gives the following expression and its integrated form:

$$\omega_z = -(\omega_{env} - \omega_{ref}) \tag{1.10}$$

$$\theta_z = -(\theta_{env} - \theta_{ref}) + c_2 \tag{1.11}$$

Again, we are ignoring the opportunity to leverage the constant of integration in (1.11) since both the flow source and the impedance are virtual. Note that if the spring in the impedance portion of the controller was a physical spring with a non-zero equilibrium position, then we could carefully choose c_2 in the flow source to compensate for that offset. Instead we will also set $c_2 = 0$. In this form ω_z and θ_z are easily recognized as error signals, and plugging into (1.9) gives us our control law:

$$\tau = k(\theta_{ref} - \theta_{env}) + b(\omega_{ref} - \omega_{env}) \tag{1.12}$$

or in block diagram form:

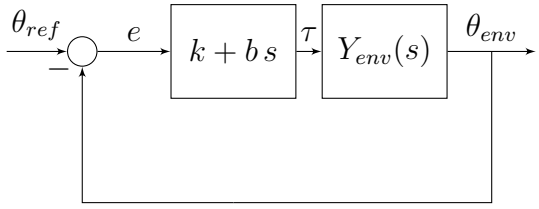

Figure 1.7: Block diagram of the general impedance controller.

The difference between this impedance controller and a Proportional-Derivative (PD) controller is that, in addition to the reference input θ_{ref}, the control gains k and b (or K_P and K_D for a PD controller) can vary. The implications of varying the gains of the controller will be discussed in the section on finite state-based impedance control. There is evidence that the human joints change their impedance during various lower limb activities such as level ground walking. A framework that allows such changes is therefore well suited for prosthetic control. In general, the impedance

of the prosthesis need not be linear. In fact, the biomechanics literature suggests that the impedance of the ankle joint in stance during level walking is nonlinear [40]. If we define the impedance parameters k and b as functions of state or time, however, the linear controller becomes nonlinear and opens up opportunities for more accurate emulation of healthy biomechanics.

A final simplification to this controller can be made if the reference position is assumed to either be constant, or to change discontinuously. In this case, ω_{ref} is either zero or undefined, and so should be removed from the control law. This could be modeled by removing the flow source from Fig. 1.8 and instead explicitly setting or switching the virtual equilibrium position dropped from (1.8). The simplified bond graph for this system is:

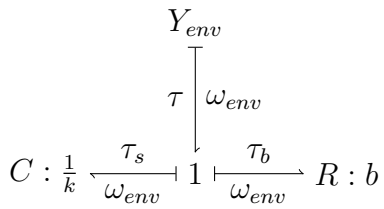

Figure 1.8: A manipulator emulating a spring and damper.

The corresponding control law becomes:

$$\tau = k(\theta_{ref} - \theta_{eq}) + b\,\dot{\theta} \tag{1.13}$$

5.2 Finite State-Based Impedance Control

In order to gain insight as to how we should specify the three inputs to the impedance controller (k, b, and θ_{ref}) from (1.12), let us examine the behavior of a single joint in two common lower limb activities: the ankle in quiet standing and level ground walking. In [41], 10 subjects displayed an average coefficient of determination (R^2)

of 0.918 in a linear regression between ankle moment and ankle angle during quiet standing, suggesting that a linear impedance would do well to emulate healthy behavior for this activity. In this case the impedance control law derived previously would devolve into a regulator with fixed θ_{ref}, and fixed gains k and b. As a result, we could instead use (1.13) to implement this behavior.

In the case of level ground walking, however, it can quickly be seen that a static impedance will not serve to properly emulate the healthy joint behavior at either the knee or the ankle. A spring and damper system is energetically conservative, and a plot of ankle joint power vs. percentage of stride indicates that the ankle joint delivers net positive energy over the gait cycle. At the very least, θ_{ref} will have to be varied in order to deliver this power. In general, however, (1.12) allows us to vary θ_{ref}, k, and b. Furthermore, it is unlikely that there is a unique mapping between joint state and impedance parameters. In other words, in different portions of the gait cycle the same joint state might produce different joint torques. It would be best, therefore, to determine the impedance parameters as a function of the percentage of the gait cycle. It may be possible to generate a continuous estimator of gait cycle percentage and use this estimate to drive varying impedance parameters. A simpler method, however, is to identify characteristic events throughout the gait cycle and use these events as cues for discrete transitions between impedance parameters. This approach forms a finite state machine where the behavior in each state is determined by a different control law. If the parameters are assumed to be constant in each state, then each state produced by such a system is guaranteed to be locally passive (since (1.13) is passive).

The only concern for system stability is therefore due to the interaction of state transitions. This is a legitimate concern, however, as hybrid systems are not necessarily stable simply because they consist of only passive systems [42–45]. A simple example of such a system can be constructed by using two controllers of the form of

(1.13) with zero references to control a simple inertia. The first state is active in the first and third quadrants (i.e. during periods of power delivery), while the other is active in the second and fourth quadrants (i.e. during periods of power dissipation). The system can be written as follows:

$$\dot{\mathbf{x}}(t) = \begin{bmatrix} 0 & 1 \\ -\frac{1}{J}k(\mathbf{x}) & -\frac{1}{J}b(\mathbf{x}) \end{bmatrix} \mathbf{x} \tag{1.14}$$

where

$$\begin{bmatrix} k(\mathbf{x}) \\ b(\mathbf{x}) \end{bmatrix} = \begin{cases} \begin{bmatrix} 50 & 2 \end{bmatrix}^T, & \text{for } x_1 x_2 > 0 \\ \begin{bmatrix} 8 & 6 \end{bmatrix}^T, & \text{for } x_1 x_2 <= 0 \end{cases} \tag{1.15}$$

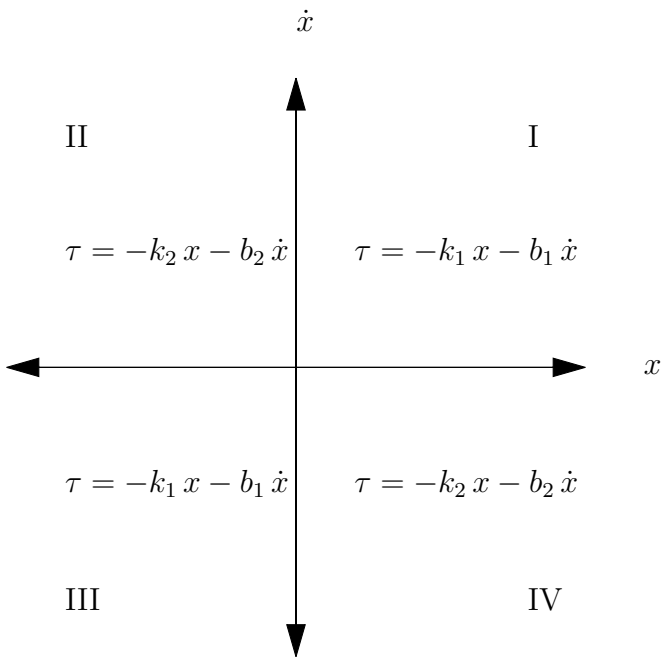

Figure 1.9: An unstable hybrid system consisting of two passive continuous systems.

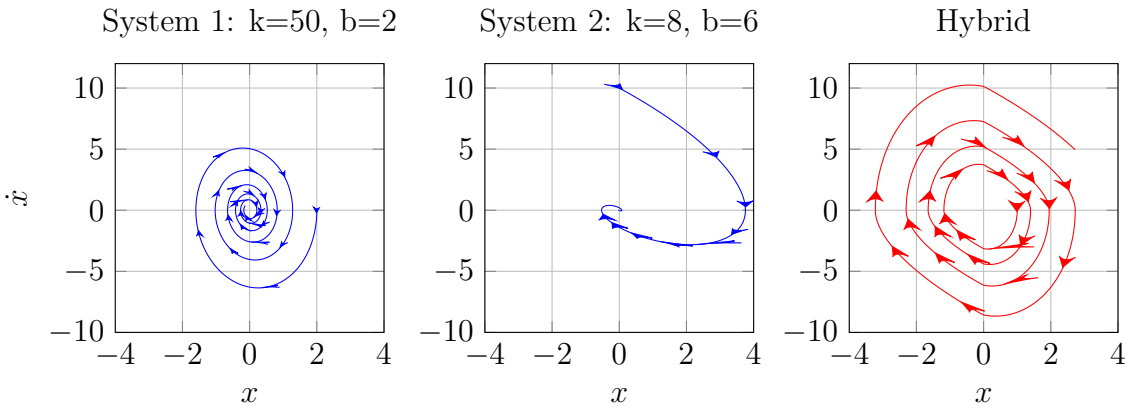

Figure 1.10: Phase portraits of two passive systems and the unstable hybrid system that results from switching between them.

The phase portraits in Fig. 1.10 show the stable behavior of each passive system along with the unstable phase trajectory that results when they are switched. Of course, this is a contrived hybrid system that is designed to be unstable. In practice, however, appropriate selection of state transitions typically prevents such unstable systems from arising.

CHAPTER II

STUMBLE RECOVERY

The introduction of power into a lower limb prosthesis has typically been motivated by the presence of deficiencies in amputee *mobility* when using passive prosthetic technology. On the other hand, deficiencies regarding amputee *stability* are of, perhaps, equal or greater importance in terms of quality of life. This chapter begins with a manuscript presented at the 32nd Annual International Conference of the IEEE Engineering in Medicine and Biology Society in Buenos Aires, Argentina, which describes a detection and classification approach for stumble recovery for an active lower limb prosthesis. This preliminary work was extended to include active responses based upon the classification of the stumble event, and was implemented in a Generation 1 prosthesis. The remainder of this chapter describes further preliminary work performed in pursuit of a Research Project Grant from the National Institutes of Health which was ultimately not funded, despite the demonstration of fully functional stumble recovery on an amputee subject wearing a powered knee and ankle prosthesis.

1. Manuscript 1: Stumble Detection and Classification for a Powered Transfemoral Prosthesis

1.1 Abstract

This paper describes an approach for the real-time detection of stumble for use in an intelligent lower limb prosthesis, using accelerometers mounted on the prosthesis, and also describes an algorithm that classifies the stumble response as either an elevating or lowering type response. In order to validate the proposed approach, the investigators collected stumble data on 10 healthy subjects using accelerometers affixed to the subjects in a manner consistent with similar instrumentation on a transfemoral prosthesis. The proposed algorithms were shown to correctly identify stumbling and correctly classify the stumble response for all 19 stumbles and 34 control strides collected in the experiments.

1.2 Introduction

The majority of commercially available lower-limb prostheses are energetically passive. Recent advances in mechanical and electrical system components have made feasible powered prosthetic lower limbs that are capable of biomechanically significant levels of joint torque and power, while still fitting within an anthropomorphic envelope. To date, several groups have demonstrated such prostheses, reporting a reduction in the metabolic energy cost of gait, improved symmetry of gait, and an improved restoration of healthy biomechanical gait, relative to passive prostheses [14, 18, 46].

In addition to improved mobility, another important characteristic of a prosthetic leg is its ability to restore stability to its user. In passive prostheses, this characteristic is often at odds with the goal of enhanced mobility; a prosthesis that allows dynamic

movement usually does so at the sacrifice of some stability in both standing and walking. In a 2001 survey of 435 community-living lower-limb amputees, approximately half reported falling in the last year, and 40.4% of those who fell reported sustaining an injury as a result of the fall [47]. With the number of lower-limb amputees in the United States at approximately 623,000 in 2005 [7], projection of the previous survey onto the larger population suggests a significant demand for prosthetic devices that are able to address deficiencies in the lower-limb amputee's stability.

The combination of intelligence (resulting from advanced control algorithms implemented on microcontrollers with high computational capabilities) and power (in the form of high-capacity batteries and power-dense brushless DC servomotors) in a self-contained prosthesis provides a unique opportunity to address stability issues for the lower-limb amputee. While previous work on the side of intelligence and control has been focused on real-time recognition of user intent [6], the objective of this work is to separate that intent from external perturbations such as slips or stumbles. If such perturbations can be quickly and correctly identified, a powered prosthesis can implement an active recovery response, and as such potentially prevent the user from falling as a result of a stumble.

Before an active response to a perturbation can be implemented, a reliable method of identification must be developed to protect the user from unexpected and independent behavior on the part of the prosthesis. This paper addresses that problem for the particular case of stumbling during the swing phase of gait (prosthetic leg only). The identification problem is broken into two segments: detection and classification. Detection is the process of recognizing that a stumble has occurred during swing, while classification identifies the type of stumble, such that the correct recovery strategy can be employed.

The human response to stumbling has been relatively well-characterized in healthy

subjects [48–56]. Most studies identify two or three recovery strategies; elevating, lowering, and occasionally a delayed lowering strategy (implemented when the elevating strategy is unsuccessful). The elevating strategy is most commonly seen as a response to perturbations in early swing. In this strategy, the human actively flexes the hip, knee and ankle to raise the swing leg. This movement produces two effects. In the event that the foot is still hindered by the obstacle after the response is activated in the leg, the elevation helps the foot to clear the obstacle to allow free swing. The other effect is that the flexion reduces the moment of inertia of the leg about the hip joint and allows a faster, longer step to be taken in order to support the trunk, which has traveled forwards and rotated more extremely due to its momentum during the extended time of the perturbed stride. After this period of flexion, a complementary extension phase is executed to prepare the leg for stance at the next heel strike.

The lowering strategy typically occurs during middle to late swing. This response is essentially a premature exit from swing at the point the where swing was impeded. The stance leg then executes an exaggerated step (similar to the elevating strategy) in order to both clear the obstacle and to properly position the foot for the next stance phase in order to arrest the forward rotation of the trunk [50].

A delayed lowering strategy occurs when an elevation strategy is executed, but the foot does not successfully clear the obstacle before the forward rotation of the trunk becomes too severe. In this case, the human aborts the active flexion while the foot is still behind the obstacle and executes a lowering strategy instead. EMG response latencies for all strategies are on the order of 100 ms [48, 55].

In order to implement these responses in the prosthesis developed by the authors, the walking state chart described in [5] needs to be modified as shown in Fig. 1. From the figure, it can be seen that the lowering strategy is inherent in the behavior of the leg, as the presence of a heel or toe load on the prosthesis will always force a transition into the stance phase of gait. Even though the prosthesis should already behave

correctly for the purpose of a lowering response, both detection and classification must be implemented in order to reliably execute an elevating strategy at the proper time. The following sections present the methods by which kinematic and inertial stumbling data were recorded for a variety of healthy subjects, and the algorithms for stumble detection and classification that were developed using these data.

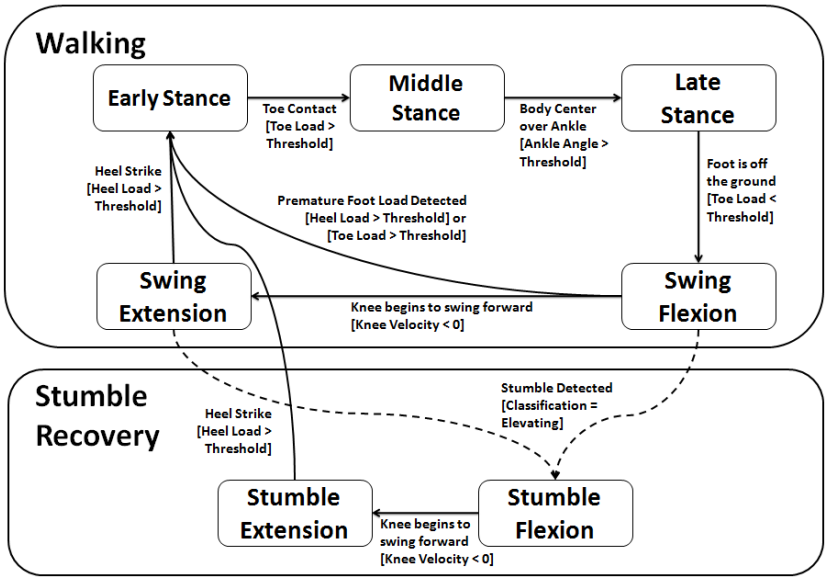

Figure 2.1: Modified state chart for the walking controller. Note that the implementation of the lowering strategy does not require execution of the detection or classification algorithms.

1.3 Methods

There are several techniques that have been used to produce authentic stumbles in human gait. Distinctions can be drawn between treadmill techniques vs. over-ground walking, and also between perturbations created by obstacle encounters vs. rope blocking. Schillings, et al. induced stumbles by dropping an obstacle on a treadmill belt at specific times in order to produce perturbations at different segments of swing [48, 49, 57, 58]. Cordero, et al. also used a treadmill, but chose to block the subject's swing by pulling on a rope attached loosely to the subject's leg [59, 60]. Other studies,

such as those performed by Pijnappels et al., Pavol et al., and Eng et al., employed custom-built devices that deployed a concealed obstacle as the subject walked along a walkway [50–56]. In the only stumbling study known by the authors to address amputees, Blumentritt et al. used rope blocking while subjects walked over ground [61].

In order to develop real-time algorithms for the detection and classification of stumble with instrumentation appropriate for embedding in an intelligent prosthesis, the authors required multiple measurements of joint angles and limb inertial accelerations, all correlated to the stumble event. Since no published studies on stumbling provided such data, the authors conducted experiments on healthy subjects to provide an appropriate database for the design and testing of stumble detection and classification algorithms.

In order to conduct these experiments, the authors chose an obstacle encounter approach in over-ground walking because it most accurately recreates a real-life stumble. A modular walkway was constructed that was composed of a series of identical platforms, one of which contained a concealed stumbling mechanism. Each module was 0.6 m long by 0.9 m wide. A total of 8 modules were built, providing a total walking distance of approximately 5 m. Since each module was visually identical, the stumbling mechanism could be placed at any point along the walkway without the subject identifying it. The stumbling mechanism was built out of wood and was mounted with a spring-loaded hinge. It was released remotely by triggering a solenoid and locked into place when fully extended. The height of the obstacle was approximately 10 cm above the surface of the walkway when deployed. The entire walkway was covered with a loose-pile carpet to disguise the seams where the stumbling block flipped out of the walkway.

Each subject was instrumented with three separate triple-axis accelerometer modules (Analog Devices, ADXL335) on the left leg: one located on the foot, shank and

thigh. The accelerometer signals were low-pass filtered at 50 Hz. The ADXL335 is a 3.3 V device, so the acceleration signals were amplified to a range of zero to 10 V before passing through a 6 m signal tether in order to ensure data integrity. The 9 signals were acquired by a PC running MATLAB's Real-Time Workshop at a sampling rate of 1000 Hz with a data acquisition card (Sensoray, Model 626). Each accelerometer module was secured to the leg with flexible straps in order to avoid constriction of the leg's movement. The modules were aligned with respect to gravity (1 g of acceleration in the vertical axis, zero in the other two axes) while the subject stood with a straight leg on the walkway.

Joint angles of the hip, knee and ankle of the left leg were measured during each trial using a motion capture setup. A single camera was used to track the locations of 5 reflective markers in the sagittal plane. Markers were placed on the iliac crest, the greater trochanter, the lateral epicondyle, the lateral malleolus, and the head of the fifth metatarsal. Video data was recorded at 90 Hz and the joint angles were computed in post-processing using MATLAB. The joint angle measurement approach was validated by comparing the computed joint angles from normal strides with representative data published by Winter [62].

Data were recorded for both normal gait and stumbles on 10 healthy male subjects of ages ranging from 24 to 42. The subjects were warned of the possibility of a stumble or fall during the experiment. Because the anticipation of a stumble could significantly alter the subject's gait pattern, several techniques were employed to reduce the ability of the subject to anticipate the event. Each subject listened to music through earphones at a loud but comfortable level of volume in order to provide mental distraction and also to mask any sounds that occurred during deployment of the stumbling block. The location of the stumbling mechanism was moved in the walkway after each stumble attempt. The stumbling block was also only deployed on randomly determined trials at a frequency of approximately 20%.

Video frames corresponding to data for a representative elevating-type and lowering-type stumble are shown in Figs. 2.2 and 2.3, respectively. These figures also show the computed link orientations (from the motion capture system), the data for knee angle as a function of time, and indicate with a vertical cursor the instant of the stumble.

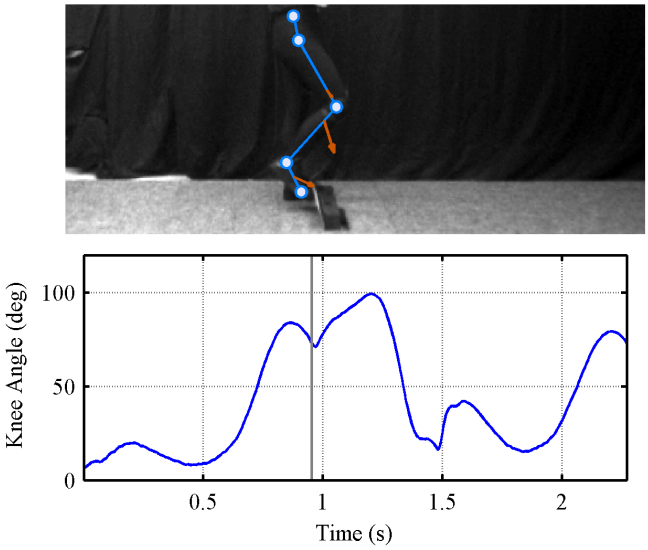

Figure 2.2: Representative measurement of an elevating type stumble response.

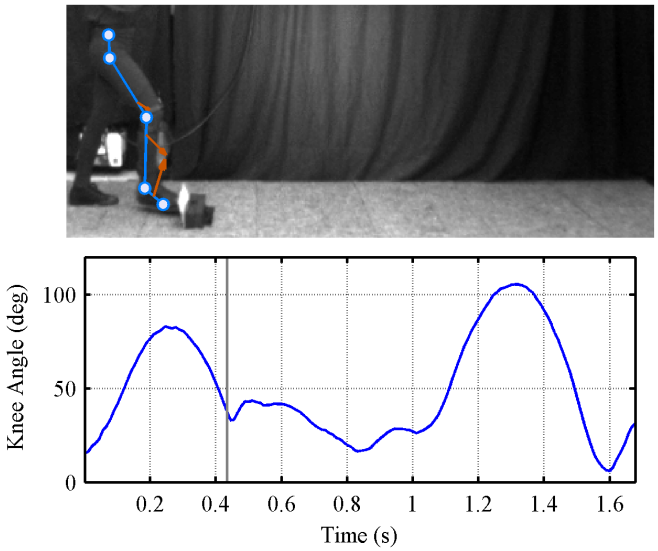

Figure 2.3: Representative measurement of a lowering type stumble response.

1.4 Detection

With a working data set of 19 successful stumbles and 34 control strides from across all 10 subjects, an algorithm was developed that utilizes the six accelerometer signals from the sagittal plane (two each for the three segments of the lower limb). Each accelerometer signal was high and low pass filtered using second order filters with 3 and 40 Hz cutoff frequencies, respectively. Whenever swing was initiated, the filtered data was used to generate frames of 64 samples (64 ms) of data with the starting points of successive frames separated by 10 samples. Since the biomechanics of swing phase contain primarily low frequency information, and since stumble events entail significant power at higher frequencies, a Fast Fourier Transform (FFT) was used to measure the amount of power at frequencies between 10 and 40 Hz. A stumble flag was raised when the power at these higher frequencies exceeded a threshold, determined relative to normal swing. If four or more signals raised stumble flags within a 100 ms interval, the algorithm reports a stumble. Figure 2.4 shows a representative FFT (from one component of shank acceleration) for a swing phase in which a stumble occurred, and for comparison to a swing phase without a stumble event.

This algorithm correctly detected stumbles (and the absence of stumbles) in all collected data, with an average delay of detection of 50 ms, and a maximum detection delay of 70 ms. Note that, as described by Schillings et al. the delay in the stumble response in healthy subjects is typically more than 100 ms, and thus the delay required by the FFT approach is well within the reaction time of healthy subjects [48, 55].

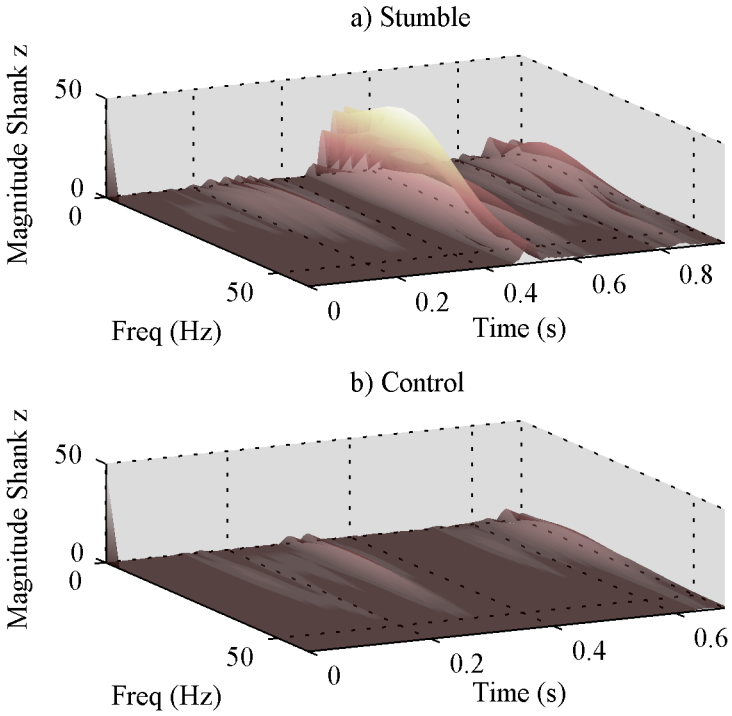

Figure 2.4: Power spectra of the shank z-axis accelerometer during swing for a stumbling trial (a) and a control trial (b).

1.5 Classification

When a stumble is detected, the event must then be classified as either a lowering or elevating event. Note that this determination is made easier due to the intact hip in the transfemoral amputee, which directly influences the accelerometer measurements on the leg segments, and thus provides information regarding the stumble strategy being employed by the user.

Figure 2.5 shows the y-direction (i.e., transverse) component of the thigh segment acceleration for 50 ms preceding stumble detection for all 19 stumbles, where the dark traces are the cases in which the subjects employed an elevating strategy, and the light traces on the cases in which the subjects employed a lowering strategy. As can be observed from the figure, the character of the acceleration is distinct between the

elevating and lowering trials. Figure 2.6 shows the root mean square of this component of acceleration for the 50 ms preceding stumble detection for all 19 stumbles. As can be seen from the figure, applying a simple threshold to this measurement is sufficient to determine the stumble strategy for all 19 stumbles.

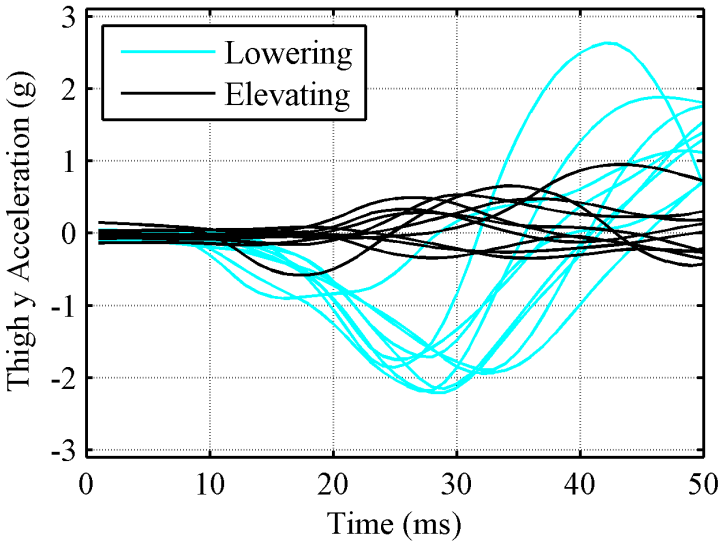

Figure 2.5: Transverse component of thigh acceleration during elevating and lowering strategies.

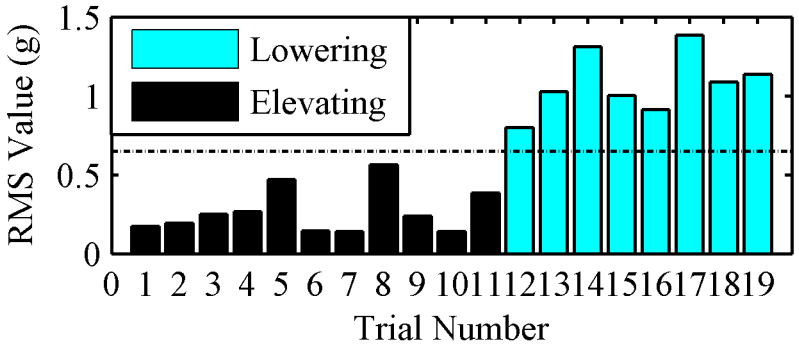

Figure 2.6: RMS values of the y-component of the thigh accelerometer signals.

1.6 Conclusion

This paper proposes a methodology for implementing detection and classification of a stumble using accelerations of the thigh, shank and foot during swing. Both FFT-based detection and threshold based classification are promising. However, larger datasets with more stumbles per subject are necessary for a more thorough validation of the presented methods.

2. Addendum to Manuscript 1: Implementation of Stumble Recovery in a Powered Prosthesis

The results of the above manuscript were compelling enough to try to implement real recovery strategies in the powered prosthesis prototype and test them on an amputee subject. The following research was conducted as preliminary work for a series of R01 proposals for the National Institutes of Health. Although the project did not receive funding, it has been shown that a powered knee and ankle prosthesis is capable of detecting, classifying, and appropriately reacting to all four cases of stumbles (elevating and lowering, ipsilateral and contralateral). Implications regarding further directions of this work are summarized at the end of this chapter.

2.1 Recovery Approaches

2.1.1 Trajectory-Based Recovery

Before the stumble recovery method described in the previous manuscript was implemented on the powered prosthesis, several approaches were considered for implementing the elevating-type recovery response in the powered prosthesis. Since the healthy elevating strategy is a fundamentally active response, the first approach considered for

recovery in the powered prosthesis consisted of a trajectory generation and execution phase following the detection and classification of the stumble. It was assumed that executing a trajectory tracking algorithm was acceptable in this condition, provided that the selected trajectory was consistent with the user's response, and that it ended in sufficient time and reverted to the finite state-based impedance framework.

In order to understand the normal human biomechanics of the stumble response, the authors constructed a data set for two subjects of similar height, weight and age. The data from the first subject was used for algorithm development and the data from the second subject was used to validate the approach. Subject A was male, 27 years old, weighed 83 kg, and had a height of 1.81 m. Subject B was male, 25 years old, weighed 84 kg, and had a height of 1.82 m.

In order to capture joint angles for each data set, a custom motion capture setup was constructed for a simple, two-dimensional analysis. A single camera captured frames at 90 Hz of a 5 m walkway. Reflective markers were placed on the iliac crest, the greater trochanter, the lateral epicondyle, the lateral malleolus, and the head of the fifth metatarsal of the subject. The locations of these markers were extracted from each frame in MATLAB and used to calculate the joint angles.

Fig. 2.7 shows the segmentation of the elevating response for a typical trial. The cross marks the contact of the subject's foot with the obstacle, and the solid lines represent the flexion and extension phases of the response. The flexion phase in the figure is delayed from the instant of stumble in order to account for the latency of the reaction in the subject. The change in knee angle during this time is due to the passive dynamics of the interaction between the foot and the obstacle.

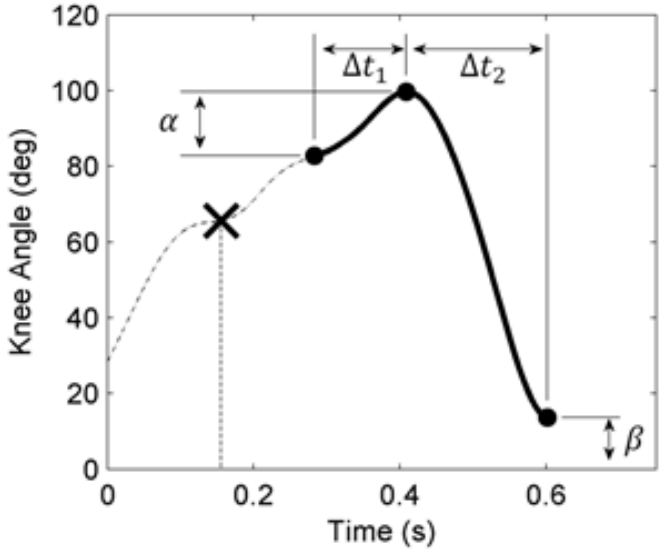

Figure 2.7: Trajectory design parameters taken from measured data.

The trajectory reference for the prosthesis is split into two components: one corresponding to knee flexion after impact with the obstacle, and a second corresponding to knee extension in preparation for stance. The transition from the flexion trajectory to the extension trajectory is governed by a finite-state model that switches based upon a zero crossing in knee velocity (corresponding to a peak in knee angle). This approach protects the prosthesis from executing a complex trajectory independent of interaction with the user. In other words, if the knee angle does not reach the specified angle in the time dictated by the trajectory, the prosthesis will wait for the inflection in knee angle before continuing with the extension phase. There are two characteristic times, $\Delta\tau_1$ and $\Delta\tau_2$, which correspond to the durations of flexion and extension, respectively. The other two parameters shown are characteristic angles: α, corresponding to the maximum flexion angle (relative to the knee angle at the time of detection) and β, the angle at heel strike. These parameters were determined from empirical data and used to help specify constraints for the trajectory generation. Their values are summarized in Table 1.

For each component of the trajectory, four constraints were set based upon both

Table 1: Empirical Parameters

Parameter	Value
α - Desired Added Knee Flexion	20°
β - Desired Knee Angle at Heel Strike	20°
$\Delta\tau_1$ - Median Flexion Duration	73 ms
$\Delta\tau_1$ - Median Extension Duration	274 ms

the empirical parameters described above and the constraints for position and velocity continuity. These constraints were used to uniquely determine third order polynomials of the form

$$\theta_{flx}(t) = \begin{cases} c_{10} + c_{11}t + c_{12}t^2 + c_{13}t^3, & \text{for } 0 < t < \Delta t_1 \\ \theta_{detection} + \alpha, & \text{for } t \geq \Delta t_1 \end{cases} \tag{2.1}$$

$$\theta_{ext}(t) = \begin{cases} c_{20} + c_{21}t + c_{22}t^2 + c_{23}t^3, & \text{for } 0 < t < \Delta t_2 \\ \beta, & \text{for } t \geq \Delta t_2 \end{cases} \tag{2.2}$$

where $\theta_{flx}(t)$ represents the trajectory for flexion, $\theta_{ext}(t)$ represents the trajectory for extension, t denotes time (relative to the beginning of each segment of the trajectory), and each c_{mn} represents a constant coefficient subject to the constraints listed in Table 2.

As is evident from the constraints listed in Table 2, the only factors that influence the shape of the response trajectory for a given stumble are the angular position and velocity of the knee at the time of detection. (Remember that the four parameters α, β, Δt_1, and Δt_2 are empirically determined, but once chosen they are implemented as constant values.) Trajectories were generated for each stumble in data sets from the two subjects. The detection point for each trial was taken as the inflection in velocity after the stumble, signifying the end of the passive dynamics and the beginning of the active human response.

Table 2: Trajectory Constraints

Constraint	Description
$\theta_{flx}(0) = \theta_{detection}$	Continuity of Knee Angle at Detection
$\dot{\theta}_{flx}(0) = \dot{\theta}_{detection}$	Continuity of Knee Velocity at Detection
$\theta_{flx}(\Delta t_1) = \theta_{detection} + \alpha$	Maximum Knee Angle at End of Flexion
$\dot{\theta}_{flx}(\Delta t_1) = 0$	Knee Velocity at End of Flexion
$\theta_{ext}(0) = \theta_{flx}(\Delta t_1)$	Continuity of Knee Angle at Detection
$\dot{\theta}_{ext}(0) = \dot{\theta}_{flx}(\Delta t_1)$	Continuity of Knee Angle at Detection
$\theta_{ext}(\Delta t_1) = \beta$	Continuity of Knee Angle at Detection
$\dot{\theta}_{ext}(\Delta t_1) = 0$	Continuity of Knee Angle at Detection

Fig. 2.8 shows the trajectory overlaid with the measured response and a control swing for a typical trial in subject B. It is important to note that the knee angle parameters were determined by tuning, and the characteristic times were selected as the median values from subject A. A detection window is shown in the figure to highlight the time from the stumble event to the latest measured muscle response in healthy subjects.

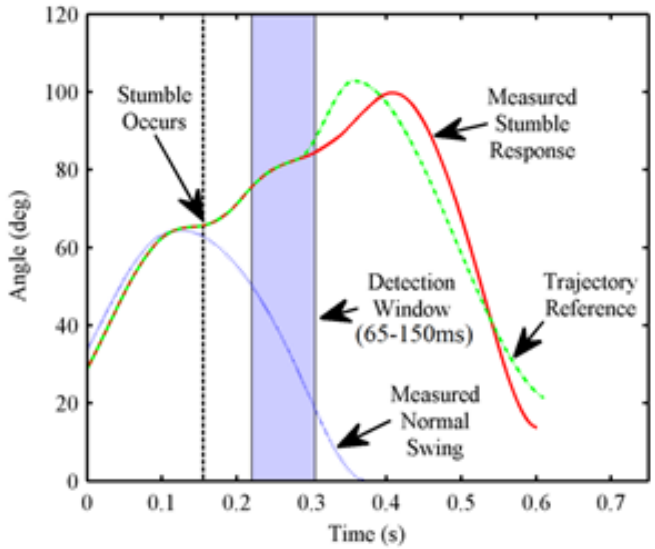

Figure 2.8: Generated trajectory as compared to the measured response.

A simulation of the presented response was performed for each stumble in order

to gage the ability of the prosthesis to effectively track the trajectory. A control law of the form

$$\tau = k(\theta(t) - \theta_{traj}(t)) + b\dot{\theta}(t) \tag{2.3}$$

was adopted in order to preserve the impedance framework already implemented on the prosthesis. In 2.3, τ represents the actuator torque, $\theta(t)$ represents the prosthetic knee angle, $\dot{\theta}(t)$ represents the prosthetic knee velocity, and $\theta_{taj}(t)$ is the reference trajectory. The gains k and b adjust the impedance used to track the reference.

During the stumble response, power can be generated by the evolution of the reference in time. At the conclusion of each segment of the trajectory, however, the reference will remain at a constant value until a state-transition occurs and therefore recapture the passive behavior. Furthermore, in the simulation the tracking of the reference occurs at a moderate impedance ($k = 5Nm/deg$, $b = 0.1Nm \cdot s/deg$). This impedance allows a fast response but still tolerates a significant amount of tracking error. The result is a more dynamic and forgiving interaction between the movement of the prosthesis and the actions of the user.

To evaluate the elevating stumble response, a simplified model of the prosthesis was used. Fig. 2.9 shows a free-body diagram of the model, implemented as a pendulum attached to a moving point. The forces acting on the prosthesis (in free swing) are the force due to the acceleration of gravity on the prosthesis's center of mass, the propagated inertial forces due to the accelerations at the knee, and the imposed actuator torque. The equation of motion for the model is given by

$$I\ddot{\varphi} = mL(\ddot{y} + g)sin\varphi + mL\ddot{(}x)cos\varphi + \tau. \tag{2.4}$$

The orientation of the prosthesis is expressed in the world coordinate system (WCS), and so it is represented by φ in order to differentiate this angle from the true

knee angle θ in eq. 2.3. The knee angle is found by the difference between φ and the orientation of the thigh in the WCS.

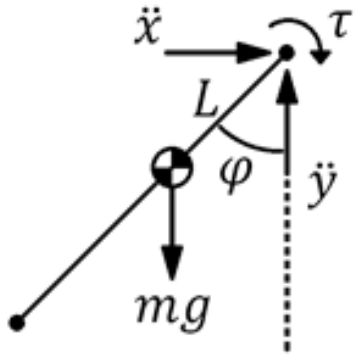

Figure 2.9: Free-body diagram of the shank model.

A simulation was performed for each trial in order to estimate the achieved trajectory of the leg had it been controlled by the suggested control law. The translational movement of the knee was constrained to the kinematics measured in the motion capture, so the validity of this approach is dependent upon the assumption that these trajectories would have been similar given the slightly varied knee kinematics.

Fig. 2.10 shows the simulated knee angles for the control implementation overlaid with the measured responses for the validation subject (subject B). Despite the noticeable deviation from the measured response in some cases, it is probable that the flexion of the prosthesis would still improve the probability of a successful placement of the foot in order to support the body and prevent a fall. In every case, the simulated prosthesis movement would have cleared the obstacle, which is critical to the execution of an elevating strategy.

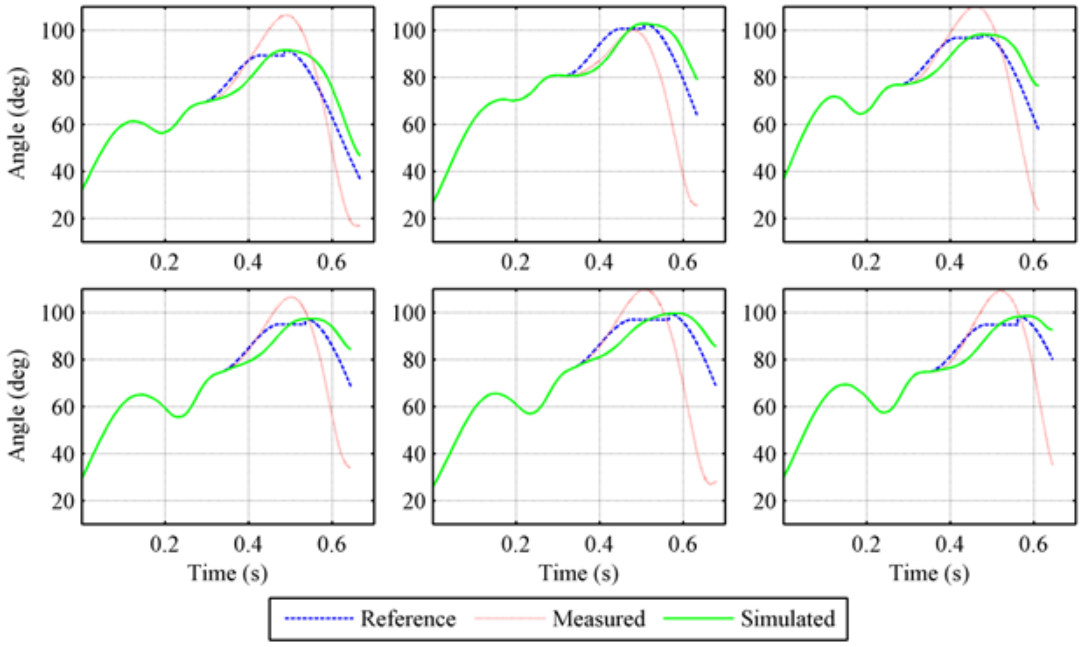

Figure 2.10: Generated trajectories as compared to the measured responses in all six trials for Subject B.

2.1.2 Impedance-Based Recovery

In order to preserve the finite state-based framework of the original control system, and in order to maintain consistency with the work presented in Manuscript 1, a two state extension to the walking controller was also considered for implemented an elevating strategy in stumble recovery. Using the same healthy subject data from the previous experiments, Frank Sup constructed a three-link (thigh, shank, and foot) planar model using MATLAB Simulink.

Inertial estimates of the actual leg segments were used for the simulation, and impedance parameters were manually tuned for each state in order to match the kinematics of a healthy stumble. The model was constrained to follow the hip joint trajectory and thigh segment angle of the healthy trial. Just as in the single degree of freedom simulation, the validity of this approach assumes that the hip dynamics would

not be substantially influenced by slight variations in the knee and ankle behavior, since this portion of the simulation is kinematically constrained.

The impedance parameters used for the knee joint in the simulation are shown in Table 3.

Table 3: Knee Impedance Parameters

Phase	K $Nm \cdot deg^{-1}$	b $Nm \cdot s \cdot deg^{-1}$	θ_k deg
Normal Swing Flexion	0.9	0.05	58
Normal Swing Extension	1.6	0.10	33
Stumble Swing Flexion	0.2	0.00	105
Stumble Swing Extension	3.1	0.17	33

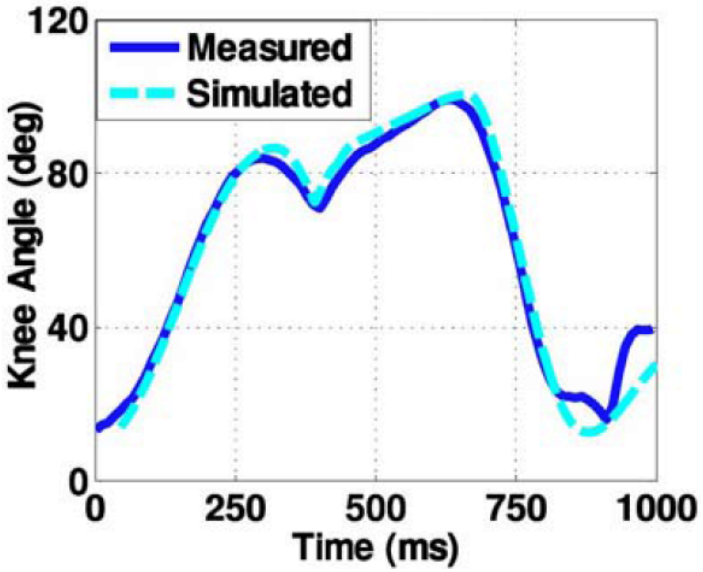

Figure 2.11: Measured and simulated knee joint angle during elevating stumble recovery (stumble event occurs at 400 ms).

2.2 Amputee Subject Testing

2.2.1 Implementation on the Powered Prosthesis

Several simplifications were made to the detection and classification approach described above in order to facilitate an efficient implementation on the embedded system of the powered prosthesis. Much of the simplification stems from the fact that the finite state machine of the powered prosthesis provides valuable information about the current phase of gait, which was lacking in the healthy subject experiments. In the healthy subject experiments, toe off and heel strike events were significant risks for false detections of stumbles, as both produced significant accelerations. Since these events correspond to state transitions in the finite state machine of the powered prosthesis, the real time stumble detection algorithm can simply ignore possible stumble events within windows of these state transitions. For this reason, a simple thresholding scheme was sufficient for detection, and a real time FFT was not conducted in the trials that follow.

2.2.2 Testing the Four Stumble Events

Because a stumble can occur on either the sound side or the affected side for a unilateral amputee, and because there are two main recovery strategies (elevating and lowering), there are four distinct stumbling scenarios. All four stumble scenarios were investigated with an amputee subject using the powered prosthesis. To begin, the subject performed what are known as "contrived" stumbles, or stumbles where he was aware of the obstacle before it perturbed his stride. In all four conditions, the prosthesis performed as designed; in early swing on the affected side the prosthesis performed an elevating strategy, and in late swing it provided support for the lowering strategy. In the case of sound side stumbles, the prosthesis remained in support during

the recovery movement of the sound leg for both elevating and lowering strategies.

Despite these promising results, when unanticipated stumbles were tested on the amputee subject, he quickly reacted to the perturbation with a learned response not seen in healthy subjects. In affected side stumbles, the prosthesis correctly detected stumbles and chose elevating responses for early swing and lowering responses for late swing, while the subject in all cases immediately performed a compensatory hopping motion on his sound side. This reaction is undoubtedly learned from walking with a prosthesis that does not inherently react to stumbles.

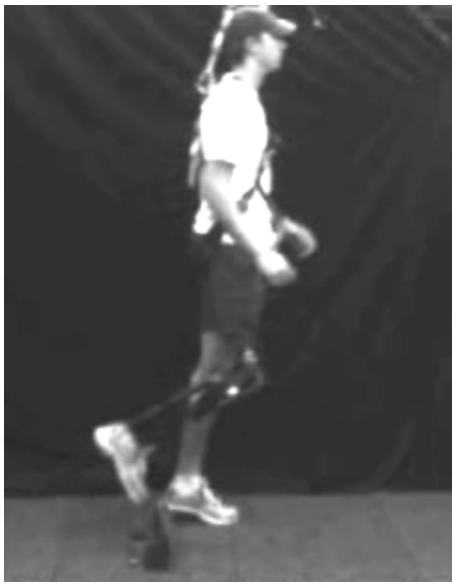

Figure 2.12: Stumble response in an amputee subject using the powered prosthesis. This is a "contrived" stumble where the subject was aware of the obstacle. In this scenario, the subject was able to use the prosthesis to clear the obstacle and subsequently receive support on the affected side. When the obstacle was unanticipated, however, the subject executed a different recovery strategy consisting of hopping on his sound side.

Continued research on stumble recovery techniques for amputees using powered prostheses may require the subjects to wear the prototype prostheses for long periods of time in order to re-learn reflex techniques during stumbling events. Because this sort of study would require commercially hardened prototypes and, possibly, FDA-approval of the devices, it was not pursued further by the author. Another possible

approach would be to test the recovery techniques of new amputees that had not already grown accustomed to using passive prostheses. Again, the selection criteria for this study excluded amputees that were less than 6 months post independent ambulation, so this approach was not pursued.

CHAPTER III

NAVIGATION OF STAIRS

A significant problem for many lower limb amputees is the navigation on terrain other than level ground. Although the lack of power in passive devices is clearly a problem for stair ascent, both stair ascent and descent are characterized by notably different impedances and behaviors than level walking. Therefore, it is not surprising that passive devices developed and optimized for level ground walking suffer a performance disadvantage during these activities. The virtual impedance characteristics of the powered prostheses described in this dissertation make them well suited to adaptable behaviors, and, as such, they can change their behavior accordingly for stair ascent and descent. This chapter consists predominantly of a manuscript that appeared in the 3rd issue of the 21st volume of the IEEE Transactions on Neural Systems and Rehabilitation, which describes stair ascent and descent controllers developed by the author using the methodology of the finite state-based impedance control framework developed by Sup [5]. Additional plots of estimated power delivery are included in an addendum, as these data were not included in the journal publication.

1. Manuscript 2: Control of Stair Ascent and Descent with a Powered Transfemoral Prosthesis

1.1 Abstract

This paper presents a finite state-based control system for a powered transfemoral prosthesis that provides stair ascent and descent capability. The control system was implemented on a powered prosthesis and evaluated by a unilateral, transfemoral amputee subject. The ability of the powered prosthesis to provide stair ascent and descent capability was assessed by comparing the gait kinematics, as recorded by a motion capture system, with the kinematics provided by a passive prosthesis, in addition to those recorded from a set of healthy subjects. The results indicate that the powered prosthesis provides gait kinematics that are considerably more representative of healthy gait, relative to the passive prosthesis, for both stair ascent and descent.

1.2 Introduction

Over the past two to three decades, two significant technological advances have helped to enhance the mobility of transfemoral amputees. In the 1980s the introduction of composites such as carbon fiber allowed the creation of energy-storing ankle-foot complexes that can return some of the energy stored in the stance phase of gait back to the limb for the swing phase. In the 1990s the integration of microprocessor control with modulated damping elements in prosthetic knee joints enhanced the capability of prosthetic knees to accommodate variation in gait speed and locomotion activity. Despite these advances, the capabilities of these joints remain deficient relative to the healthy joint, particularly during stair ascent and descent. The inability to achieve biomechanically healthy stair ascent is largely due to the fact that the emulation of healthy stair ascent requires significant net positive power at the knee and ankle joints

[63–65]. An energetically passive prosthesis is fundamentally unable to provide such net power at either joint. The inability of existing prostheses to provide biomechanically healthy stair descent is not due to a lack of power generation capability, per se, but rather due to the inability of existing prostheses to appropriately configure the ankle joint prior to foot strike. That is, stair descent is characterized by forefoot strike rather than heel strike, which enables the ankle joint to dissipate substantial power during the loading phase of gait. A typical passive (compliant) ankle/foot prosthesis is unable to provide the appropriate ankle posture during the terminal swing phase to set up forefoot strike and is similarly unable to absorb energy (without later releasing that energy) during the loading phase of stair descent. Although various powered lower limb prosthetic devices are emerging [3–6, 12, 14, 18, 66], to the knowledge of the authors, no literature is currently available regarding the implementation of stair descent or ascent with a powered knee and ankle transfemoral prosthesis. It should be noted that Koganezawa, et al. presented a passive transfemoral prosthesis designed to provide reciprocal stepping; however, no data was presented, and it was conceded that active knee extension and ankle plantarflexion were not possible [67].

As such, the authors present here the design, implementation, and experimental validation of a stair ascent and descent control system for a powered knee and ankle prosthesis previously developed by the authors. The authors have previously described controllers for level and sloped standing and walking [3–6]. In this paper, the authors describe the design of the control system for stair ascent and descent, implement the system in the aforementioned powered prosthesis, and compare the resulting joint kinematics during stair ascent and descent with those provided by a passive prosthesis and healthy subjects.

1.3 Methods

1.3.1 Powered Prosthesis

The controllers presented in this manuscript were designed for and implemented on the powered prosthesis prototype pictured in Fig. 3.1. This prosthesis is the second generation of the prosthesis prototype described in [5]. The second generation prosthesis uses the same hierarchical control structure as the first, consisting of a supervisory controller that infers the user's intent and selects an appropriate activity mode and an activity-level controller that runs a state machine to select the internal phase of the activity. The knee and ankle actuators are brushless DC motors that are controlled by custom servo-amplifiers integrated into the embedded control system. Sensors in the prosthesis include a shank axial load sensor, angle sensors at the knee and ankle joints, and a 6-axis inertial measurement unit. The embedded electronics are contained on a single printed circuit board located on the shank of the prosthesis (excluding small circuit boards required for sensor interfacing). The power source is a lithium-polymer battery, and the prosthesis attaches to an amputee's socket with a standard pyramid connector. The current prototype can achieve approximately 100 Nm of torque at the ankle joint and 90 Nm of torque at the knee joint. The prosthesis prototype shown in Fig. 3.1 weighs 4.3 kg (9.5 lb), not including the mass of the shoe or height adaptor shown.

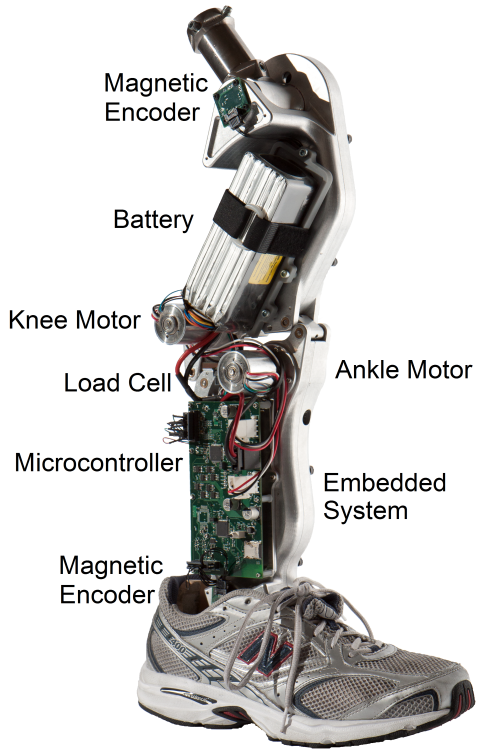

Figure 3.1: The powered prosthesis previously developed by the authors and used in the experiments.

The activity-level controllers in the device are implemented in the form of a finite state machine (FSM). Each state within the FSM generates torque commands for the knee and ankle joints that ensure passivity within the state. The torque command is a function of joint angular position and velocity, and is given by

$$\begin{aligned} \tau_k &= k_k(\theta_k - \theta_{eq_k}) + b_k\dot{\theta}_k \\ \tau_a &= k_a(\theta_a - \theta_{eq_a}) + b_a\dot{\theta}_a \end{aligned} \tag{3.1}$$

where τ denotes the commanded torque, θ denotes the joint angle, and $\dot{\theta}$ denotes the joint angular velocity. The subscripts k and a denote knee and ankle, respectively. The three remaining parameters in each equation are easily recognized in this form as a stiffness term, equilibrium position, and a damping coefficient (k, θ_{eq}, and b, respectively). This control law, therefore, can be viewed as an emulation of a spring and

damper within each state. The primary goal behind implementing such a controller is that the behavior of the prosthesis within any given state will be passive, yet energy can be introduced into the system by changing the potential energy of the virtual spring arbitrarily during transitions between finite states. Since state transitions are based on mechanical cues from the user, the user retains control over the introduction of power into an otherwise passive system.

1.3.2 Stair Ascent Controller

The stair ascent controller consists of 5 phases, each of which is accessed sequentially during a single stride of stair ascent. The conditions for state transitions for stair ascent are listed in Table 6, and the state machine is depicted in Fig. 3.2. Stair ascent begins in Phase 4, which is called the pre-landing phase. This phase is tuned for a relatively high impedance to prepare the prosthesis for loading once the user positions the prosthetic foot on the first step. This high impedance allows the user to register a load on the prosthesis even though the knee is relatively bent. The registration of this load triggers the T40 transition, and the prosthesis enters Phase 0.

Phase 0 is the main power delivery phase of the stair ascent controller. In this phase, the knee extends and lifts the center of mass of the user. The knee extension is achieved by selecting a high impedance for the knee and choosing an equilibrium position near zero such that the knee generates a large moment at the beginning of this phase.

The transition from Phase 0 to Phase 1 (T01) occurs when the knee and ankle angles both straighten significantly. This straightening is due in part to the extensive knee torque provided by the impedance set in Phase 0, and also by a simultaneous exertion of hip torque in flexion from the user. This torque coincides with ground contact on the contralateral side and is the signal for the ankle to start pushing off

in preparation for swing. Phase 1 ends when ground contact is lost, as measured by a minimum threshold in the load sensor.

Phase 2 is characterized by a large knee flexion produced by a moderate impedance and a large knee equilibrium angle. When the knee velocity inflects during swing (after the knee angle passes its equilibrium position and, consequently, the knee torque inflects), the controller transitions into Phase 3, the swing extension phase. Once the knee has extended sufficiently under a low impedance, the controller transitions back to Phase 4, where it maintains a moderate impedance in anticipation of loading on the next step.

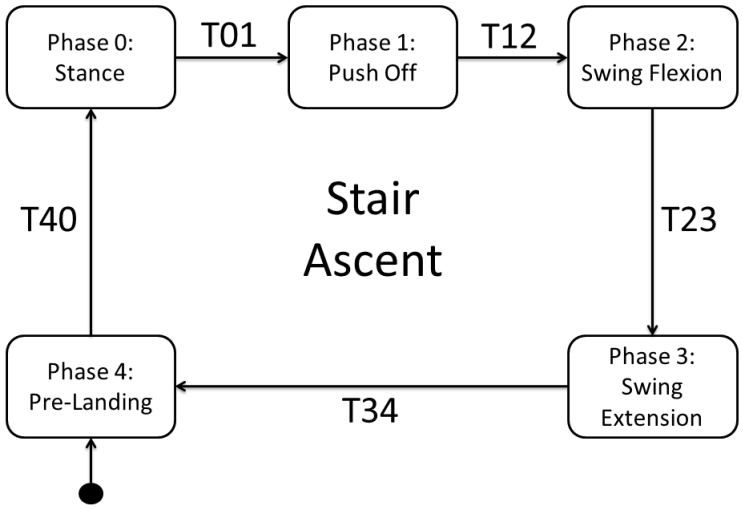

Figure 3.2: The finite state model for the stair ascent controller.

1.3.3 Stair Descent Controller

The stair descent controller is similar in form to the ascent controller, although with several significant differences in the nature of the finite states. The first major difference is that the lifting portion of the stance phase is replaced with a lowering portion as the user's center of mass moves down the steps. The second difference is that there

Table 4: Finite State Transitions for the Stair Ascent Controller

Transitions	Description	Condition
T01	The knee is straightened and ankle push-off begins.	Load is high Load is high Ankle is close to zero
T12	The toe leaves the ground after pushing off.	Load is low
T23	The knee reaches maximum flexion in swing.	Knee velocity inflects Knee exceeds a certain angle
T34	The knee finishes extending and prepares for foot landing.	Knee returns to proper angle
T40	Ground contact is established and the next stride begins.	Load is high

is no push-off phase for the ankle; the small amount of swing flexion seen at the knee is actively provided by the knee actuator.

The conditions for state transitions for stair descent are listed in Table 7, and the state machine is depicted in Fig. 3.3. The prosthesis enters stair descent in Phase 3, the swing extension phase. This phase has a moderate impedance and serves both as the phase that extends the knee at the end of a stride and also as the pre-landing phase for the next instance of ground contact. Additionally, the ankle equilibrium position is substantially plantar-flexed in anticipation of ground contact. The pre-landing phase and the knee extension phase are not distinct in the stair descent controller because a high impedance is not necessary on ground contact, since the leg is preparing to yield to the weight of the user.

Once ground contact is established, as measured by the load cell, the prosthesis enters the forefoot strike phase, Phase 0. In this phase, the knee is moderately stiff, and the ankle is highly damped. Since the ankle begins this phase in plantarflexion, it will passively flex as the user loads the prosthesis. Eventually a threshold is met with respect to the ankle angle, and the controller transitions to the stance phase, Phase 1. In this phase, the knee becomes highly damped with no stiffness, and the result is a net knee flexion produced by the weight of the user, allowing him or her

to descend the step.

There is no push off phase after stance, and instead the prosthesis enters the swing flexion phase, Phase 3, when the load signal passes a minimum threshold, indicating that the user has shifted weight onto the contralateral limb. Swing knee flexion is therefore active in this controller, although the amount of additional flexion after stance is minimal (just enough to enable the prosthesis to clear the step). Once the velocity reaches an inflection point, just as in the stair ascent controller, the prosthesis transitions to the swing extension phase and remains in this phase until ground contact is again established.

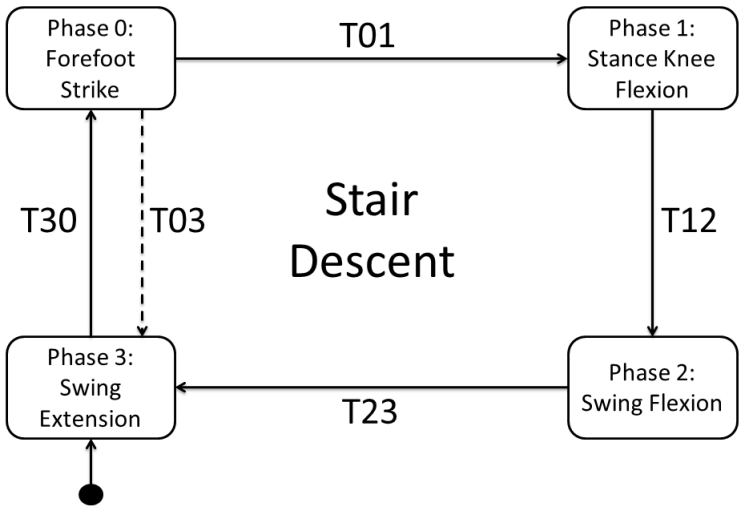

Figure 3.3: The finite state model for the stair descent controller.

1.3.4 Experimental Validation

The stair ascent and descent control system was implemented on the powered prosthesis previously developed by the authors and subsequently tested on a unilateral transfemoral amputee subject. The previously described impedance parameters were

Table 5: Finite State Transitions for the Stair Descent Controller

Transitions	Description	Condition
T01	The ankle finishes conforming to the ground and knee flexion begins.	Ankle is sufficiently flexed
T12	Stance is reached on the contralateral limb, begin swing flexion.	Load is low Knee is sufficiently flexed
T23	Maximum flexion is reached, begin knee extension.	Knee velocity inflects
T30	Forefoot strike is detected and the next stride begins.	Load is high
T03	If the foot landing phase is aborted, return to the end of swing.	Load is low

manually tuned for this subject in order to achieve appropriate stair ascent and descent behaviors. The amputee subject was a 23 year old man whose right side transfemoral amputation was the result of a traumatic injury. At the time of the experiments, he was 5 years post-amputation, and his daily use prosthesis was an Otto Bock C-Leg knee and a Freedom Innovations Renegade ankle/foot (i.e., a microprocessor-modulated damping knee, and a carbon fiber ankle/foot). In order to form a baseline for evaluation of the amputee subject's gait, kinematic data were also collected on 10 healthy male subjects with a mean age of 26.8 years (std. dev. 4.5 years). Specifically, motion capture data were collected during both stair ascent and stair descent on a wooden 8-step staircase with 16.5 cm risers and 25.4 cm runners. Kinematic data were recorded with motion capture using a 12 camera Optitrack system from NaturalPoint. Marker data was collected at 120 Hz and converted to a skeletal model within NaturalPoint's ARENA software environment and then exported as a BVH file resampled to 100 Hz. Sagittal plane joint angles were then extracted from the BVH files using MATLAB. Prior to testing, approval was received from the Vanderbilt University Institutional Review Board and all subjects gave informed consent, including permission for the publication of video and photographs.

Each subject ascended and descended the staircase in 10 trials. The second and

third steps with each limb were used for analysis from each trial, totaling 20 strides for both ascent and descent for each subject. The same procedure was used for the amputee subject, although the use of a hand rail was allowed on the subject's sound side. For the amputee subject, trials were performed first with his daily use prosthesis (where he was instructed to attempt a step-over-step strategy for stair ascent, compensating for the lack of knee extensive torque with excessive hip extensive torque and by using the hand rail) and then with the powered prosthesis. It is important to note that the subject indicated that his preferred method of stair ascent with his daily-use prosthesis was to ascend each step with only his sound side. However, this method was selected for the comparison, since like the other cases (healthy and powered prosthesis), it represents step-over-step walking, and therefore arguably represents a fairer basis for comparison. For stair descent with the daily-use prosthesis, the subject chose the same strategy described in [68]. In this strategy, the prosthetic heel is placed approximately half a foot length from the edge of the step and the foot rolls over the edge of the step, effectively using the interface between the stair edge and foot as a proxy for the ankle joint.

1.4 Results

1.4.1 Stair Ascent

Fig. 3.4 and 3.5 show the knee and ankle joint angles versus stride for stair ascent for the three experimental cases previously described. In Fig. 3.4, the top row shows the left and right average knee joint angles from the 10 healthy subjects, wherein each healthy subject dataset represents 20 strides. The middle row contains the average left (intact) and right (prosthetic) knee joint angles over 20 strides from the amputee subject with the powered prosthesis and previously described stair ascent controller. The bottom row contains the average left (intact) and right (prosthetic) knee joint

angles over 20 strides from the amputee subject with his daily use passive prosthesis. The average stride times for stair ascent were 1.20 seconds (std. dev. 0.06) for the healthy subjects, 1.80 seconds (std. dev. 0.05) for the powered prosthesis, and 1.41 seconds (std. dev. 0.16) for the passive prosthesis. Since the ground reaction force was not measured in these experiments, mean curves for each healthy subject were computed by parsing the strides in a manner similar to the kinematic reference signal presented in [69]. Instead of using the vertical position of a foot marker, however, heel strike was determined by the small but sharp inflection present in the ankle angle. The same plots for the ankle joint are shown in Fig. 3.5.

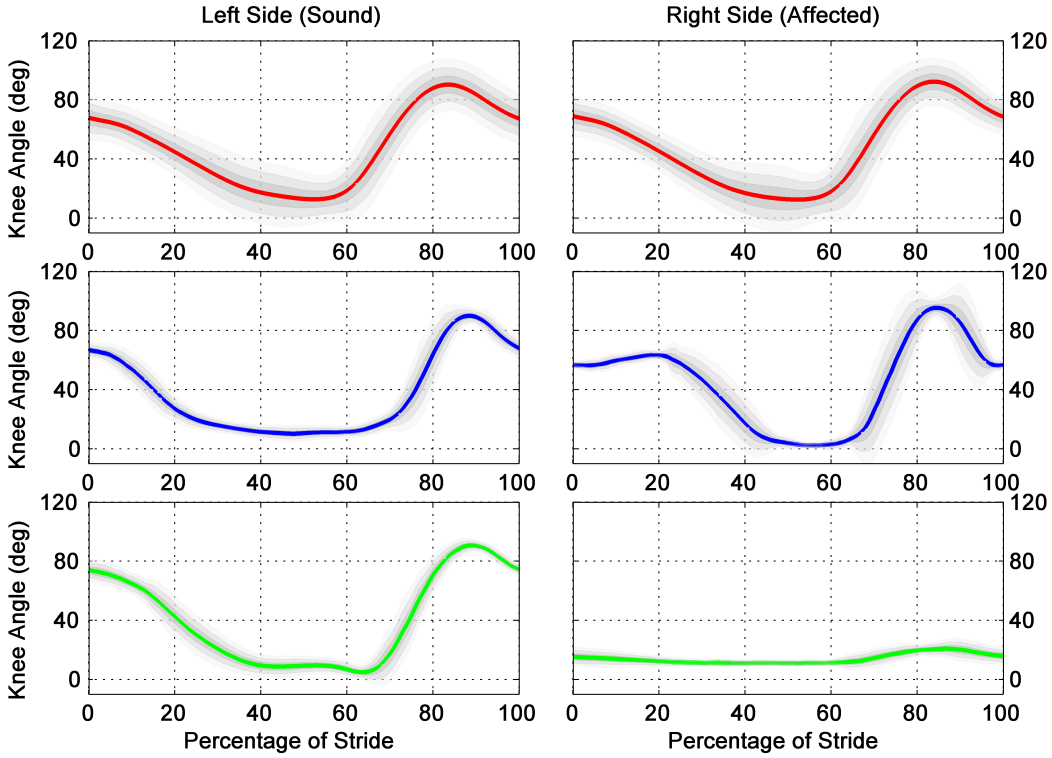

Figure 3.4: Kinematics comparison for the knee angle in stair ascent. The top two plots show the left and right side averages of ten healthy subjects. The middle two plots show the averages for the amputee subject using the powered prosthesis. The bottom two plots show the averages for the amputee subject using his daily use prosthesis. All plots show +/- 1, 2, and 3 standard deviations in sequentially lighter gray bands.

Table 6: Max/Min Knee and Ankle Angles for Stair Ascent

Measure	Healthy		Passive		Powered	
	μ	σ	μ	σ	μ	σ
Max Knee	91.1/93.0	5.4/5.2	**90.8/21.5**	1.4/1.7	90.2/96.3	1.9/1.9
Min Knee	11.7/11.3	5.1/5.6	4.1/10.5	1.1/0.8	9.5/2.0	1.3/0.7
Max Ankle	24.0/25.9	3.6/3.8	**32.6/14.3**	2.0/1.2	19.8/20.8	1.6/0.6
Min Ankle	-5.7/-0.9	3.9/3.6	**-29.8/4.3**	1.4/0.4	-28.7/-16.1	1.8/0.8

* Differences between right and left measures greater than 15° are highlighted in bold print.

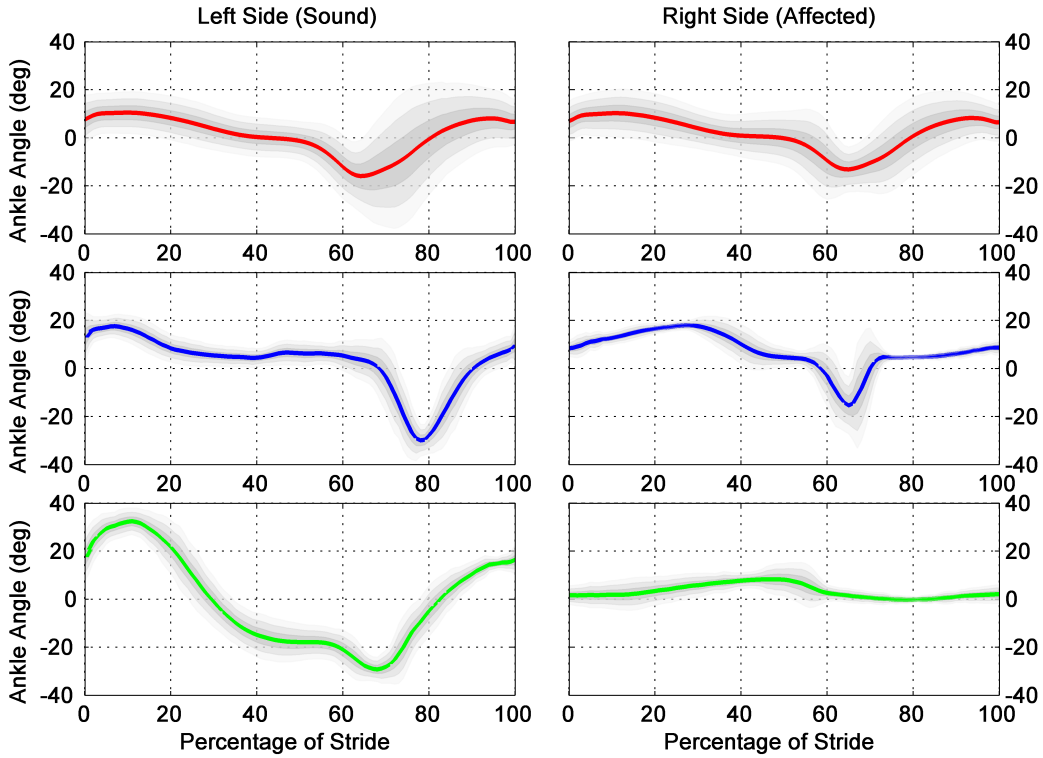

Figure 3.5: Kinematics comparison for the ankle angle in stair ascent. The top two plots show the left and right side averages of ten healthy subjects. The middle two plots show the averages for the amputee subject using the powered prosthesis. The bottom two plots show the averages for the amputee subject using his daily use prosthesis. All plots show +/- 1, 2, and 3 standard deviations in sequentially lighter gray bands.

1.4.2 Stair Descent

Stair descent knee and ankle kinematics are shown in the same form as for stair ascent in Fig. 3.6 and 3.7 (also for 20 strides in all plots, and for 10 subjects in the healthy subject case). The average stride times for stair descent were 1.09 seconds (std. dev. 0.06) for the healthy subjects, 1.36 seconds (std. dev. 0.05) for the powered prosthesis, and 1.10 seconds (std. dev. 0.08) for the passive prosthesis.

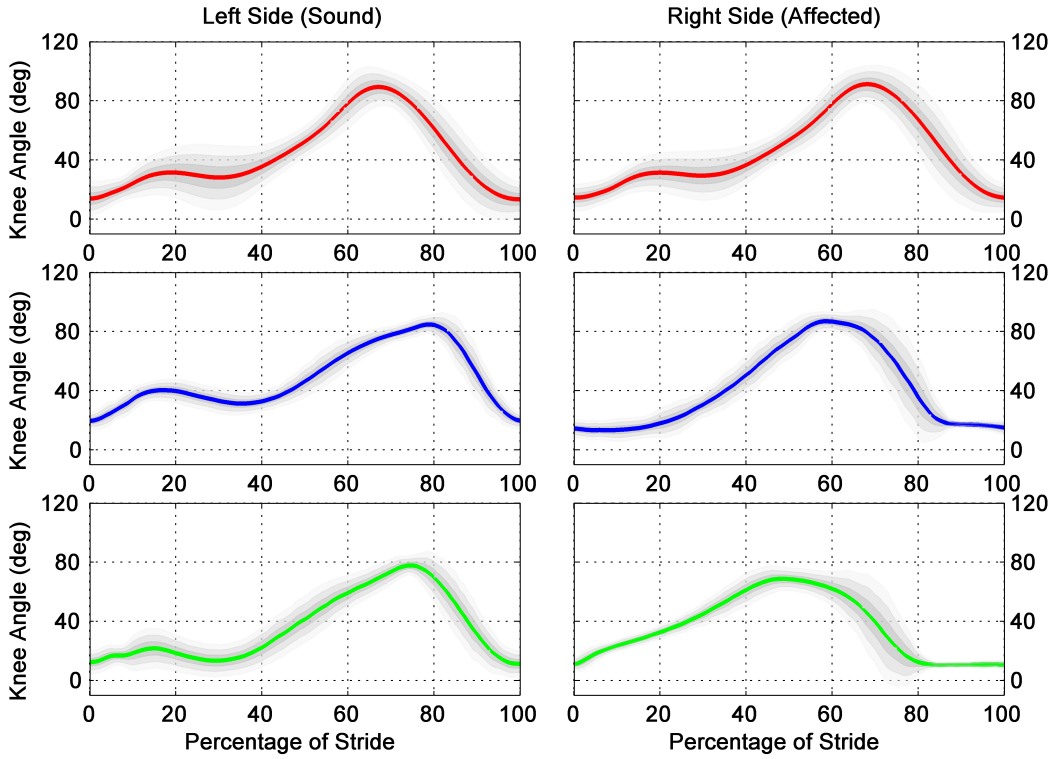

Figure 3.6: Kinematics comparison for the knee angle in stair descent. The top two plots show the left and right side averages of ten healthy subjects. The middle two plots show the averages for the amputee subject using the powered prosthesis. The bottom two plots show the averages for the amputee subject using his daily use prosthesis. All plots show +/- 1, 2, and 3 standard deviations in sequentially lighter gray bands.

Table 7: Max/Min Knee and Ankle Angles for Stair Descent

Measure	Healthy		Passive		Powered	
	μ	σ	μ	σ	μ	σ
Max Knee	90.4/92.5	3.9/3.7	78.6/69.4	1.7/2.8	85.3/87.6	2.0/1.8
Min Knee	11.8/12.9	3.6/2.7	9.7/9.8	2.5/0.6	18.4/12.1	1.4/2.4
Max Ankle	34.2/36.5	3.5/5.0	**31.3/7.4**	4.4/1.1	28.8/28.6	0.9/2.1
Min Ankle	-17.7/-14.2	3.6/4.0	**-23.1/2.2**	2.0/0.5	-27.0/-13.0	1.5/0.5

* Differences between right and left measures greater than 15° are highlighted in bold print.

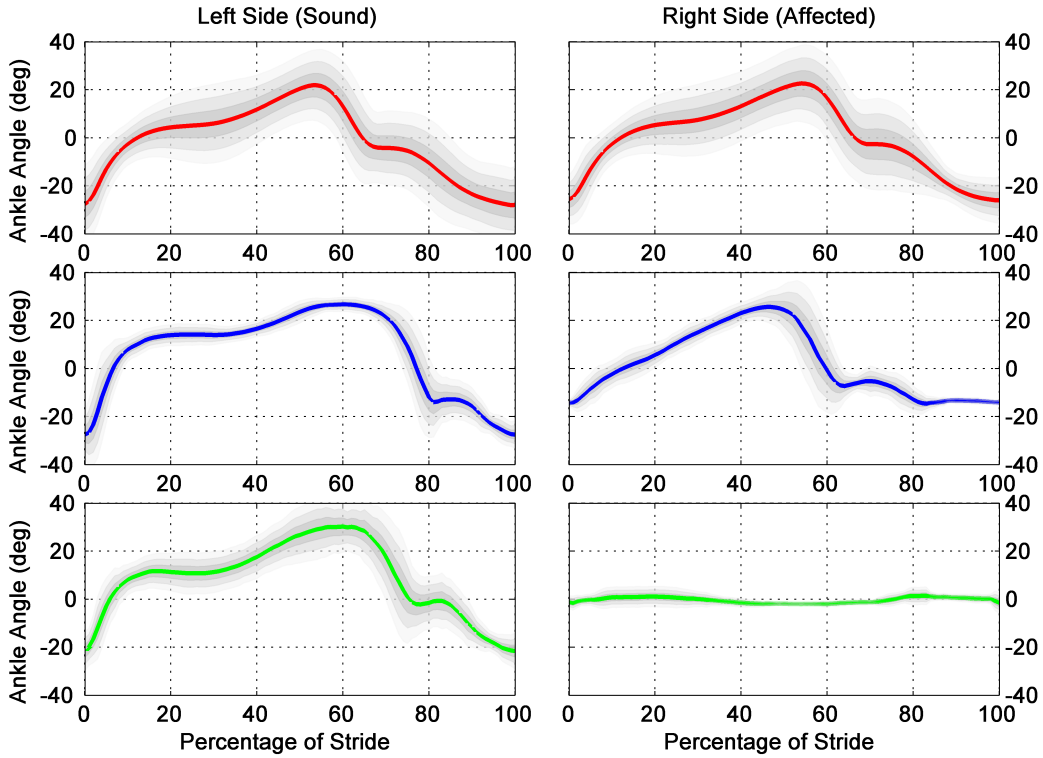

Figure 3.7: Kinematics comparison for the ankle angle in stair descent. The top two plots show the left and right side averages of ten healthy subjects. The middle two plots show the averages for the amputee subject using the powered prosthesis. The bottom two plots show the averages for the amputee subject using his daily use prosthesis. All plots show +/- 1, 2, and 3 standard deviations in sequentially lighter gray bands.

1.5 Discussion

It is important to note the limitations of using averaged kinematic data across subjects as a standard for evaluating gait. Firstly, averaging the mean curves of each subject with respect to either time or normalized time (in terms of percentage of stride) can artificially reduce peaks in the data. For instance, if the instant of peak swing knee flexion varies from subject to subject, this will result in a smearing of the average peak knee flexion, producing what appears to be a wider, softer swing phase. Additionally, one would expect the averaged data to exhibit an increased symmetry between limbs, assuming that kinematic anomalies specific to each subject are equally distributed between the right and left limbs. In light of these issues, it is important to remember that the healthy subject data plotted in Fig. 4, 5, 6, and 7 depict gait cycles that were never performed by a single individual. These effects are relatively minor, however, as can be seen by consulting Tables III and IV, which show the means and standard deviations of the maximum and minimum knee and ankle angles for the left and right sides for all trials.

Despite these limitations, reasonable evaluations of a particular gait cycle can still be made by comparing to these averaged data. It is clear from the stair ascent data in Fig. 4 and 5 that the powered prosthesis provides a significantly better approximation of healthy joint kinematics than the passive knee and ankle counterparts (i.e., comparing the data in the right column of these respective figures). In stair descent, the passive and powered knees perform similarly (right column of Fig. 6), although the powered ankle clearly provides a significantly better approximation of healthy ankle behavior than the passive ankle (right column of Fig. 7).

1.5.1 Stair Ascent

As depicted in Fig. 4, the knee angle of the powered prosthesis in stair ascent contains all the essential features of biomechanically normal stair ascent. There is a net knee extension in stance (i.e. the knee angle begins stance at approximately 70° and ends near 10°, lifting the user up the step) and knee flexion in swing comparable to the healthy data (approximately 90° of knee flexion). However, the stance knee extension for the powered prosthesis appears slightly late relative to the healthy subject data. Additionally, the amputee subject's sound side stance knee extension appears to occur earlier than in the healthy subject data. This asymmetry occurs due to a slight pause in the amputee subject's gait as he checks the position of the prosthetic foot on the step and prepares for the transition to Phase 0, the stance phase where the prosthetic knee extends. The reason for this pause is due in part to the lack of proprioception on the amputee's affected side. Extra care and confirmation is therefore needed on the part of the amputee to confirm that the limb is configured in a safe way for the next step. If the pause were removed from the parsing of the stride, the knee kinematics would match extremely closely to the healthy average. In consideration of the safety and confidence of the subject, however, the authors felt it would be inappropriate to discourage this pause during the training of the subject.

The ankle kinematics (Fig. 5) for the powered prosthesis also exhibited similar trends to that of the healthy subjects, although there was less symmetry in this case between the amputee subject's sound and affected sides. Specifically there was a heightened plantarflexion of the sound side ankle, though its peak of -30° is still within approximately 2 standard deviations of the healthy subject data. This peak suggests some sound-side compensation when using the powered prosthesis, although there is no evidence of vaulting during middle stance (no plantarflexion before 60% of stride).

With regard to the characteristics of the passive prosthesis in stair ascent, a lack of power generation capability largely precludes net knee extension during stance phase, and so the amputee subject adopted a strategy of hip circumduction in order to achieve reciprocal stepping in this case. Specifically, the subject placed the prosthetic foot on the subsequent step, and with the knee mostly straight on the step above him, he made an extended and exaggerated ankle push-off, along with significant assistance from the sound side hand rail (see video included in the supplemental material). Additionally the early portion of the stance phase of the sound ankle showed evidence of vaulting, as the ankle plantarflexes at 30% of stride instead of 60%. Although joint torques were not measured in these experiments, the subject presumably used excessive hip torque to vault over the passive device.

1.5.2 Stair Descent

Since the knee acts primarily as a damper in stair descent, the subject's passive knee prosthesis is able to provide a high degree of functionality for this activity. Indeed, both the passive and powered knees provide fairly good facsimiles of healthy knee joint kinematics during stair descent. In both cases, however, there is a notable lack of early stance knee flexion (i.e., loading response) on the affected side. Although the framework of the powered prosthesis does allow for such stance knee flexion, the authors chose not to enable this feature, since it was effectively present via the compliance in the socket interface.

An essential difference between the powered and the passive prostheses was the speed of stance knee flexion. Although the degree of damping in both the passive and powered prostheses can be adjusted (meaning that either one could be tuned to be faster or slower), the reason that the powered prosthesis exhibits a steeper knee flexion slope in descent is because the total descent in the powered prosthesis is split

into two portions. In the first portion of stance the descent is due to ankle flexion (Phase 0). After the ankle has dorsiflexed sufficiently, the controller transitions to Phase 1 and the knee flexes, continuing the descent. This damped ankle flexion is impossible in the case of the passive carbon fiber ankle-foot complex because it cannot actively plantarflex in anticipation of a descending forefoot strike. The difference is shown clearly in the ankle kinematics, where an initial ankle angle of almost -20° is achieved by the powered prosthesis before forefoot strike. Because the user must position the middle of the passive prosthetic foot over the edge of the step in order to allow knee flexion for descent, it is impossible to supply a moment to the ankle in stair descent, and, as a result, the ankle remains almost entirely motionless during the gait cycle. Thus, although the passive prosthesis enables effective stair descent, it could be argued that the passive prosthesis provides a less stable platform, since the prosthetic foot is not flat on the ground while the knee flexes in descent.

1.6 Conclusion

This paper presents the design and preliminary validation of a control system for stair ascent and stair descent with a powered knee and ankle prosthesis. Experimental results on a single amputee subject indicate that the powered prosthesis with the stair ascent controller provides knee and ankle joint kinematics during stair ascent that are considerably more reflective of healthy knee and ankle joint kinematics, relative to a passive prosthesis. Experimental results of stair descent indicate that both the passive and powered prostheses provide appropriate knee joint kinematics during stair descent, while the powered prosthesis provides ankle joint kinematics considerably more reflective of healthy joint kinematics, relative to a passive ankle joint.

2. Addendum to Manuscript 2: Estimated Power in Stair Ascent and Descent

The powered prosthesis logs the electrical current supplied to the knee and ankle motors, along with the velocities of the knee and ankle joints (although these could be readily computed from the angles). In order to estimate the supplied power during stair ascent and descent, the knee current was scaled with the motor torque constant and the transmission ratio in order to estimate the torque output (neglecting losses due to inefficiency in the transmission). The resulting torque was then further refined by applying an offset due to Coulomb friction according to the sign of the velocity signal. This torque was multiplied by the velocity and normalized in terms of percentage of stride. The mean of this estimated signal is plotted in Fig. 3.8 for stair ascent and Fig. 3.9 for stair descent.

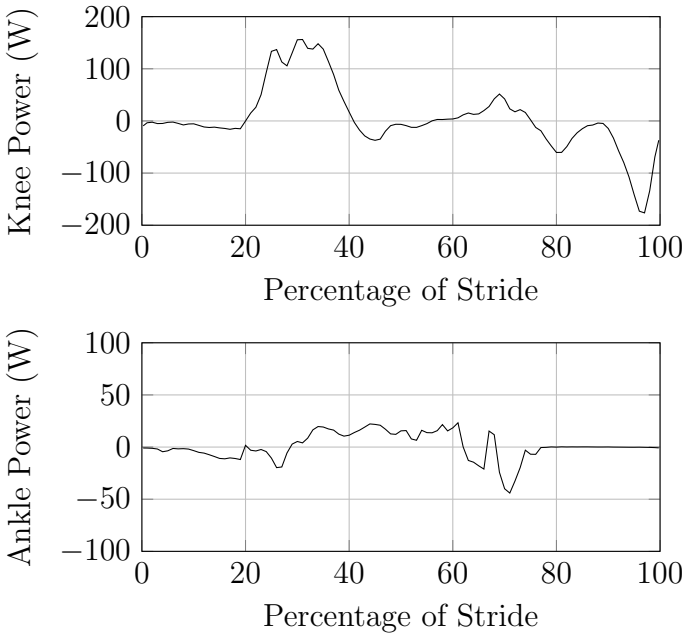

Figure 3.8: Stair ascent joint power.

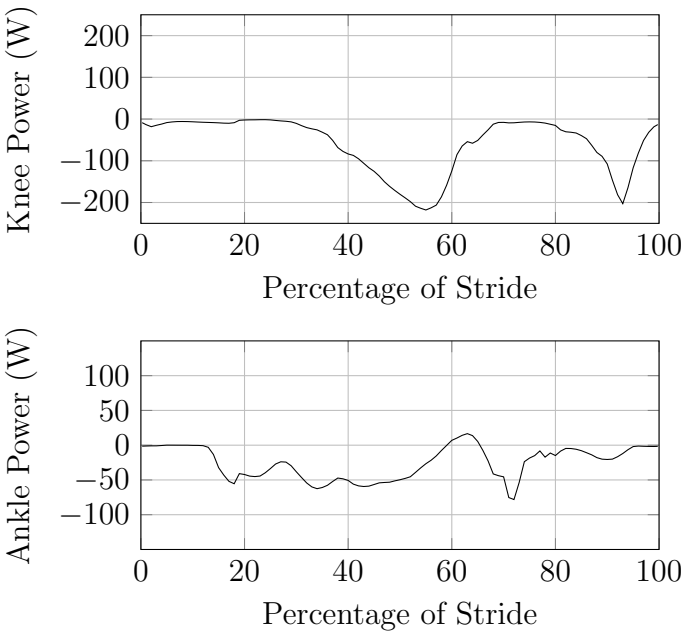

Figure 3.9: Stair descent joint power.

In the estimated power plots provided in Fig. 3.8, the power delivered during the stance knee extension phase (Phase 0), is clearly seen between 20% and 40% of the stride. The peak power for the knee during this phase was approximately 150 W. The amputee subject used in these experiments weighed 85 kg, resulting in a body-mass normalized peak knee power of approximately 1.75 W/kg. Unfortunately the literature does not present a clear consensus on the average peak knee power for healthy subjects. Depending possibly upon factors such as stair inclination, subject selection, gait speed, and even the calculation technique, numbers ranging from 1.1 W/kg to 3.4 W/kg have been reported [6-8, 22]. The authors feel that this level of power delivery is reasonable considering the fact that the subject's relatively short residual limb (55% the length of the sound side) placed a limitation on the comfortable level of achievable knee torque. An additional, unmeasured, source of power delivery during this phase is the sound side hand rail, with which the subject may have been able to offload some of the requirements of the prosthetic limb.

As would be expected, the knee power plot for stair descent is entirely dissipative. It deviates from published literature on healthy subject data primarily in its lack of a preliminary dissipative hump due to the initial stance knee flexion previously described as absent for this tuning [63, 65, 70]. Negative peak powers for both the knee and ankle are lower than reported for healthy subjects, although the ankle power remains substantially negative for a longer period of time. This phenomenon explains why the ankle angle for the powered prosthesis adopts a longer, less steep trajectory than that seen in the healthy subject data. For a given speed of stair descent, any remaining energy not dissipated by the powered prosthesis during the descent phase would either be dissipated by the affected side hip, or by the subsequent forefoot strike of the sound side.

CHAPTER IV

HYBRID CONTROL: A MODIFIED IMPEDANCE FRAMEWORK

One of the primary disadvantages of the finite state-based impedance control framework is that its functionality relies heavily on the careful selection of a relatively large number of parameters. For a transfemoral prosthesis, each finite state consists of six parameters (k, b, and θ_{eq} for the knee and ankle). Most activities contain five or six states. Since walking is subdivided into three different tunings for variable cadence (slow, medium, and fast), and four different tunings for slopes (down 10°, down 5°, up 5°, and up 10°), there are ten different activities for the supervisory controller to choose between. This many states produces over 300 impedance parameters that could be individually varied. If we consider that we might want to tune thresholds for state transitions, this number can easily grow beyond 400 parameters. Furthermore, the methodology behind selecting impedance parameters is grounded in an intuitive understanding of second order systems. This type of knowledge may be common for engineers, but is often quite foreign for prosthetists or medical professionals. Therefore, the problem of tuning the powered prosthesis may be considered intractable for the target demographic when using a pure finite state-based impedance control framework.

Clearly, trends in impedance parameters are likely to appear across subjects. Two of the most probable correlating factors are subject height and weight. With enough data across enough subjects, it is entirely feasible that functional "open loop" tunings

could be derived for a new user based upon an empirical model. It is very unlikely, however, that any empirical model would be accurate enough to eliminate the need for expert tuning, at least in order to obtain optimal performance. As a result, prosthetists would still be required to have a strong understanding of impedance parameter tuning in order to ensure proper fitting and training for new amputees.

Additionally, the degree of flexibility in the parameter tuning process allows for local optimizations of impedance parameters within a particular activity. In other words, two prosthetists could arrive at "optimal" behaviors for the prosthesis in a given activity, but could have done so with two different sets of impedance parameters. It would be important, therefore, in the development of a tuning database, to use explicit and consistent rules to adjust impedance parameters, and also to always start from the same initial conditions. Otherwise a variety of locally optimized impedance tunings could be intermixed, reducing the effectiveness of the empirical model.

Regardless of the difficulties in building a unified model for impedance parameter tuning, doing so requires resources beyond that of a mechanical engineering research laboratory. The number of subjects involved, along with the number of identically constructed and calibrated prosthesis prototypes, necessarily requires this process to be delayed until the pre-production stage of the commercial development of a device. As an alternative approach to the impedance parameter problem, the author has attempted to construct a simplified activity controller framework that significantly reduces the number of adjustable parameters. The philosophy behind this control system leverages the fact that certain states in the state machine are effectively unstable in the sense that the user cannot practically cause the prosthesis to remain in such a state for infinite time.

The example in section I.5.2 demonstrated that a hybrid system composed of linear passive system behaviors is not necessarily stable. In the walking controller, several states exhibit this behavior. The transition out of swing flexion occurs when the knee

velocity inflects (i.e. after peak knee flexion). It is generally not feasible for the user to prevent any extensive motion whatsoever at the knee, and, as a result, it is virtually impossible to cause the knee to remain in the swing flexion state. Furthermore, the swing extension state automatically transitions to pre-landing state when the knee reaches an extended position. This threshold is generally close to or matching the knee equilibrium value in the swing extension state, and so the knee is guaranteed to meet this threshold unless the user intentionally obstructs the extension through contact with the environment. Of course, subsequent state transitions do require more active involvement of the user, and so the overall state machine is not unstable in the sense of being self-exciting or sustaining. If the user stops interacting with the device, it will come to rest passively in a single impedance state. The caveat is that this phenomenon is not achievable in any arbitrary state. In practice, the prosthesis comes to rest in one of two states in the walking controller if the user ceases to interact with the device. If the user keeps the prosthesis unloaded after swing, the prosthesis comes to rest in the pre-landing state, awaiting a load signal that signifies heel strike. If the user ceases to walk while bearing a load on the prosthesis, it comes to rest in the middle stance state, awaiting a significant ankle dorsiflexion from the user to signify the start of push off.

The implication of only having two realizable passive behaviors in the walking controller is that the other "transient" finite states are enforcing local passivity needlessly. Their switching interactions are locally unstable, and so the advantage of being internally passive is lost. The goal, now, is to exploit this fact in order to reduce the number of parameters in the system and simplify the tuning process to generate the desired movements. When a push off condition is met (i.e. the transition in the walking controller from middle stance to late stance is initiated), the prosthesis might as well make a deliberate, transient motion and then automatically switch back to a passive behavior. This motion can be generated in any way the designer chooses, so

long as it ends in a pre-specified finite amount of time and is not likely to re-excite the push off trigger such that it becomes self-sustaining.

The new control system is therefore labeled as a hybrid controller in that it combines both passive finite state behavior and an active trajectory tracking and power delivery behavior. Note that the use of the term hybrid here is distinct from the notion of a hybrid system as a system containing both discrete and continuous dynamic behaviors. (Both the original finite state-based impedance controller and the new hybrid controller are technically hybrid systems.) In the new system the walking controller consists of two states: a passive impedance state for stance and a timed trajectory tracking state for push off and swing. The active state is triggered in the same manner as the transition from middle stance to late stance in the original controller; a threshold is set for ankle dorsiflexion in stance. One this threshold is met, a trajectory is generated for each joint, and the prosthesis executes this trajectory using the impedance control law with the equilibrium position as the trajectory reference. The gains, k and b, are tuning for good tracking performance in swing (i.e. when the external forces on the prosthetic foot are negligible). In general these gains are different from those used in the passive stance state. When the trajectory phase has completed, the prosthesis automatically reverts to the passive stance state until another trigger condition is met in the ankle angle signal.

The trajectory phase of this controller is executed across two significantly different configurations of the prosthesis: stance and swing. In stance, there are significant external forces placed upon the prosthesis by the environment and the user. In swing, the ability of the user to exert forces on the prosthesis is greatly diminished since ground contact is lost. Because the dynamics in these conditions vary so greatly, it is difficult to tune a set of gains for the trajectory controller that achieve good performance for both scenarios. Instead, the gains are tuned for good performance in swing. This method allows for only a moderate impedance during swing, which

helps to safeguard against stumbles by retaining some degree of compliance. With this tuning, however, too much error is allowed during push off, and power delivery during this portion of the gait cycle is diminished. Instead of changing the gains during the transition of stance to swing, which would start to re-introduce the parameterization problem of the original controller, an open loop pulse of transient torque is introduced during push off. The size and duration of this torque pulse is tunable by the user or prosthetist. This approach gives the tuner direct control over the "amount of push" produced by the device, which is a concept readily understood without an engineering background. In the same way, modifications can be made to the reference trajectory to exactly control performance metrics such as the amount of knee flexion. The prosthetist or user no longer needs to understand how knee flexion is achieved; he or she simply needs to observe that knee flexion is too low, and then directly change the reference to accommodate. The resulting system therefore not only significantly reduces the number of parameters requiring tuning, but also provides parameters that more directly correlate with the performance metrics prosthetists use for fitting and training.

The hybrid controller is also easily extended for achieving variable cadence. In healthy biomechanics, not only do the rates of the trajectories of the knee and ankle joints change as a function of cadence, but so do the shapes of the trajectories. Although the hybrid controller could accommodate variable cadence simply by playing the reference trajectories at a speed determined by an internal estimation of cadence, a more biomechanically correct behavior can be generated by dynamically changing the shape of the trajectory as well. In order to do so, control points for the spline generation must be provided to the controller. Three sets of control points (one set each for a slow, normal, and fast cadence) are used for interpolation to generate a specific set of control points for a specific speed. The trajectory generation process is depicted in Fig. 4.1.

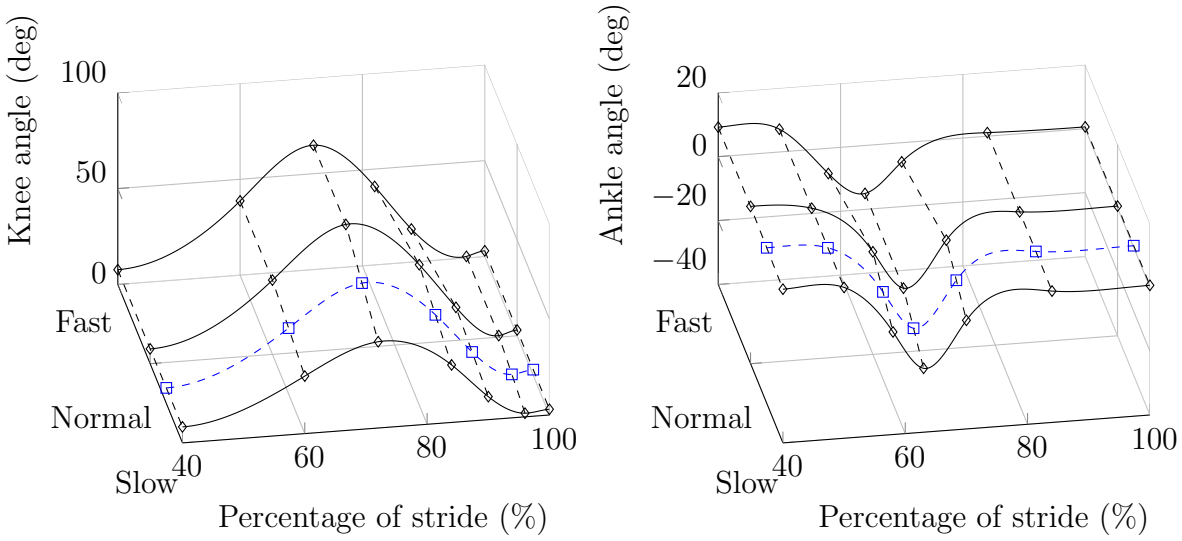

Figure 4.1: Variable cadence trajectory generation. The diamonds are the tunable control points for the three reference splines. The squares are the interpolated control points based upon the selected cadence. The dashed trajectory denotes the reference passed to the trajectory controller for a given stride.

The remainder of this chapter contains a manuscript submitted to the Robotics and Automation Magazine for a Special Issue on Wearable Robotics. This manuscript presents both the design and control of the third generation of the Vanderbilt Powered Prosthesis, and includes level walking data on three subjects using the hybrid control system.

1. Manuscript 3: A Powered Knee and Ankle Prosthesis for Transfemoral Amputees

1.1 Abstract

This article describes the design and control of a powered knee and ankle prosthesis for transfemoral amputees. The prosthesis embodies a number of the same design

traits as a haptic interface, and the design principles underlying it are largely drawn from technical insights offered by the haptic interface community over the past couple of decades. Specifically, each joint of the prosthesis is designed to be capable of emulating a generalized mechanical behavior, and as such, each joint is designed to provide a high bandwidth of output across a wide dynamic range. With such output capability, the prosthesis is able to emulate the variegated behaviors of the human neuromuscular system and is able to reproduce the neuromuscular and biomechanical behaviors of the healthy limb. In this article, the authors describe the design of a new prosthesis prototype, describe the structure of a controller utilized to coordinate actions of the prosthesis with the biomechanical movement of the user, and present biomechanical data to demonstrate and validate the design and control approach.

1.2 Introduction

Lower limb prostheses have traditionally been energetically passive devices (i.e., they can store or dissipate power, but cannot produce net power). Amputees who utilize passive limbs generally walk more slowly, expend significantly more energy during ambulation, are more limited in the types of terrain they can traverse and types of activities they can perform, and fall frequently relative to healthy counterparts [47, 68, 71–77]. The intent of a prosthesis is to replace the biomechanical functionality of the healthy limb. The joints of the healthy limb provide a variety of biomechanical behaviors which vary considerably within and between activities, and which are in general characterized by power dissipation, storage, and generation. As such, it is reasonable to assume that endowing a prosthesis with power, and by extension with the ability to emulate the range of biomechanical behaviors exhibited by the healthy limb, would enable a more capable prosthetic intervention. Such an intervention could potentially restore healthy biomechanical function to a greater extent than

conventional prostheses, particularly across a variety of activities.

Although investigations of powered prostheses were conducted several decades ago (see, for example, [78, 79]), recent research activity in the field has increased substantially, presumably facilitated in part by recent improvements in the power density of brushless DC motors, the energy and power density of lithium-polymer and lithium-ion batteries, and the availability of compact and efficient microcontrollers and integrated-circuit-based inertial measurement units (IMUs). Research efforts toward the development of powered prostheses are enumerated in the recent review articles [80, 81]. Early results incorporating these powered prostheses in small-scale trials indicate more accurate reproduction of healthy limb kinematics and kinetics, the potential for reduced pathologies in intact joints, and the potential for reduced metabolic costs during locomotion [3–5, 12, 28, 32, 34, 82].

1.3 Vanderbilt Powered Prosthesis Design Philosophy

Various powered prostheses have been developed with differing design and control approaches and philosophies. The prosthesis described here was designed essentially as a haptic interface, such that each joint is capable of emulating the variety of biomechanical behaviors exhibited by the joints of the healthy limb. As prescribed in the haptic interface design literature, the development of a high-fidelity haptic device requires that each joint of the device be designed to provide a high bandwidth of output across a wide dynamic range. Doing so requires that the device enable power flow in both directions (i.e., the actuated joints be fully back-drivable), and is further facilitated by incorporating several design practices, such as minimizing open-loop phase lag, sensor quantization, and sampling delay (see, for example, [83]), and avoiding non-collocated closed loops, particularly those characterized by compliance and hard nonlinearities such as friction and backlash (see, for example, [84]).

Assuming the prosthesis is designed as such, and is capable of reproducing the variegated behaviors of the healthy limb, a second design issue arises, which is how to select these joint behaviors such that the limb moves in biomechanical coordination with the user. The authors argue that the need for a system and structure that integrates the movement of the prosthesis with the movement of the user is an issue that is unique to robotic limbs. The only motive power source for a conventional, energetically passive prosthesis is the user. As such, a passive prosthesis is inanimate; it cannot move without the user swinging his or her residual limb to propel the prosthetic leg forward. Because the user must "sling" the passive leg around, such prostheses fundamentally move in concert with the user—albeit in a biomechanically deficient manner. Unlike an energetically passive prosthesis, a powered prosthesis contains its own motive power source, and can both act and react. The control interface between the prosthesis and user therefore becomes substantially more important with a powered leg. Such legs have the capability to emulate healthy biomechanical function, but this capability also enables them to move independently of the user, or to move in discord with the user's movement or intent.

This article describes the design of a powered knee and ankle prosthesis for transfemoral amputees. As per the preceding discussion, the prosthesis is designed essentially as a haptic interface, such that each joint is capable of emulating a generalizable mechanical behavior, and is capable of moving between various types of mechanical behavior, as governed by a coordination controller. Additionally, the article describes a control approach that leverages the notion of localized passivity, as discussed by [85], to provide safe and coordinated interaction between the user and prosthesis. Following a description of the prosthesis, biomechanical data are presented from walking trials with three amputee subjects to demonstrate and validate the design and control approach.

1.4 Prosthesis Design

1.4.1 Actuation and Structure

A rendering of the powered prosthesis, with some sections cut away to show design components, is shown in Fig. 4.2. As shown in the figure, the prosthesis consists of a powered knee unit and a powered ankle unit, separated by a standard prosthetic pylon, allowing alignment adjustments between the knee and ankle axes, as well as adjustability of the shank length. As shown in the figure, the knee unit includes a battery and embedded system that powers and controls both joints. The knee unit additionally incorporates a load cell, which essentially measures the ground reaction force along the shank. The knee and ankle units are electrically connected by a flexible wire tether to accommodate height adjustability.

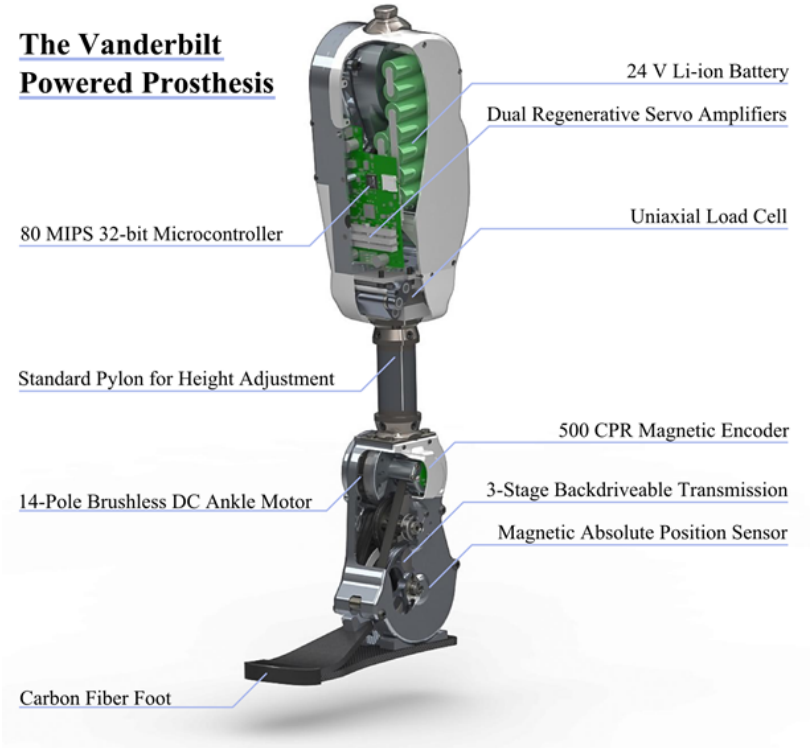

Figure 4.2: A rendering of the CAD model of the powered prosthesis.

Both the knee and ankle units are actuated by the combination of a brushless DC motor and a three-stage belt/chain speed reduction transmission. Specifically, the knee incorporates a Maxon EC30 brushless motor, which drives the knee joint through a 176:1 speed reduction, the combination of which is capable of generating a maximum active torque of approximately 85 Nm through its actuated range of motion of 120 deg (5 deg hyperextension and 115 of flexion). The ankle joint incorporates a Maxon EC60 brushless motor, which drives the ankle joint through a 115:1 speed reduction, the combination of which is capable of generating a maximum active torque of approximately 110 Nm through its actuated range of motion of 70 deg (25 deg dorsiflexion and 45 deg plantarflexion). The actuator output at the ankle joint is supplemented by a carbon-fiber leaf spring incorporated into the foot, which is characterized by a stiffness of approximately 6 Nm/deg, and engages at approximately zero degrees in the ankle range of motion. The spring biases the output capabilities of the ankle towards plantarflexion, which is consistent with the biomechanical characteristics of the ankle during locomotion [14]. At typical ankle angles during late stance, the spring provides around 60 Nm of supplemental torque.

Table 8: Mechanical and Electrical Characteristics of the Powered Prosthesis

Characteristic	Value
Maximum Knee Torque	85 Nm
Maximum Ankle Torque	110 Nm (from motor)
Knee Range of Motion	-5° to 115°
Ankle Range of Motion	-45° to 25°
Battery Capacity	125 W·hr
Maximum Battery Current	30 A
Maximum Motor Current	18 A
Nominal Mass	4.75 kg

The structural components of the knee and ankle units are machined from 7075 aluminum alloy. The knee and ankle structures are designed to accommodate users of up to 115 kg body weight in addition to the internal loads imposed by the actuators, with a minimum safety factor of 2 against structural failure.

Given the respective sizes of the knee and ankle units, the minimum build height of the prosthesis corresponds to a measurement between the knee center and ground of 425 mm, which corresponds to a 10th percentile female dimension, as given by [86] (i.e., the prosthesis should fit all adult males, and 90% of the adult female population). The prosthesis is shown within the envelope of a 50th percentile male leg in Fig. 4.3. For a 50th percentile male, the mass of the current prosthesis prototype is approximately 5 kg.

Figure 4.3: The powered prosthesis inside an anthropomorphic envelope.

1.4.2 Sensing

In addition to a 6-axis IMU in the shank, the prosthesis includes sensing for the knee and ankle angles and angular velocities, and for the axial load in the shank. All sensing is based on contactless sensors to enhance reliability and lifetime. The angular positions of the knee and ankle joints are measured by absolute magnetic encoders located coaxially with the joints, and also by incremental magnetic encoders located coaxially with the motor shafts. These angle measurements are fused with complementary filters to avoid the influence of high-frequency transmission dynamics in the feedback controller. The angular velocities of the knee and ankle joints are calculated from the incremental magnetic encoders on the motor shafts. The axial load in the prosthetic shank is measured through the linear displacement of a double parallelogram four-bar linkage, which is situated just distal to the knee unit (see Fig. 4.2). The linkage is constrained to move axially with respect to the shank, and the load is related to axial displacement via a helical compression spring with a stiffness of approximately 360 N/mm. A linear magnetic encoder measures the displacement across the spring and produces a measure of the shank axial load.

1.4.3 Embedded Electronics

The essential components of the prosthesis electrical system are depicted in the schematic shown in Fig. 4.4. A photograph of the embedded system is shown in Fig. 4.5. The prosthesis power supply is a nominal 24 V lithium-ion battery pack, rated at approximately 125 W•hr. The main processing element is a 32-bit microcontroller from Microchip Technologies, which runs the primary control loop at 500 Hz. In this loop the main controller executes the joint torque controllers (described subsequently), in addition to performing secondary functions such as logging data, communicating with the servo controller, and servicing other peripherals (such as

communication with the IMU over SPI). A secondary processing element (a 16-bit digital signal processor from Microchip Technologies) receives motor current commands from the main controller at 500 Hz, and uses these references to control current in the brushless DC motors via a pair of custom regenerative servoamplifiers, each of which samples motor current at 150 kHz, runs closed-loop current control at a sample rate of 4.6 kHz (based on a filtered version of the sampled motor current), and switches the MOSFET bridges at a PWM rate of 45 kHz. The current control loop for each motor consists of the combination of a feed-forward motor model supplemented with a PI feedback loop.

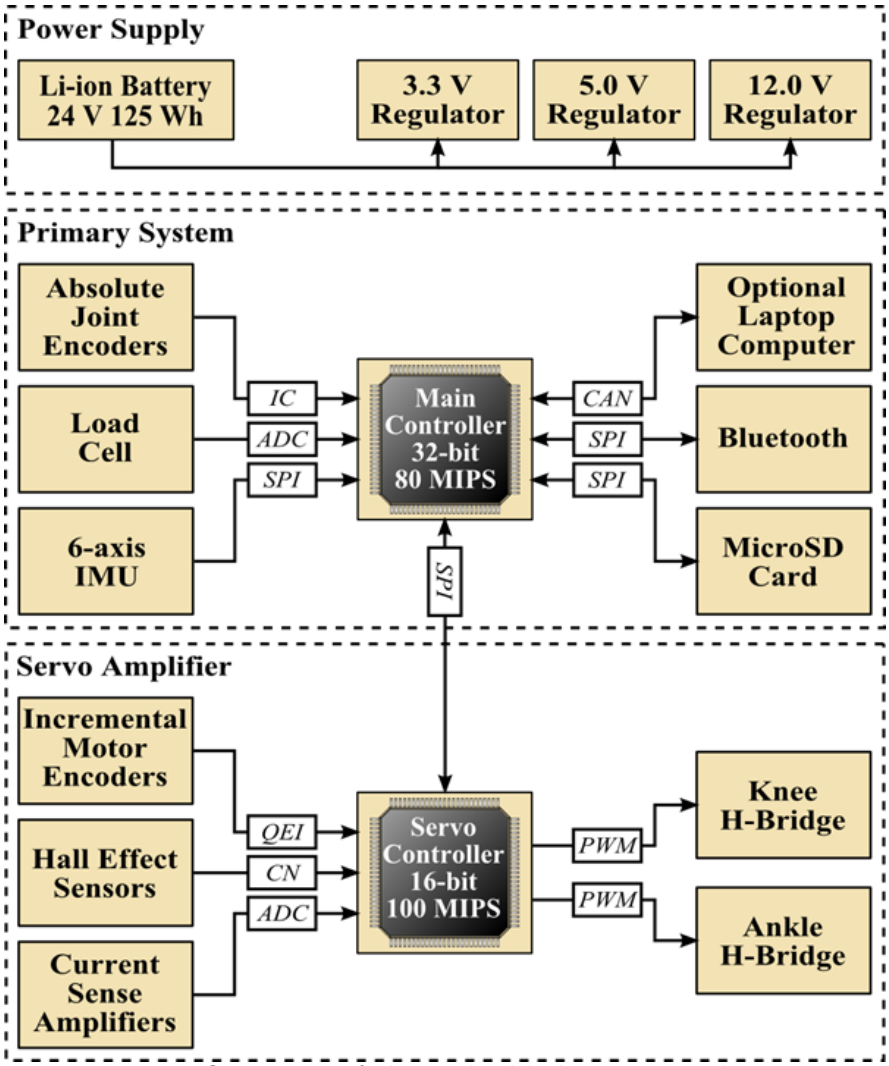

Figure 4.4: Overview of the embedded system architecture.

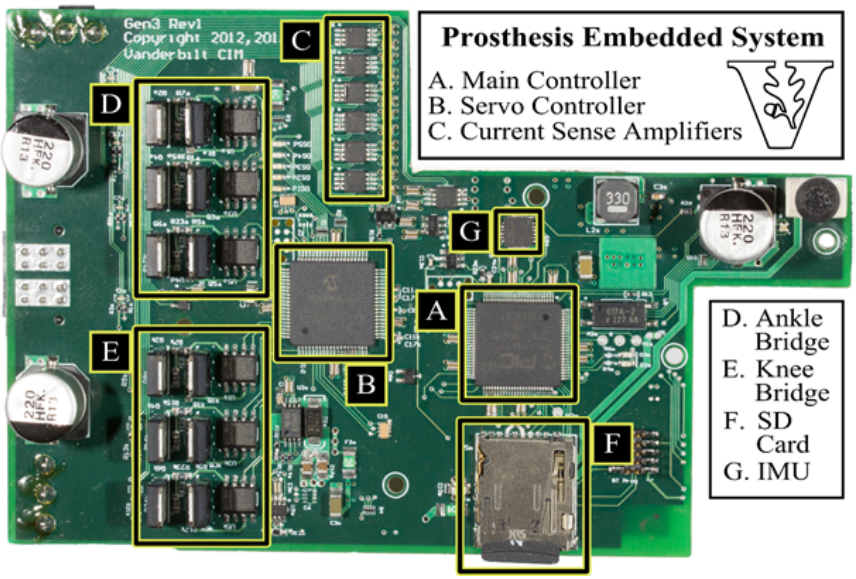

Figure 4.5: Photograph of the embedded system.

1.5 Control Approach

The prosthesis control system consists of a hierarchical state machine, the top layer of which is called the supervisory controller. The states of the supervisory controller are called "activities." An activity is itself a finite state machine, the states of which are called "phases." An example of an activity in the supervisory controller would be standing, and an example of a phase in the standing activity controller would be weight bearing.

The supervisory controller governs transitions from one activity to another, while each activity controller dictates transitions from one internal phase to another. There are four activities contained in the supervisory controller. These activities are shown in the state machine depicted in Fig. 5. Within any given phase of any given activity, impedance parameters and equilibria are specified for the knee and ankle joints. The impedance control law for each joint is given by

$$\tau = k(\theta - \theta_{eq}) + b\dot{\theta} \tag{4.1}$$

where τ is the commanded torque, k is the proportional gain or stiffness, θ is the joint angle, θ_{eq} is the desired joint angle equilibrium position, and $\dot{\theta}$ is the joint angular velocity. These parameters are enforced through lower level controllers, which form a cascaded control structure mapping the joint states (angular position and angular velocity) to motor currents.

The impedance control law (4.1), which is discussed in more detail in [5, 29], emulates a spring and damper within each state. The control structure provides two substantial features. First, joint impedances can be selected that are representative of impedances exhibited by the healthy joint, which facilitates interaction with the ground and provides to the user a more natural feel relative to a (high impedance) position controlled joint. Second, the behavior of the prosthesis within any given phase will be passive, yet energy can be introduced into the system by changing the stiffness or equilibrium position of the virtual spring during transitions between phases. Since phase transitions are based on mechanical cues from the user, the user retains control over the introduction of power into an otherwise passive system.

Despite the features provided by this piecewise-passive impedance-based control approach, the approach is somewhat parameter-intensive, since each phase for each joint requires selection of three impedance parameters. As such, for a piecewise-passive impedance-based control approach for level walking with five phases, the two joints would require selection of thirty impedance parameters. In order to reduce the number of control parameters, a hybrid control approach was implemented for the walking controller. Specifically, since the effect of joint impedance is most evident when the prosthesis is in the stance phase of gait (i.e., when the user is interacting with the ground, a high-impedance environment), and less evident when the prosthesis is

in swing, the authors implemented a control approach that incorporates a piecewise-passive impedance control approach during the stance phase of gait, but incorporates a trajectory-tracking high-impedance controller during the swing phase of gait. The hybrid walking controller consists of three phases, as depicted in Fig. 6. The first two phases, early stance and middle stance, are basic impedance states that roughly correspond to the first 40% of the gait cycle. The early stance portion begins at heel strike and ends at peak stance knee flexion, entering middle stance. Middle stance continues until an ankle angle threshold is reached, at which point the prosthesis initiates a step with a powered push-off.

Once the third phase is reached, the prosthesis will perform a powered push-off and enter swing. Instead of executing a series of piecewise passive phases, each of which would entail impedance parameter selection, the hybrid controller executes a trajectory at a relatively high impedance, where the trajectory for each joint follows a spline defined by a set of reference points interpolated from healthy walking data at different walking speeds. To achieve a variable cadence, the interpolation is based upon the length of time spent in the preceding stance phase, as determined by a timer that increments while the load signal is above a given threshold. Once the trajectory has finished, the prosthesis automatically reverts to the first phase, early stance, in anticipation of heel strike. In order to provide the energetic role of push-off in late stance, a feed-forward torque command is superimposed at the onset of the trajectory phase. The torque command is a single period of a unity-offset cosine wave, which is scalable in both width (time) and height (magnitude). This torque pulse provides an intuitive parameter for the tuning of the "amount of push" delivered to (and perceived by) the user. Note that the strength of the powered push-off largely determines the net amount of energy delivered to the user over the stride.

1.6 Experimental Implementation and Biomechanical Results

The efficacy of the powered prosthesis design and control approach was assessed in experiments with three transfemoral amputee subjects. The ability of the powered prosthesis and controller to provide level walking functionality was assessed by characterizing the knee and ankle joint biomechanics (e.g., joint angles, torques, and powers) during over ground walking, and comparing these to the biomechanical behavior of the knee and ankle joints in the healthy limb.

1.6.1 Biomechanical Assessment

Three subjects were recruited through local prosthetists for the assessment. The subjects' anthropomorphic data, along with data concerning the configuration of the prosthesis, are given in Table 9. Approval to perform these assessments was granted by the Vanderbilt Institutional Review Board and informed consent was obtained for each subject prior to each assessment. Subjects additionally gave verbal permission for the publication of photographs and video. Figure 4.6 shows a photograph of one of the subjects walking with the powered prosthesis.

Figure 4.6: A subject walking with the powered prosthesis.

The prosthesis was fit to each subject, and the controller parameters were manually tuned. The primary controller parameters requiring tuning are the impedance parameters, the push-off trigger angle, and the push-off strength (see Table 10). The impedance parameters were tuned, starting with a set of nominal parameters obtained from healthy subject data (see discussion in [29]), to achieve subject comfort and sense of synergy with the prosthesis, and to achieve a biomechanical movement in the stance phase representative of healthy gait (e.g., appropriate stance knee flexion). The push-off trigger angle and strength were adjusted to provide a powered push-off that was comfortable to the user. A summary of the control parameters used for each subject is given in Table 10. It is notable that not all the impedance parameters

needed to be adjusted between subjects to obtain a comfortable gait. Also, note that the push-off trigger angle appears to be a function of user height and step length, where the taller subject preferred more dorsiflexion before push-off (10 deg), while the two subjects similar in height preferred less dorsiflexion (8 deg, 7 deg respectively).

Table 9: Subject Data and Prosthesis Configuration

	Subject A	Subject B	Subject C
Height	1.93 m	1.83 m	1.83 m
Weight	79 kg	95 kg	86 kg
Age	25 yrs	24 yrs	46 yrs
Cause of Amputation	trauma	trauma	cancer
Years Post-Independent Ambulation	7 yrs	3 yrs	2 yrs
Amputation Side	right	left	left
Prosthesis Configured Weight	5.09 kg	5.04 kg	5.05 kg
Prosthesis Configured Height	54.0 cm	51.9 cm	50.5 cm
Prosthetic Foot Size	28 cm	28 cm	28 cm

1.6.2 Biomechanical Data

Once tuned, each subject walked over ground on the prosthesis at a self-selected speed. Figures 4.8 through 4.9 show the averaged biomechanical data from the knee and ankle joints for each of the three subjects, specifically averaged over twelve consecutive strides. Note that the data shown in these figures were computed in post-processing using sensor data from the prosthesis. Specifically, the joint angles and angular velocities were measured with the absolute and incremental encoders at each joint. The joint powers were calculated as the product of the joint torques and angular velocities, where the joint torques were calculated from the combination of motor current and joint angle data. Specifically, the joint torques experienced by the user were computed using a model of the passive characteristics of the motor, transmission

(i.e., inertia, friction), and, in the case of the ankle joint, the parallel spring. Finally, note that stride data were parsed based on load cell data, and in accordance with standard presentation, plotted as a function of stride percentage. In all cases, the data are plotted along with data characterizing plus and minus one standard deviation around the corresponding mean behavior of the knee and ankle joints during healthy level walking at a self-selected speed, as provided by [62].

Table 10: Subject Data and Prosthesis Configuration

	Subject A	Subject B	Subject C
Height	1.93 m	1.83 m	1.83 m
Weight	79 kg	95 kg	86 kg
Age	25 yrs	24 yrs	46 yrs
Cause of Amputation	trauma	trauma	cancer
Years Post-Independent Ambulation	7 yrs	3 yrs	2 yrs
Amputation Side	right	left	left
Prosthesis Configured Weight	5.09 kg	5.04 kg	5.05 kg
Prosthesis Configured Height	54.0 cm	51.9 cm	50.5 cm
Prosthetic Foot Size	28 cm	28 cm	28 cm

Figure 4.7 shows averaged knee and ankle joint angles for each subject exhibited by the prosthesis during walking. For all subjects, the prosthesis provides knee and ankle joint kinematics with the essential characteristics of healthy joint behavior. Specifically, as in healthy walking, the knee joint exhibits stance knee flexion between 0 and 30% of stride, although peak flexion values for the amputee subjects are somewhat less than the healthy average. In the authors' experience, amputee subjects tend to prefer slightly less stance knee flexion, perhaps due to the compliance of the socket interface and/or the lack of proprioception in the limb.

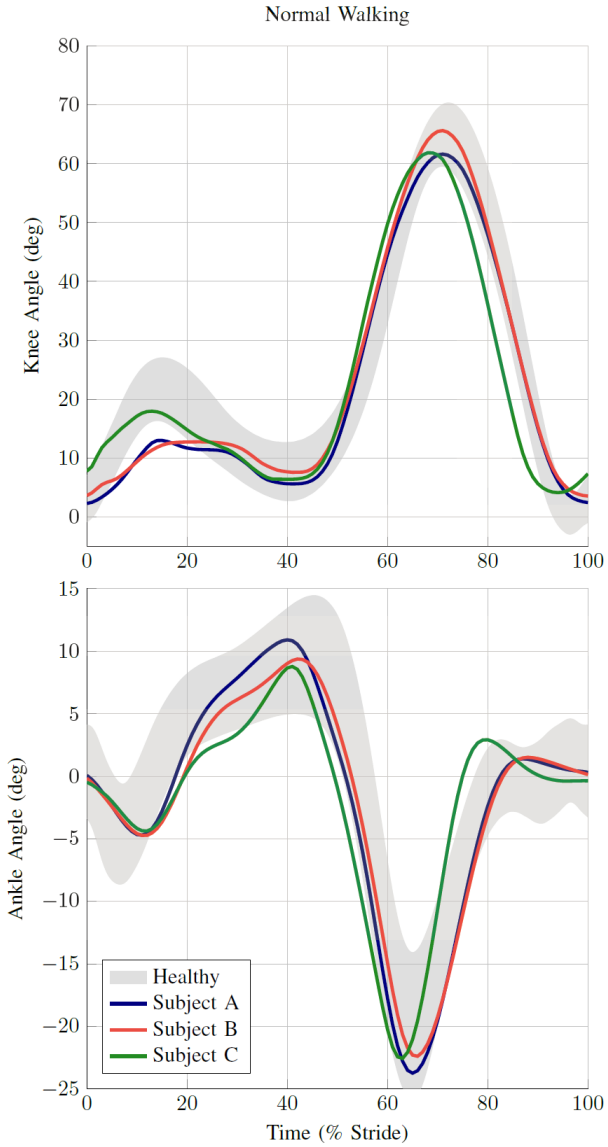

Figure 4.7: Knee and ankle kinematics for 3 amputee subjects using the powered prosthesis. For the knee joint, 0 deg corresponds to full knee extension, and flexion is positive. For the ankle joint, positive angles represent dorsiflexion and negative angles represent plantarflexion.

All subjects' ankle behaviors also closely match those of healthy subjects. Most notable is the significant plantarflexion of the ankle joint around 60% of stride. During this period the ankle joint is delivering net positive power, which is a characteristic unique to an active device. Furthermore, the prosthesis actively returns from plantarflexion after toe-off in order to provide ground clearance at the toe during the

swing phase of walking.

Figure 4.8 shows the body-mass-normalized knee and ankle joint torques provided by the prosthesis as a function of stride for each subject, also compared to the band of typical healthy subject knee and ankle body-mass-normalized torques. Like the joint kinematics, the joint torques for all subjects are strongly representative of healthy subject data. Regarding the knee torques, the amplitudes for the stance phase reflect the somewhat diminished stance knee flexion relative to healthy subjects. As in the healthy subject data, during the beginning of powered push-off (approximately 45% of stride), the powered prosthesis provides for each subject a flexive torque to counteract the hyperextensive torque supplied by the ground reaction force.

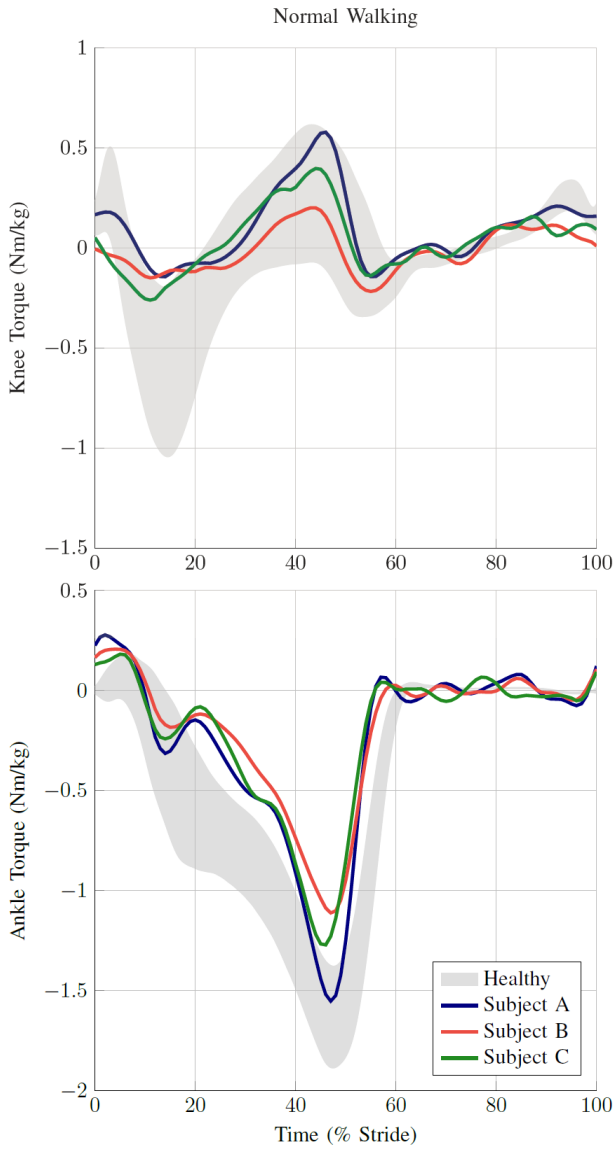

Figure 4.8: Knee and ankle kinetics for 3 amputee subjects using the powered prosthesis. For the knee joint, a positive torque is a flexive torque. For the ankle joint, positive torque is a dorsiflexive torque.

At the ankle, the prosthesis provides an initial dorsiflexive torque immediately following heel strike, followed by a period of increasing plantarflexive torque during the stance phase of walking. As in the healthy subject data, the ankle torque increases throughout stance, and peaks during the powered push-off period between 40 and 60% of stride. Once the toe is off the ground, the external forces on the ankle are small, due to the foot's low moment of inertia, and so little external torque is present during

this period.

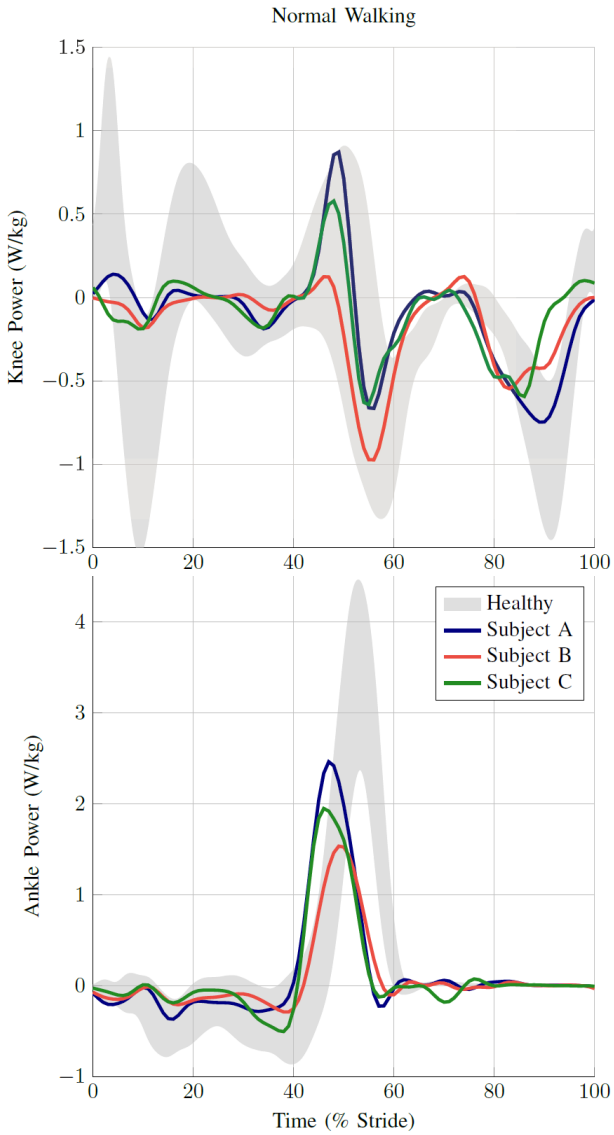

Figure 4.9: Knee and ankle powers for 3 amputee subjects using the powered prosthesis. For both joints positive power represents power delivered by the joint, and negative power represents power absorbed by the joint.

Body-mass-normalized knee and ankle joint powers for each subject are plotted in Figure 10. As seen in the joint power data, power characterizing the knee and ankle joints falls largely within the healthy subject norms. Regarding the knee joint, power associated with stance knee flexion during early to middle stance is diminished, corresponding to the previously mentioned lessened stance knee flexion. However,

knee joint power during late stance and swing is quite representative of healthy knee joint power data.

As in the knee joint, the power associated with the ankle joint is quite representative of healthy norms. Specifically, for each subject, the ankle primarily absorbs power during the early and middle phases of stance, and subsequently generates a pulse of power between approximately 40 and 60% of the stride cycle, in accordance with the powered push-off phase of walking. Note that the peak power associated with this push-off is on the low side of the healthy mean. This phenomenon is related to torque and power limitations of the hardware. Nonetheless, these data are still in character with the biomechanical behavior of the healthy joint.

1.7 Conclusion

The authors describe in this article the design and control of a powered knee and ankle prosthesis for transfemoral amputees. The prosthesis was designed essentially as a haptic interface, such that each joint is capable of emulating a generalizable mechanical behavior, and also of moving between various types of mechanical behaviors, as governed by the prosthesis controller. A prosthesis controller is described herein that combines passive impedance-type behaviors at the respective joints during most of the stance phase of gait, and relatively high-impedance trajectory control during the swing phase of gait, the combination of which provides coordinated interaction with the user and minimal controller parameterization. The powered prosthesis was demonstrated on three transfemoral amputee subjects, and shown in all cases to provide knee and ankle joint biomechanical behaviors that are highly representative of healthy joint biomechanics during walking. Finally, although level walking was described and demonstrated, the authors note that one of the most unique and compelling attributes of a powered prosthesis, such as the one presented here, is its ability

to adapt its behavior to a variety of activities and terrain types, and thus provide to the user appropriate biomechanical behaviors across a wide variety of activity. Accordingly, fulfilling the potential of powered prostheses will require the continuing development of coordination controllers for multiple types of activities, in addition to algorithmic structures that recognize when a user intends to transition from one activity to another.

CHAPTER V

BILATERAL CONTROL

Since unilateral amputees often perform compensation strategies with their sound side in order to compensate for deficiencies in their prosthesis, the question arises of how a bilateral amputee would be affected by the use of powered prostheses. In order to investigate this problem, this chapter begins with preliminary work using able body adapters on a healthy subject to develop a control system for bilateral amputees. The latter half of this chapter consists of a manuscript that has been accepted with minor revisions to the IEEE Transactions on Biomedical Engineering. In this work, a coordinated bilateral control system is implemented and tested on an amputee subject.

1. Healthy Subject Experiments

In order to assess the feasibility of using powered prostheses as an intervention for bilateral, transfemoral amputees, a pair of unilateral powered prostheses was tested on the author using able body adapters. The results and observations from this experiment were used to influence the development of the bilateral control system subsequently described. This system was then implemented on the powered prostheses and they were connected with the CAN data tether. The author also tested this new system to confirm that coordination between the prostheses enhanced safety

and reliability in the system. During the testing of the coordinated controller, the author also donned a pair of passive prostheses as a baseline, since gait using able body adapters does not exactly recreate amputee gait.

1.1 Able Body Adapters

The purpose of an able body adapter is to mimic an amputation in a healthy person, allowing the person to don a prosthesis. Applications for such a device are limited, and so typically these devices are custom fabricated for research purposes. When constructing an able body adapter to facilitate use of a transfemoral prosthesis, the subject's shank is usually held in a flexed position (somewhere close to 90°) by a brace. Since the knee joint of the healthy subject cannot be removed, the prosthetic knee must be offset. For sagittal plane studies and unilateral applications, this offset is usually made in the coronal plane, such that the axis of the prosthetic knee is collinear with the (approximate) axis of the healthy knee. The two main advantages of such a configuration are that (1) the knee axes are symmetric on both sides of the body (in a unilateral application), and (2) the natural height of the subject can be preserved. For a bilateral application, the advantage of knee axis symmetry is irrelevant since both knee joints must be moved. Furthermore, offsetting the prosthetic knees in the coronal plane puts significant moments on the prostheses and the able body adapters, resulting in a system that is uncomfortable for the user and can potentially impact his or her gait.

The other popular position for knee axis relocation (and the method used in this work) is directly underneath the able body adapter (offset in the sagittal plane). This position creates artificially long thighs, but allows the subject to bear weight in a much more comfortable and stable way. Furthermore, the attachment point of the prosthesis can be repositioned forward and aft to balance the center of gravity

of the folded healthy limb. A minor concern is that the hip angle of the subject is necessarily offset in the anterior direction, though enough range of motion typically remains for activities such as level ground walking.

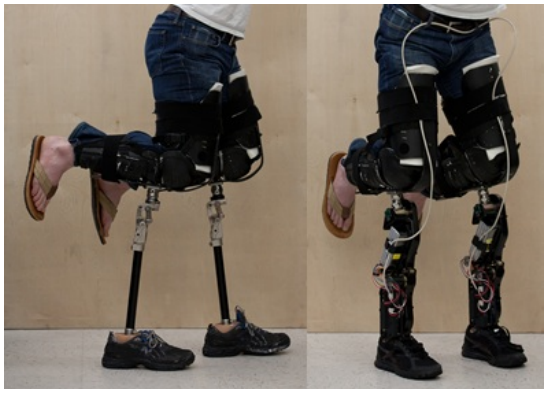

Figure 5.1: The author wearing able body adapters with the passive and powered prostheses.

The able body adapters used in this work can be seen in Fig. 5.1. They are constructed from PVC, aluminum bar stock, and commercially available athletic padding. Standard prosthetic pyramid adapters can be mounted along the shank portion of the adapters in increments of 0.5 inches. The adapters are attached to the subject with hook-and-loop straps in four places on the thigh and shank.

1.2 Bilateral Experimental Setup

Kinematic data were collected on the author using all three prosthetic configurations (passive, unilateral powered, coordinated powered) through the use of a 12 camera motion tracking system from NaturalPoint. Marker data was collected at 120 Hz and converted to a skeletal model within NaturalPoint's ARENA software environment and then exported as a BVH file resampled to 100 Hz. Sagittal plane joint angles were then extracted from the BVH files using MATLAB.

The use of a treadmill was necessary in order to obtain a sufficient number of

strides at steady state within the confines of the capture volume for this motion capture system. For stability purposes, parallel bars were installed along the sides of the treadmill and the author used them for support in all trials.

1.3 Powered Prostheses with Unilateral Control Systems

In the first set of trials the powered prostheses were each programmed with the unilateral control system. Because the unilateral controller is intrinsically designed, there is no inherent preclusion from using two unilateral prostheses for a bilateral application. At the beginning of the trials, a parameter set that was tuned for a unilateral transfemoral amputee of similar height and weight to the author was used. After practicing for several trials, the only parameter change necessary was to reduce the ankle angle threshold to achieve the transition from middle stance to push off. Note that this threshold marks the largest introduction of power in the gait cycle and is typically the threshold to which users are the most sensitive.

Fig. 5.2 shows the knee and ankle kinematics of the best 20 consecutive strides achieved by the author in a trial of 38 total strides with the unilateral controller operating on both powered prostheses. The green line represents the right limb mean and the blue line represents the left limb mean. The dotted lines represent ± 1 standard deviation from the means.

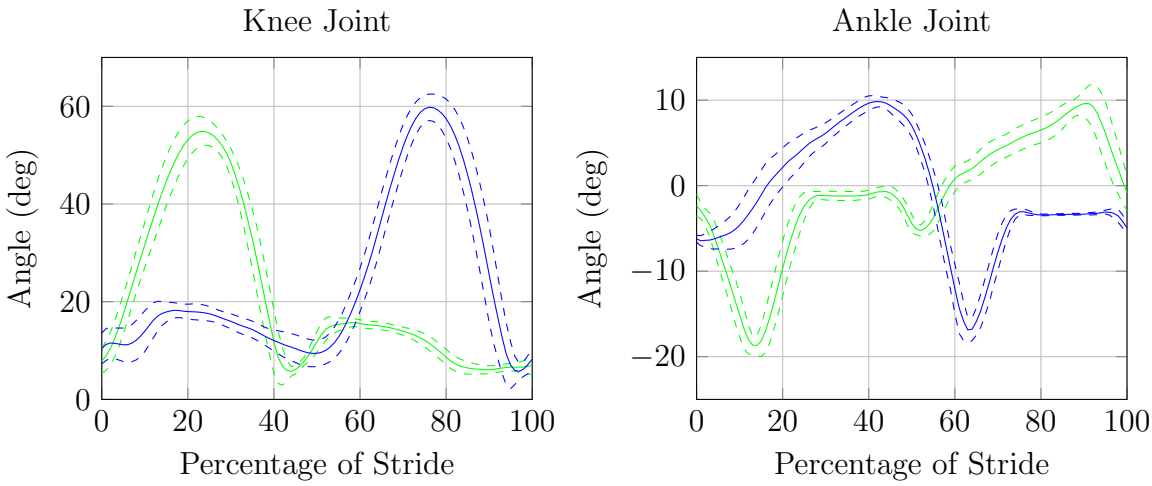

Figure 5.2: Lower limb kinematics for 20 consecutive strides with the unilateral control system.

Figure 5.3: Screenshots depicting the phases of the right powered prosthesis during one stride from video (top) and motion capture (bottom).

All the essential features of level ground walking are present in both the knee and ankle kinematics for these 20 optimal strides. However, in this, the most successful trial consisting of 38 strides, two illuminating errors occurred. On the 4^{th} stride the author failed to bring the ankle angle to a high enough degree of dorsiflexion to trigger the T12 transition (the push off threshold mentioned previously). As a result, the right side prosthesis did not enter swing and the prosthesis remained stiff and straight

during this non-weight bearing period. During the 33^{rd} stride, the author achieved a premature push off on the left side. The knee flexion during push off (late stance) made it difficult for the author to continue to supply an axial load on the shank. As a result, the left prosthesis entered swing flexion before the occurrence of heel strike on the ride side. Consequently, the left prosthesis buckled and the author was forced to support himself with the parallel bars.

Although Fig. 5.2 clearly suggests that biomechanically normal gait is possible with this controller in bilateral applications for a healthy subject, the main goal of this work is to provide stable control for bilateral amputee subjects in over-ground walking without external stability aids. Therefore, it is important to evaluate the deficiencies in the control structure that might preclude this goal.

The two anomalies mentioned earlier recurred in several of the trials. Although the frequency of such anomalies diminished as the author adapted to walking on the prostheses, the possibility of their occurrence in over-ground walking without a stability aid is a significant risk. The missed push off anomaly (stride 4) is a lower risk event, as the subject is transitioning away from a weight bearing phase on the device that missed its cue. The author was able to continue the stride by swinging his right side prosthesis despite the fact that it remained in middle stance (Phase 1).

The premature push-off of the left side prosthesis during stride 33 poses a more significant problem for the subject. In the unilateral controller, the transition from a stiff knee to a soft knee in the push off phase is triggered by a threshold in knee angle. The preferred signal for this transition would be the detection of the contralateral heel strike, but the unilateral controller is unable to directly measure this event. When the knee angle threshold is used as a proxy, a premature push off can cause the knee to buckle because this threshold will be met before the user's weight has started to transition onto the contralateral limb. Without the use of external stability aids, the result would most likely be a fall.

1.4 Passive Prostheses

Before the bilateral controller was implemented to enhance the reliability of the powered prostheses, the author performed a series of treadmill tests using a pair of passive prostheses. The knee unit was the Ossur Total Knee 2000, and the ankle unit was the Freedom Innovations Pacifica LP carbon fiber ankle-foot complex. The knee was connected to the ankle with a standard aluminum pylon and the complete prosthesis weighed 1.80 kg with its foot shell. The first photograph in Fig. 5.1 shows the passive prostheses mounted to the able body adapters on the author.

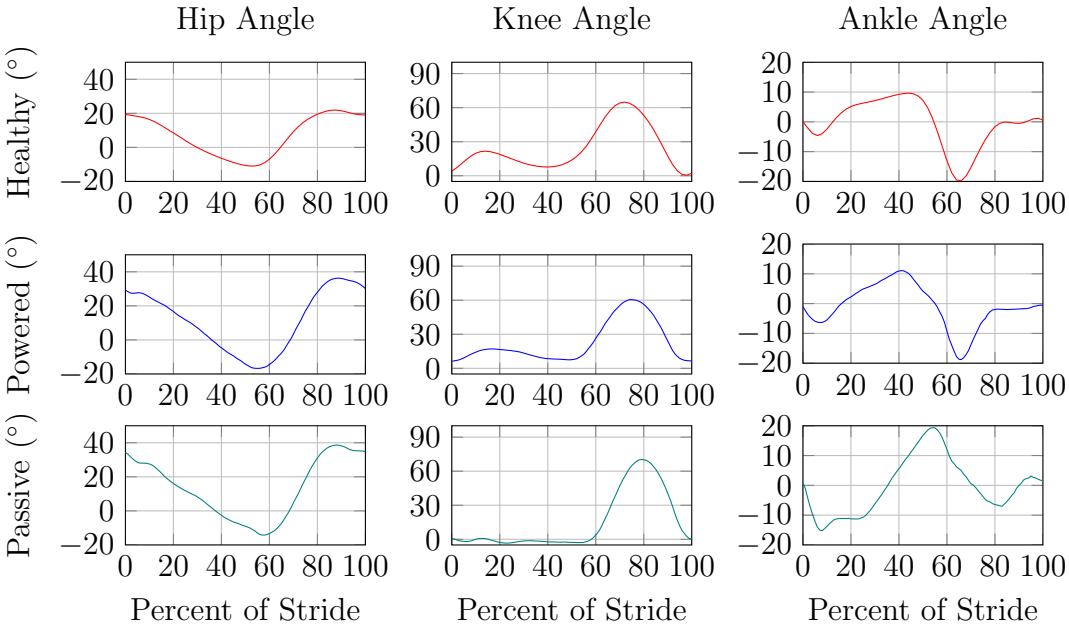

Figure 5.4: Comparison of lower limb kinematics between healthy subjects, the author using coordinated powered prostheses, and the author using passive prostheses.

The kinematics achieved with the passive prostheses are plotted Fig. 5.4 (along with healthy data and the results from the coordinated powered prostheses). It was the author's experience that the passive devices required significant hip torques to generate sufficient extension of the knee in swing. Additionally, a hyper-extensive torque was applied to the knee by the hip throughout stance to guarantee stability.

This behavior is seen in the plot of the knee angle, as the knee stays virtually at zero throughout the stance phase. The hip also reached a higher peak flexion as a result of the exaggerated swing necessary to properly position the passive prosthesis for heel strike. The offset in the prosthetic ankle during stance is a kinematic reaction to the hyperextension of the knee, and the lack of plantar flexion at toe off is clearly the result of a non-powered push off.

1.5 Powered Prostheses with Coordinated Control System

In order to avoid the two errors previously described in the unilateral system, a Controller Area Network (CAN) communication scheme was implemented to share data between the prostheses. The main purpose of this communication was to lock out certain states in the contralateral prosthesis. Details of the implementation of this system on a healthy subject can be found in [87]. With the data tether installed and the coordinated controller implemented, the averaged kinematics achieved by the pair of powered prostheses did not differ significantly from that achieved with the unilateral controller (see Fig. 5.4). The important difference, however, is that no strides resulted in the loss of support due to a premature push off, since the transitions surrounding push off are now constrained by the internal mode of the contralateral prosthesis. Double support is a guaranteed feature of the coordinated control system, so long as the communication channel between the legs is intact.

2. Manuscript 4: A Coordinated, Powered Prosthetic Intervention for a Bilateral Transfemoral Amputee

2.1 Abstract

This paper presents the design and validation of a control system for a pair of powered knee and ankle prostheses to be used as a prosthetic intervention for bilateral transfemoral amputees. The control system leverages inter-communication between the prostheses for enhanced awareness and stability, along with power generation at the knee and ankle joints to better restore biomechanical functionality in level ground walking. The control methodology employed is a combination of an impedance-based framework for weight-bearing portions of gait along with a traditional trajectory-based approach for the non-weight-bearing portions. The control system was implemented on a pair of self-contained powered knee and ankle prostheses previously developed by the authors and tested by the second author, who is, himself, a bilateral amputee. This user was able to achieve kinematics at the prosthetic and intact lower joints (hip, knee, and ankle) that were substantially more indicative of healthy gait than that achieved with passive prostheses.

2.2 Introduction

It is difficult to estimate the number of bilateral lower limb amputees living in the United States. In the largest amputee demographic study known to the authors, persons suffering multiple amputations were not distinguished, although the total number of amputees was shown to be both large (with over 600,000 being either above the knee, below the knee, or the foot) and rapidly growing (projected to double over the next 50 years) [7]. The absence of an explicit report of the number of bilateral transfemoral amputees in the preceding study suggests that the population may be

relatively small compared to the total number of persons living with a lower limb amputation.

Several studies do distinguish multiple amputations, however. For the period of April 1, 2006 through March 31, 2007, 4% of the 4574 referrals to the 43 prosthetics service centers in the United Kingdom were bilateral lower limb amputees [88]. In a review of 1846 lower limb amputees admitted to the Dundee Limb Fitting Centre in Scotland between 1965 and 1989, 18% were bilateral, with 3.6% being bilateral, transfemoral [89]. If these numbers are comparable for the U.S. population, then the number of persons living with bilateral, transfemoral amputations is likely to be quite small.

The size of the population could be a major contributing factor in the lack of dedicated research concerning prosthetic interventions for bilateral, transfemoral amputees. Such a small population does not draw a strong commercial interest in a free market society, and, as such, bilateral amputees that choose to utilize prostheses are forced to select from a family of prostheses developed almost exclusively for the needs of the unilateral amputee. A review that included 11 bilateral, transfemoral amputees from a particular regional amputee rehabilitation center over the period between July 1988 and December 1989 evaluated functional status at discharge from the center and 3 months later [90]. Of the 11 patients, none at any point were able to achieve either "limited community" or "community" ambulation classifications, and 6 of the 11 at the 3 month follow up were classified as "wheelchair-bound." The "limited community" classification was defined as "a patient who can walk 152 m (500 ft), can participate in some avocational activity, but is not gainfully employed."

A separate study investigating the mobility of wounded veterans included 50 bilateral lower limb amputees from both the Vietnam War and Operation Iraqi Freedom/Operation Enduring Freedom (OIF/OEF) [91]. 33% of the members of the Vietnam group abandoned their prostheses in favor of a wheelchair, while only 5% of

the members of the OIF/OEF group did so. The vast majority of the abandoned prostheses in the Vietnam group were purely mechanical (as opposed to microprocessor-controlled passive devices), with a similar trend in abandonment for mechanical prostheses amongst the OIF/OEF veterans. This result suggests that increasing the functionality of the prosthesis may reduce the likelihood of abandonment, which has been shown to be quite high in bilateral, transfemoral amputees [92].

2.2.1 Bilateral Transfemoral Gait

Unilateral lower limb amputees typically exhibit significant compensatory behaviors in their intact limb (sound side) in order to accommodate the deficiencies of a typical passive prosthesis. Such compensatory actions include a longer stance phase on the sound side (presumably for stability) [73], increased hip extensor and ankle plantarflexor work on the sound side [75], and vaulting (which is a mid-stance plantarflexion of the sound ankle to provide extra ground clearance during swing of the prosthetic limb). These compensatory actions may be partially responsible for the increase in metabolic energy experienced by unilateral amputees during level walking [72, 93, 94].

Bilateral amputees have no intact limb to provide these compensatory behaviors, and they are significantly more limited in their ability to ambulate with prostheses. All control of and compensation for the prostheses must come solely from the hips. Since most prostheses are passive devices, the hips are over-taxed in terms of power generation, leading to excessive hip torques and a substantially increased metabolic cost of transport [95–98].

2.2.2 Emergence of Powered Prostheses

Traditionally, lower limb prostheses were passive by necessity; the technology required to construct a powered device comparable in size and weight to the anatomical limb has only emerged over the last five to ten years. Now that the supporting technology has arrived (power-dense motors/batteries and efficient microprocessors), the field of prosthetics is beginning to incorporate active elements. A number of research groups have published preliminary results on a variety of powered lower limb devices.

The prosthetics and orthotics company Ossur has released two versions of a powered knee joint called the Power Knee. This knee prosthesis is designed to be used in conjunction with an off-the-shelf passive prosthetic ankle/foot. Because the Power Knee has only existed as a commercial product, no literature is publicly available concerning its design.

Herr *et al.* have developed a powered ankle for transtibial amputees which leverages both series- and parallel-elastic actuation [12–16]. By measuring the deflection of a series spring (with known spring constant K_s), an estimate of the ankle torque can be determined. An added benefit of series elasticity is that the introduction of compliance in between the prosthetic foot and the actuator softens the transfer of impulses from shock loading (i.e. heel strike), which may reduce wear on the mechanical transmission. The parallel spring reduces the peak torque required from the actuator at the high-power push off event in the late stance phase of level walking. In a study on 3 transtibial amputees comparing the use of a passive ankle with the powered prototype, it was shown that the powered ankle was able to reduce the energetic cost of transport by 7-20% [12]. In addition, the control approach demonstrated in [16] incorporates intrinsic speed adaptation, allowing an efficient gait across a range of walking speeds.

A separate effort in powered ankle design conducted by Sugar *et al.* has produced

a two degree of freedom ankle named SPARKy 3, which stands for Spring Ankle with Regenerative Kinetics [17, 18]. An important goal in this effort was to enhance the agility of active users by providing the power necessary for running and jumping, along with providing actuation in the coronal plane. As a result, the designers opted to use two Maxon EC30 Powermax motors operating in parallel to provide 400 W of continuous power, with estimated peaks of up to 1500 W.

Lefeber *et al.* have just reported on another powered ankle that uses an electric motor to store energy in a spring during stance [99]. This design reduces the power requirements of the motor by spreading the energy deliver over a longer period of time (all of stance instead of the brief moment of powered push off). Testing of the design shows energy delivery that matches or exceeds healthy subject data.

Other research efforts are using electromyography, inertial measurement, and other techniques to enhance control systems for powered knees or ankles [20–28, 35, 36, 100**?** , 101]. To date, however, this is the first work known to the authors concerning the application of integrated powered knee and ankle prostheses for bilateral amputees.

2.3 Methods

2.3.1 Powered Prosthesis

The authors have previously developed and reported on a powered transfemoral prosthesis prototype. The device has been shown to perform level walking [5], real-time intent recognition [6], upslope walking [4], ground adaptive standing [3], and stair ascent and descent [34]. Although the prototype has undergone a series of revisions, the fundamental design has remained consistent. In the current revision (see Fig. 5.5), the number of sensors on the prosthesis has been reduced by replacing the heel and toe load sensors with a single, axial load cell in the shank as a measure of weight bearing, and removing the optical encoders on the motors in favor of the integrated

Hall Effect sensors as a measure of motor position and velocity. The joint angles are now directly measured with absolute magnetic encoders, which means that all control signals are derived from non-contact sensors, which is intended to substantially improve lifetime and reliability.

The prosthesis is controlled by an embedded system that consists of two microcontrollers: a 32-bit general purpose microcontroller for high level control and a 16-bit digital signal processor (DSP) for low level control. The 32-bit microcontroller runs the control system as described in this manuscript, and performs overhead functions such as data logging and inter-prosthesis communications. The DSP implements closed-loop current control on the knee and ankle motors and receives a current reference from the 32-bit microcontroller over a serial peripheral interface (SPI). The impedance control loop and state machines are updated at a sampling rate of 500 Hz, while the current control loop runs at approximately 5 kHz.

Figure 5.5: The Vanderbilt Powered Prosthesis.

2.3.2 Walking Controller

The original control system for the unilateral transfemoral prosthesis consisted of a finite state-based impedance control framework, as described in [5]. For level walking, the gait sequence was parsed into discrete states accessed sequentially through biomechanical cues measured by sensors in the prosthesis. Within each state, a simple impedance control law was implemented to approximate the impedance seen in healthy gait. The following linear control law was utilized in each state:

$$\tau = k(\theta - \theta_{eq}) + b\dot{\theta} \tag{5.1}$$

where τ represents the commanded joint torque (for either the knee or ankle joint), θ represents the joint angular position, and $\dot{\theta}$ represents the joint angular velocity. k, b, and θ_{eq} are tunable parameters that define a virtual spring and damper, where k is the spring stiffness, θ_{eq} is the spring equilibrium position, and b is the damping coefficient.

In this paper, the control system includes provisions specific to bilateral applications. In particular, a data tether using the Controller Area Network (CAN) protocol has been implemented to share information between the two prostheses. At a rate of 500 Hz, the prostheses exchange the following signals:

- run_time - counter that increments every sample
- control_modes - state information for the control system
- knee_position - angle of the knee joint
- knee_velocity - velocity of the knee joint
- ankle_position - angle of the ankle joint
- ankle_velocity - velocity of the ankle joint

- shank_load - axial load in the shank
- prc_stride - percentage of stride for the current stride

The number of states and state behavior has also been modified from the original finite state-based impedance control framework. The bilateral controller has three distinct states for the level walking gait cycle (see Fig. 5.6). In each state, eq. 5.1 is implemented for both the knee and ankle joints. In the stance state, the impedance parameters are constant, thereby producing a locally passive system that will always come to rest in the absence of disturbances or input from the user. In this state both joints are tuned to behave as stiff, over-damped systems when supporting the user's body weight. Neither joint should be overly stiff, however, to allow for stance knee flexion and ankle plantarflexion for shock absorption after heel strike.

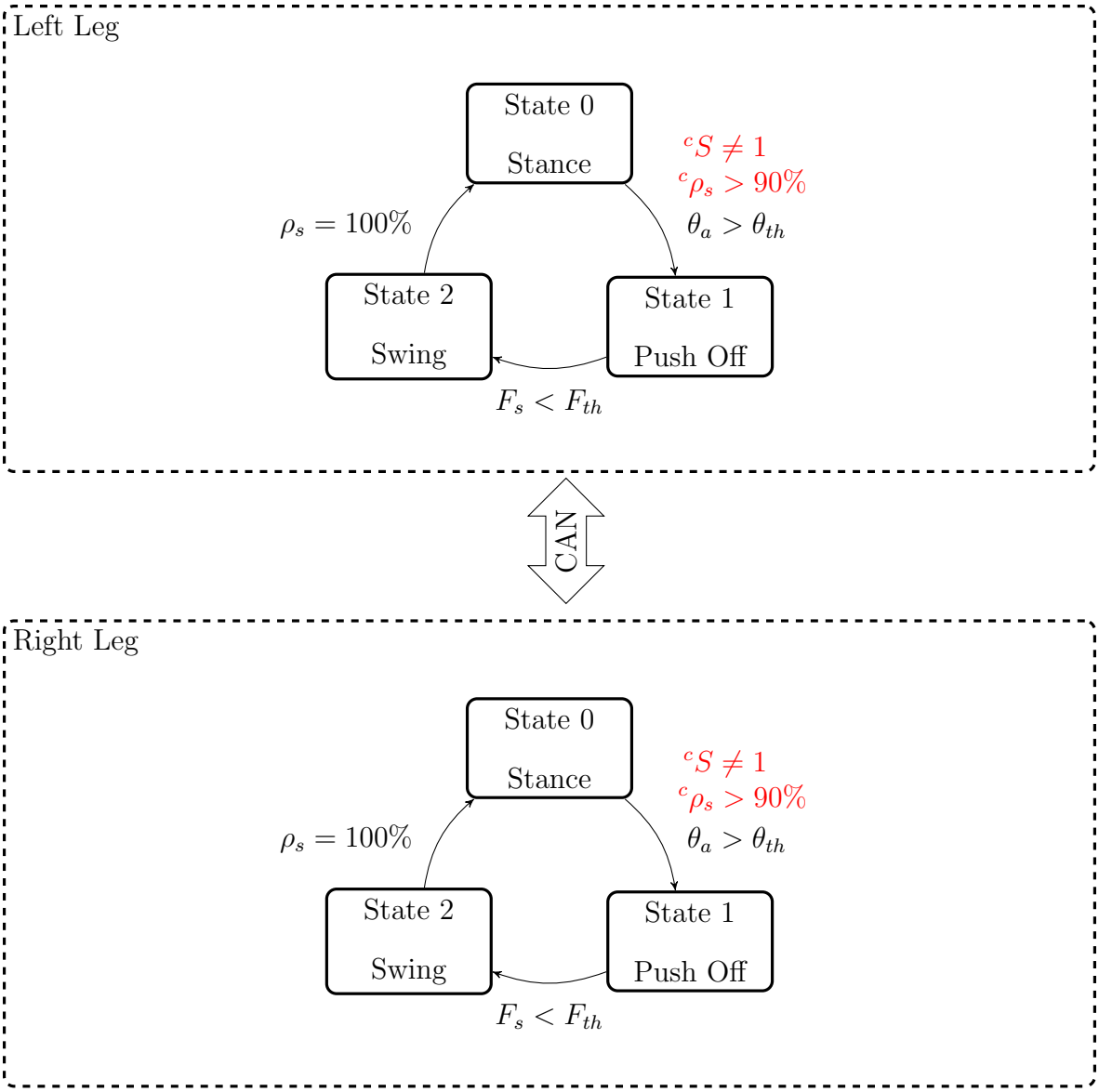

Figure 5.6: The finite state machines executed by the prostheses. θ_a is the ankle joint angle, which is compared to a predetermined threshold, θ_{th}, to trigger the transition into the ankle push off state. F_s is the axial load in the prosthetic shank, which is compared to a predetermined threshold, F_{th}, to trigger the transition into swing. The swing state executes a trajectory and automatically reverts to the stance state when the trajectory ends, which corresponds to the percentage of stride, ρ_s, reaching 100%. The red conditions on the transition from State 0 to State 1 are safety conditions that are dependent upon the contralateral signals ${}^{c}\rho_s$ and ${}^{c}S$, which are the contralateral percentage of stride and contralateral state, respectively.

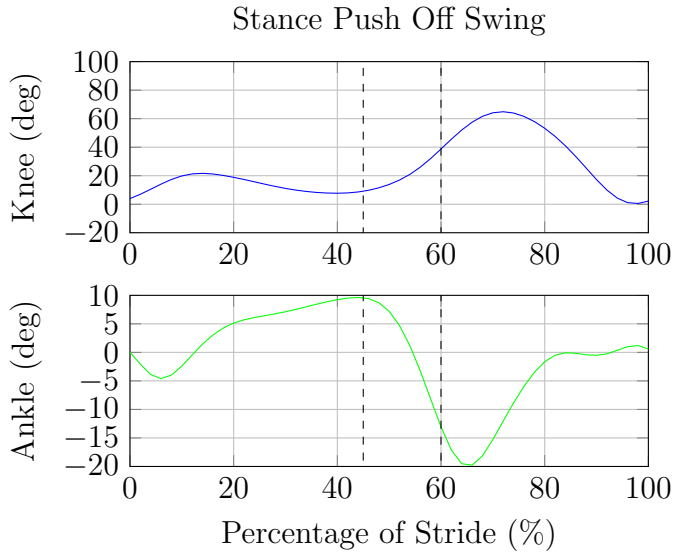

Figure 5.7: Ideal joint behavior.

In the push-off state, the ankle impedance parameters are also constant, though the equilibrium position of the ankle is moved from a neutral value (tuned specifically for the user) to an appropriate plantarflexed value to generate the energy and motion for powered push-off. By arbitrarily changing this equilibrium value, a finite amount of energy is introduced to the system, creating a transient response but then immediately reverting to a locally passive system.

In order to simplify the tuning process, however, the knee behavior is modified in the push-off state. While the stiffness and damping coefficient of the knee joint remain fixed during push off, the equilibrium position becomes a function of the ankle angle. During push off, which takes place between approximately 45% and 60% of stride (see Fig. 5.7), the knee angle and ankle angle have an approximately linear correlation. This observation has been noted previously in the literature and leveraged for the design of a passive prosthesis [102]. A linear least squares relationship was determined from the healthy data presented in [62] and is depicted in Fig. 5.8. This relationship is used to continuously calculate the knee equilibrium position in the push off state. As a result, the knee and ankle angles are kinematically linked in

this state. As the user unloads the ankle, the knee begins to yield in a synchronous manner, giving the user direct control over the duration of this state through the modulation of load on the prosthesis.

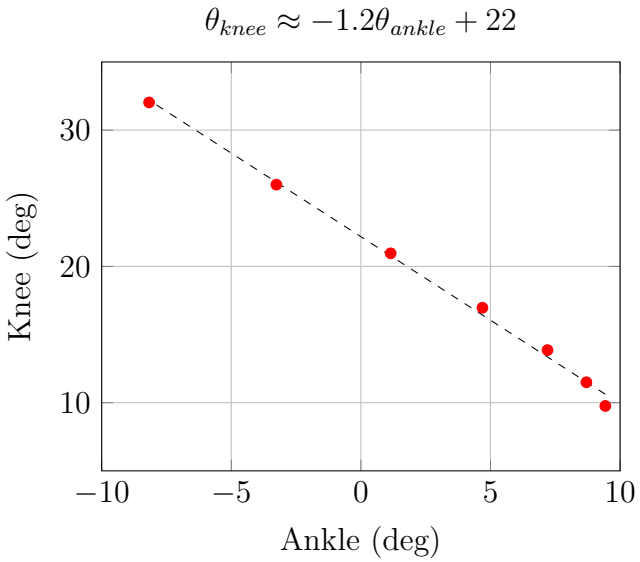

Figure 5.8: The approximately linear relationship between knee angle and ankle angle during level walking in healthy subjects between 45% an 60% of stride.

The third and final state consists of the swing phase of gait. Because the prosthesis is non-load bearing in this state, the classical advantages of pure impedance-based control would not be fully realized. The two primary advantages of the finite state-based impedance control framework presented in [5] are that the behavior of the prosthesis is not explicitly time-dependent (i.e. the user, as opposed to the device, has control over the speed at which the device moves), and that the forces produced by the prosthesis are specifically tuned to interact safely with the environment. These features are in direct opposition to the nature of high-gain trajectory control, which specifies precisely the time-dependency of the motion at a high, disturbance-rejecting impedance. If the walking speed is known, however, the time-dependent nature of trajectory execution in the prosthesis simplifies to a problem of proper initiation of

the trajectory. This is the same problem seen in the pure finite state-based framework, as the thresholds for state transitions must be timed accordingly for each user. Additionally, the high impedance used in trajectory tracking will not accommodate unknown interactions in the environment, such as the varying load placed upon the prosthesis by the user. In a non-weight bearing phase of gait such as swing, however, external loads are minimal. Since the authors have previously demonstrated an algorithm to detect and classify stumbles [33], a robotic prosthesis could easily be programmed to change its behavior in the event of a stumble, meanwhile retaining high gain trajectory control during the swing phase.

For these reasons, the swing phase of the walking controller has been reduced to a single state that executes appropriate trajectories at the knee and ankle joints. Upon completion of the trajectories, the controller reverts to the initial state (stance), previously described. The trajectories are produced by a spline interpolation generated upon entry into the state. Both the shape and duration of the trajectories are determined by an estimate of the cadence, as subsequently described.

2.3.3 Inter-prosthesis Communication

Using the control signals exchanged between the prostheses, each prosthesis implements several safety features to avoid inappropriate mode transitions which could potentially destabilize or injure the user. Firstly, the prostheses are constrained to only allow alternating steps. Neither prosthesis can enter the push off state a second time before the contralateral prosthesis has done so. There is a 2 second time-out on this feature, such that standing for a moment will re-enable push off on both prostheses. Additionally, once one prosthesis has entered the push off state, the contralateral prosthesis is locked out from also entering the push off state until the ipsilateral prosthesis has reached the last 10% of the stride. It is important to allow the triggering

of a contralateral push off before ipsilateral heel strike in order to achieve dynamic walking similar to healthy biomechanics. An earlier push off, however, could result in premature destabilization on the ipsilateral (stance) leg and might produce a fall, and, as such, must be avoided.

2.3.4 Variable Cadence

The stance and push off states of the controller inherently accommodate a variable cadence, since there is no explicit time dependence in the control law. In these phases, therefore, the user can control cadence simply by modulating the speed at which he or she moves the hip. At faster cadences the ankle transition (State 0 to State 1) and the load transition (State 1 to State 2) occur sooner. For the swing state, which executes trajectories for the knee and ankle joints, the duration and shape of the trajectories are altered for each stride. A timer is initialized at the beginning of the push off phase (Phase 1), and its value at the end of this phase determines the speed and shape of the trajectory executed in the swing phase (Phase 2). At this point in the stride, the speed of the stride is determined until the subsequent heel strike, at which point the control behavior reverts to the non-time-varying impedance control law of eq. 1.3. Although the duration of the push off state is only a portion of the stance timing available for cadence estimation, allowing the beginning portion of stance to be independent of cadence provides an important safety and control mechanism for bilateral amputees. During the stance phase (early and middle stance, specifically), a bilateral amputee may take more time than a healthy subject to stabilize at the hip and achieve an appropriate balance. This time may not be a function of the user's desired cadence, and, consequently, it is not used in the cadence estimation.

The duration of the trajectories executed in the swing phase are directly proportional to the duration of the previous push off phase. The shape of the trajectories,

however, is also adjusted according to this measure of cadence. Three reference trajectories are specified at nominal, slow, and fast cadences via seven points. The duration of time spent in the push off phase is used to interpolate between the closest two of these three sets of points, creating a new spline that corresponds to the cadence. Although the differences between the reference splines are adjustable at each control point, in this work the only control points that were modified were the ones that affected the maximum knee flexion, as can be seen in Fig. 5.9. Effectively, the maximum knee flexion is reduced at slower cadences and increased at faster cadences.

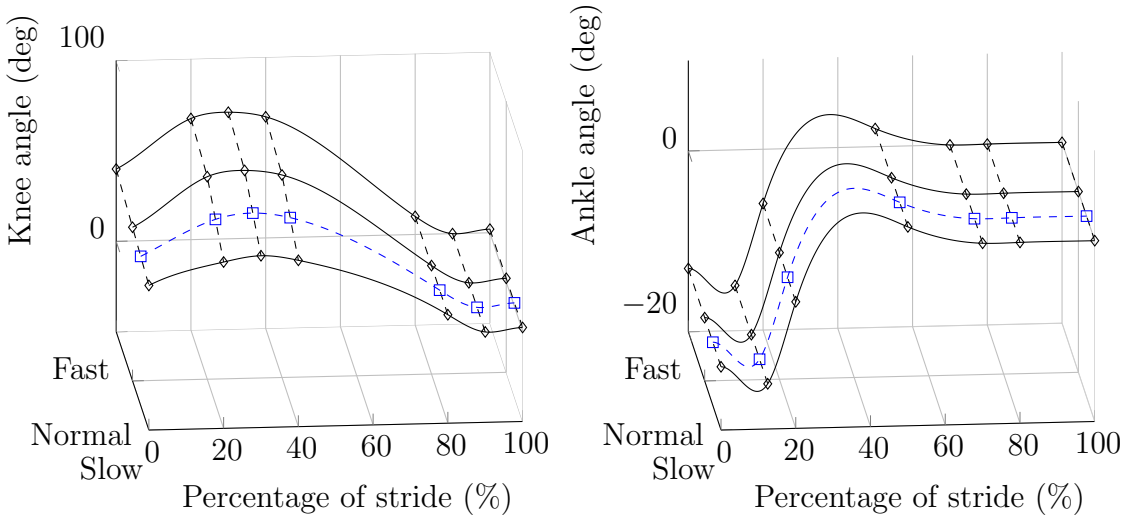

Figure 5.9: The three reference trajectories and an estimated trajectory for the swing phase of walking at the knee and ankle joints.

2.3.5 Experimental Validation

The control system was implemented on a pair of prostheses and vetted through the use of able body adapters on healthy subjects [103]. The system was then implemented on a bilateral transfemoral amputee subject (one of the authors). The subject was 38 years of age, and his bilateral amputations were the result of a traumatic injury at age 18. He wore Ossur Rheo knees (microprocessor controlled knees, or MPCs) and College Park Soleus ankles (dynamic-elastic response ankles, or DERs) for daily

use and for comparison in this study. He weighed approximately 70 kg at the time of the testing. After several testing and development sessions, a kinematic assessment was performed on both daily use (passive) prostheses and the powered prostheses. Approval for this study was given by the Vanderbilt University Institutional Review Board and informed consent was obtained before the assessment.

For each pair of prostheses, the subject walked at two comfortable walking speeds of his choosing over ground in a motion capture laboratory. He was fitted with a full skeletal marker set for motion capture with a NaturalPoint Optitrack motion capture system. Data was collected for ten trials using both the powered prostheses and the subject's daily use, passive prostheses. Because of the limited capture volume (approximately 36 square meters), the middle two strides were selected from each trial for analysis. The motion capture data was exported in the Biovision Hierachy (BVH) file format and imported into Matlab for post-processing. Heel strikes were manually selected in Matlab and the Cardan angles specified in the BVH file were converted to homogeneous transformation matrices. From these matrices, sagittal joint angles were extracted for the hip, knee, and ankle joints for each limb. Each stride was then normalized in terms of percentage of stride using the heel strikes selected previously.

2.4 Results

The joint angles for the right side hip, knee, and ankle are plotted in Fig. 5.11 for able bodied subjects (reprinted from [62]), the amputee subject using the powered prostheses, and the amputee subject using his daily use, passive prostheses. A video is included in the supplementary that shows the subject walking on both pairs of prostheses outside of the motion capture laboratory. The healthy subject data did not explicitly state walking speeds or cadences, but the data reprinted here are specified as a slow cadence, which most closely represents the subject's selected cadences. On

the powered prostheses the subject walked with an average cadence of 66 steps per minute at a self-selected slow speed and 83 steps per minute at a self-selected normal cadence. On his daily-use prostheses the subject walking with an average cadence of 70 steps/min at a self-selected slow speed and 97 steps/min at a self-selected normal cadence. The subject used a stability aid in his right hand for all trials (a forearm crutch for the powered trials and his daily use cane for the passive trials). Several representative photographs of the subject walking with the powered prostheses are shown in Fig. 5.10.

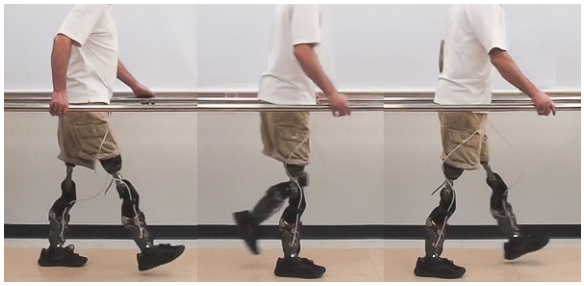

Figure 5.10: The subject walking with the powered prostheses.

In addition to the motion capture data, the powered prostheses log internal data at a rate of 250 Hz, providing an estimate of joint torques through the measurement of the motor currents. An approximation of the amount of mechanical energy delivered can be made using the motor current, motor torque constant (0.0276 Nm/A), the drive train's transmission ratio (196:1), and the ankle velocity. This approximation can be refined with an empirical measure of the transmission's frictional characteristics. In this case, the friction in the transmission was modeled as a combination of Coulomb friction and viscous damping. The model parameters were estimated by iteratively increasing their values from zero until the system no longer remained stable with otherwise zero input. With this approach, the system demonstrated stability with Coulomb friction no higher than 5 Nm and a damping coefficient no higher than 0.01 Nm·s/deg. Fig. 5.12 depicts the powered ankle behavior for a characteristic stride

(at the normal self-selected cadence), including the torque and power estimates. An integration of the power in the stance and push off phases yields -7.67 J and 11.47 J, respectively, demonstrating that this behavior would not be possible in a passive system and confirming that the powered prostheses delivered powered push-off.

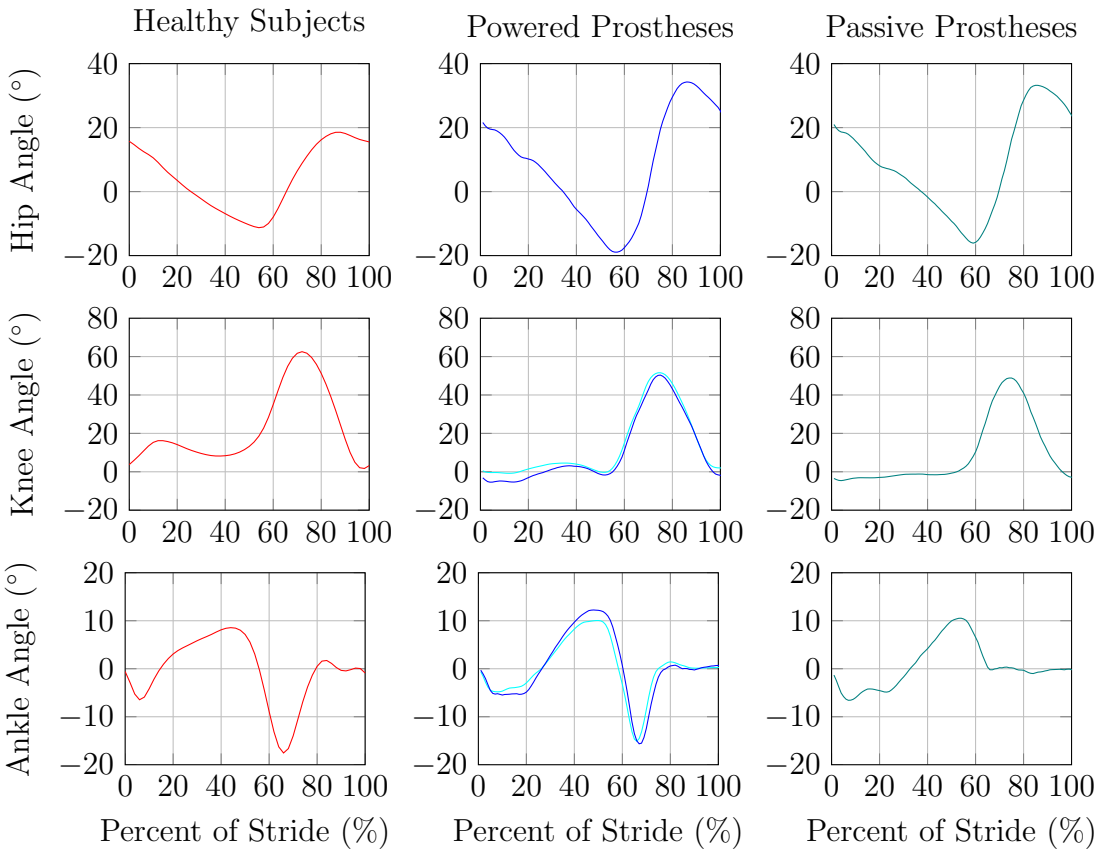

Figure 5.11: Joint angles for the right side hip, knee, and ankle for able bodied subjects (reprinted from [62]), the amputee subject using the powered prostheses, and the amputee subject using his daily use, passive prostheses. The knee and ankle joint plots for the powered prostheses include the internally measured joint angles from the powered prosthesis in lighter blue.

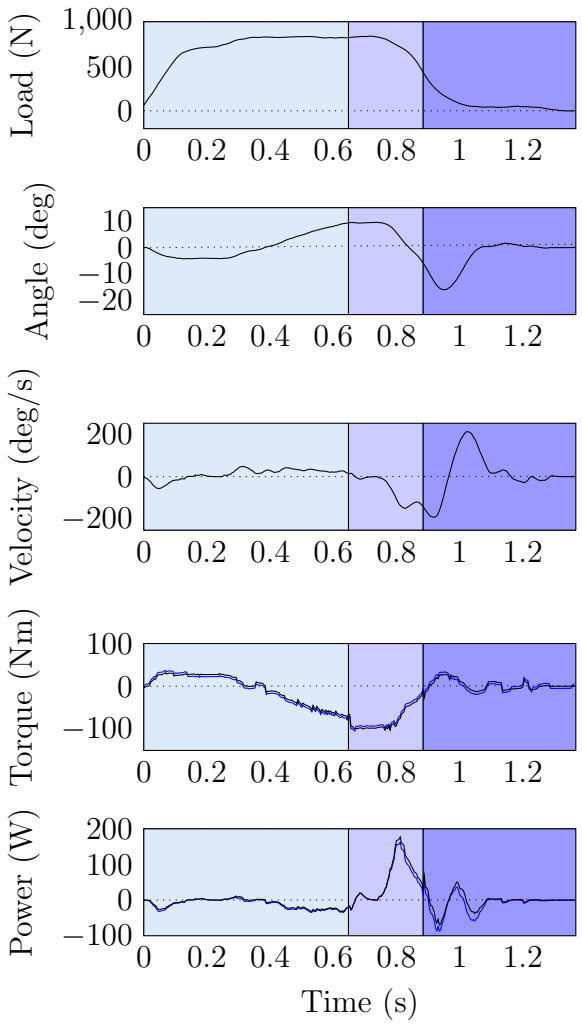

Figure 5.12: The powered ankle behavior for a characteristic stride. The top plot shows the axial load in the shank as measured by the onboard magnetic load cell. This signal is roughly proportional to the vertical component of the ground reaction force. The next two plots show the ankle angle and angular velocity, respectively. In the fourth plot, the black line represents the output torque of the ankle given 100% transmission efficiency, and the blue line represents the output torque assuming the transmission friction model described.The final plot shows the estimated power output of the ankle without (black line) and with (blue line) the transmission friction model. The three colored regions of the plots denote the three phases of the controller: stance, push off, and swing. With the transmission friction model, the net energy contribution in the stance phase was -7.67 J, while the net energy contribution in the push off phase was 11.47 J.

2.5 Discussion

The powered joint data show several kinematic features of healthy gait that are absent in the passive data. Most notable, perhaps, is the evidence of powered push- off from the ankle joint. The powered ankle exhibits evidence of an active push-off with a strong plantarflexion of the joint just after 60% of stride. This phenomenon can be verified by consulting the power plot in Fig. 5.12. During the push off phase, the powered ankle delivers almost 50% more energy than all of the energy both dissipated during heel strike or (virtually) stored during middle stance. Contrarily, the passive ankle returns to its nominal position (zero degrees) once unloaded, and, although its energy contribution is not explicitly measured, it is fundamentally constrained to return only an amount of energy equal to or less than what was stored through dorsiflexion in middle stance.

For the prosthetic knee joint, a period of stance knee flexion is observed in the powered trials. Stance knee flexion aids in shock absorption from heel strike and helps to lower the body's center of mass through segments of the stride. The MPC knees cannot provide an extensive torque greater than the externally applied torque since they only exhibit passive behavior. As a result, stance knee flexion cannot be achieved with such a device unless the user supplies a torque from the hip to extend the knee once it flexes. Such an action is not biomimetic, and it also gives the user a sense of instability in stance. As such, the passive data show a strongly hyperextended knee in stance that breaks (moves past zero into flexion) only at the initiation of swing. The ability of the powered prostheses to provide full support with flexed knees is a feature that could also enhance safety for bilateral amputees, as it is safe for the user to load the prosthesis regardless of the knee configuration. Specifically, the powered prostheses will provide supportive torque at all times in this controller, therefore eliminating the stance phase yielding that would occur in an MPC knee

that was loaded whilst not in hyperextension. Furthermore, the active swing from the powered prosthesis is guaranteed (within the torque limits of the device) to extend and provide support, even in the event that it experiences a disturbance such as a stumble or scuff. Finally, landing prematurely on the device will not sacrifice its ability to support the user, as the active swing extension will still extend the knee.

For both the powered trials and the passive trials, the intact hip joints exhibited comparable ranges of motion which were significantly larger than that seen in healthy subjects. Over-active hip motion is consistent with the literature that points to increased hip torques and metabolic costs for bilateral transfemoral amputee gait [95–98]. It is anticipated by the authors, however, that the restoration of active behavior at the ankle will serve to alleviate this over-taxing of the hips in the long term. However, this particular subject has approximately 20 years of training on passive devices and only several hours of development and testing on the powered prosthesis prototypes. As such, it is not surprising that learned kinematic compensations at the hip were not readily modified by the restoration of powered ankle push-off. Despite this fact, these data show that a pair of powered knee and ankle prostheses can be designed and controlled such that a bilateral transfemoral amputee can achieve a gait that better reflects healthy kinematics at the knee and angle joints.

3. Conclusion

The design and control of a powered prosthetic intervention for bilateral transfemoral amputees has been presented and demonstrated on an amputee subject. The control system can achieve variable cadence walking with a reduced number of user-dependent parameters relative to previously reported controllers for powered transfemoral prostheses. The prosthesis prototypes and control system described in this work have been shown to provide improved kinematics for level walking at the prosthetic knee

and ankle joints over the subject's daily use prostheses, relative to healthy data. The authors plan to extend this controller to other lower limb activities, as well as investigate lower limb kinetics in bilateral transfemoral amputees in future work.

CHAPTER VI

CYCLING

Cycling, like gait, is periodic in nature. The dynamics of cycling in steady state conditions can therefore be fully characterized by examining the behavior relative to the evolution of the crank angle over a single rotation. Furthermore, it may be possible to design a control system that performs its control action as a function of crank angle. Doing so is similar to estimating the phases of gait in order to introduce the proper control behaviors at the proper times for a controlled prosthesis. In gait, however, it is difficult to obtain a real time estimation of the percentage of the gait cycle, and instead, most controlled prostheses parse gait into discrete modes corresponding to the biomechanical phases of gait. The control action in these modes is then derived from joint angles, velocities, and external loads. In cycling, however, when the assumptions are made that the foot remains in contact with the pedal and the rider remains in contact with the saddle, then leg follows a path that is kinematically constrained. The consequence of forming this closed kinematic chain is that the motion of the prosthesis can be used to precisely measure the angle of the crank. Knowing the crank angle with a precision and latency comparable to the knee angle would open up the possibility of defining control laws based directly on the crank angle instead of local behaviors for the knee. As a preliminary investigation, the following manuscript has been submitted to the 36th Annual International Conference of the IEEE Engineering in Medicine and Biology Society in Chicago, Illinois, USA. The manuscript outlines

and evaluates an algorithm for the estimation of the crank angle of a bicycle using only measurements internal to an intelligent transfemoral prosthesis.

1. Manuscript 5: Estimation of Crank Angle for Cycling

1.1 Abstract

In order for a prosthesis to restore power generation during cycling, it must supply torque in a manner that is coordinated with the motion of the bicycle crank. This paper outlines an algorithm for the real time estimation of the angular position of a bicycle crankshaft using only measurements internal to an intelligent knee and ankle prosthesis. The algorithm assumes that the rider/prosthesis/bicycle system can be modeled as a four-bar mechanism. Assuming that a prosthesis can generate two independent angular measurements of the mechanism (in this case the knee angle and the absolute orientation of the shank), Freudenstein's equation can be used to synthesize the mechanism continuously. A recursive least-squares algorithm is implemented to estimate the Freudenstein coefficients, and the resulting link lengths are used to reformulate the equation in terms of input-output relationships mapping both measured angles to the crank angle. Using two independent measurements allows the algorithm to uniquely determine the crank angle from multi-valued functions. In order to validate the algorithm, a bicycle was mounted on a trainer and configured with the prosthesis using an artificial hip joint attached to the seat post. Motion capture was used to monitor the mechanism for forward and backward pedaling and the results are compared to the output of the presented algorithm. Once the parameters have converged, the algorithm is shown to predict the crank angle within 15° of the externally measured value throughout the entire crank cycle during forward rotation.

1.2 Introduction

As lower limb powered prostheses begin to emerge in the commercial market, amputees will likely desire to use these devices for activities outside of those necessary for everyday living. The majority of research on powered prostheses focuses on the mobility and stability benefits of walking on level ground, slopes, and stairs [5, 12, 25, 66, 104]. Cycling, however, is both a popular recreation and also a tool used for fitness and rehabilitation. It is also an activity that is characterized by significant net power generation at the hip, knee, and ankle joints [105–108]. It can be predicted, then, that lower limb amputees would suffer significant performance disadvantages when using passive prostheses for cycling. Some recent work has been done exploring cycling in transtibial amputees (with passive ankles), but the authors know of no comparable studies for transfemoral amputees [109]. This manuscript marks the beginning of an investigation into what is necessary for a powered knee and ankle prosthesis to contribute power during cycling in transfemoral amputees.

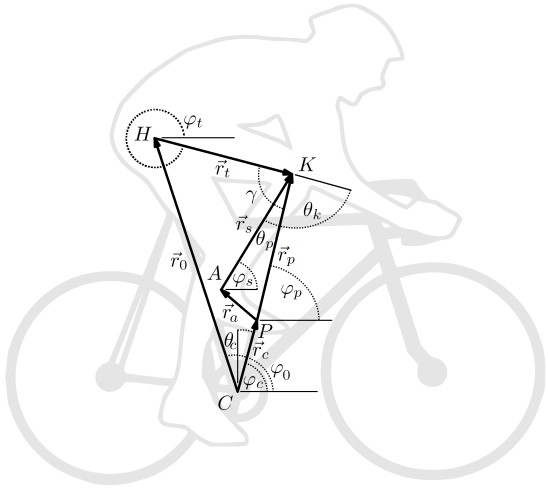

Figure 6.1: Kinematic diagram of the four bar linkage model.

In healthy biomechanics, the majority of the external work done by the pedaling limb is performed during what is known as the power stroke. The power stroke consists of knee and hip extension and ankle plantarflexion when the crank arm is in the forward half of its revolution. If the angle of the crank is denoted by θ_c and the convention shown in Fig. 6.1 is adopted, then the power stroke occurs between approximately 30° and 120° for the particular configuration shown. The power stroke region will generally vary as a function of the seat tube angle (φ_0 in Fig. 6.1), as the mechanical advantage of the lower limb joints with respect to the crank is a function of their relative angles and not their orientation with respect to gravity. For example, the power stroke for a recumbent bicyclist would be approximately 90° earlier than for an upright bicyclist.

If a powered prosthesis is going to supply torque to supplement an amputee's effort during cycling, an estimate of the crank angle is critical. The crank cycle is generally divided into 4 strokes: top, power, bottom, and recovery [109]. The transmission of torque from the knee to the crank inverts during the top and bottom strokes. The crank angle, along with the direction of rotation, must be known to the prosthesis to avoid supplying an extensive torque during the recovery stroke or a flexive torque during the power stroke. At the very minimum, therefore, an estimator is needed that can determine the initiation and termination of the power and recovery strokes.

1.3 Methods

It is assumed that the prosthesis can measure θ_k and φ_s. For the powered prosthesis previously developed by the authors, θ_k is measured by an absolute magnetic encoder, while φ_s is measured by an inertial measurement unit (IMU). With these two measurements, the relative lengths of each link in the four bar mechanism can be determined, and the result can then be used to uniquely determine the crank angle.

1.3.1 Estimation of Link Lengths

For the purposes of this work, the rider/prosthesis/bicycle system is assumed to be appropriately modeled by a planar four-bar linkage. This model therefore assumes that (1) the hip joint remains in a fixed location relative to the crank axis and (2) that the ankle joint is capable of remaining infinitely stiff such that the shank and foot can be treated as a single link. Under these conditions, this single degree-of-freedom mechanism can be completely characterized by the generalized coordinate φ_c, which is the angle of the crank shaft with convention as shown in Fig. 6.1. Note that this convention is different from that generally used in the biomechanics literature (denoted in Fig. 6.1 by θ_c), which defines the top-dead-center (TDC) position of the crank arm as zero, with forward rotation being positive [105, 109]. Because this is a single degree-of-freedom system, φ_c uniquely determines the configuration of the system under the further assumption that the knee cannot hyper-extend. (If hyperextension were allowed, there would be two assembly modes for the mechanism.) However, this mapping is a function of the relative link lengths of the mechanism, and so these link lengths must be determined if the relationship between φ_c and an internal prosthesis measurement, such as the knee angle, θ_k, is going to be exploited to determine the crank angle.

In general, it would be best to avoid specifying the geometry of the system explicitly since these parameters will likely change between riders and bicycles. Therefore, only the following parameters are specified: the seat tube angle, φ_0 (for most bicycles, this is close to 75°), r_p, and θ_p. With these parameters set and assuming at least 3 known input and output angles of the mechanism, the link lengths can be determined uniquely through classic analytical methods. If φ_p and φ_t are used (which can be uniquely determined from the measured angles θ_k and φ_s), then Freudenstein's equation can be written in the following form (derived from the loop close equation:

$\vec{r}_c + \vec{r}_p = \vec{r}_0 + \vec{r}_t$).

$$K_1 \cos\varphi_{t0} + K_2 \cos\varphi_{p0} + K_3 = \cos\varphi_{tp} \tag{6.1}$$

where the notation φ_{ab} denotes $(\varphi_a - \varphi_b)$. The coefficients are given by

$$\begin{aligned} K_1 &= \frac{r_0}{r_p} \\ K_2 &= -\frac{r_0}{r_t} \\ K_3 &= \frac{r_0^2 + r_t^2 + r_p^2 - r_c^2}{2 r_p r_t} \end{aligned} \tag{6.2}$$

The orientation of the shank with respect to gravity (and, through the knowledge of φ_0, also with respect to the bicycle frame representing the fixed link of the four bar mechanism) is estimated in real time by combining the high frequency portion of the integral of the in-plane angular rate measured by a solid state gyroscope with the low frequency portion of the inverse tangent of the in-plane accelerometer signals through the use of first order complementary filters with time constants of one second. The orientation of the thigh is determined by adding the knee angle (less θ_p) to the shank orientation. As the prosthesis moves through the cycling motion (initially generated, at least, by effort from the hip or the contralateral limb), pairs of angles are continually generated that should be consistent with the geometry of a particular four-bar mechanism. A continuous time recursive least-squares (RLS) estimator was implemented in MATLAB Simulink to achieve a best fit from the measured angles in real time. The implementation of the least squares estimation follows that presented in [110]. The covariance matrix was initialized as the identity matrix, and the forgetting factor was set to unity.

1.3.2 Estimation of Crank Angle

Either of the independent angles (the knee angle or the IMU orientation) used for the link length estimation can be used to find the crank angle. In each case, however, the mapping is both multi-valued and, at certain points, ill-conditioned. First consider the mapping from γ, which is the supplementary angle for the quantity $(\theta_k - \theta_p)$, to φ_c.

$$\varphi_c = \varphi_0 - \arccos\left(\frac{r_c^2 + r_0^2 - r_p^2 - r_t^2 + 2r_p r_t \cos\gamma}{2r_c r_0}\right) \tag{6.3}$$

The inverse cosine ($y = \arccos x$) is typically defined over the principal domain of $\{-1 \leq x \leq 1\}$ and range of $\{0 \leq y \leq \pi\}$ to avoid ambiguity. The crank angle, however, must be allowed to evolve from 0 to 2π, and so (6.3) alone will be insufficient for calculating φ_c.

φ_c can also be written as a function of φ_p,

$$\varphi_c = 2\arctan\left(\frac{-B_p \pm \sqrt{B_p^2 - 4A_pC_p}}{2A_p}\right) \tag{6.4}$$

where the coefficients A_p, B_p, and C_p are nonlinear functions of the link lengths and φ_p.

Even if a four-quadrant inverse tangent is applied, the quadratic expression still yields two possible values for φ_c. Consequently, (6.4) is also multi-valued. Within a reasonable tolerance, however, one output from each expression should be in agreement, resolving the ambiguity. The estimation algorithm therefore continuously evaluates the four conditions and selects the two closest values of φ_c as the most likely estimates for each expression.

Using two estimates of φ_c not only resolves the multi-valued problem, but it also provides an opportunity to minimize the errors resulting from singularities in either

estimate. A linear combination of the two estimates is constructed using normalized weights calculated from the relative magnitudes of the derivatives of (6.3) and (6.4). Although explicit differentiation of (6.3) and (6.4) is difficult, the derivatives can be expressed implicitly as

$$\frac{d\varphi_c}{d\gamma} = -\frac{r_t r_p \sin\gamma}{r_0 r_c \sin(\varphi_0 - \varphi_c)} \tag{6.5}$$

and

$$\frac{d\varphi_c}{d\varphi_p} = -\frac{r_p \sin(\varphi_p - \varphi_t)}{r_c \sin(\varphi_c - \varphi_t)} \tag{6.6}$$

respectively. The weights for the γ and φ_p estimates, respectively, are given by

$$G_\gamma = 1 - \frac{(\frac{d\varphi_c}{d\gamma})^2}{(\frac{d\varphi_c}{d\gamma})^2 + (\frac{d\varphi_c}{d\varphi_p})^2} \tag{6.7}$$

$$G_{\varphi_p} = 1 - \frac{(\frac{d\varphi_c}{d\varphi_p})^2}{(\frac{d\varphi_c}{d\gamma})^2 + (\frac{d\varphi_c}{d\varphi_p})^2}. \tag{6.8}$$

The weights as functions of the output are plotted in the bottom graph of Fig. 6.2. As each derivative approaches infinity, its respective contribution to the crank estimate approaches zero. Note also that, in general, the derivative of the output with respect to the knee angle measure is smaller than the derivative with respect to the shank angle measure, causing the knee measure to dominate the estimation except near its singularities.

1.4 Validation

A powered knee and ankle prosthesis previously developed by the authors was fitted to a bicycle and connected to an artificial passive hip joint mounted to the seat post.

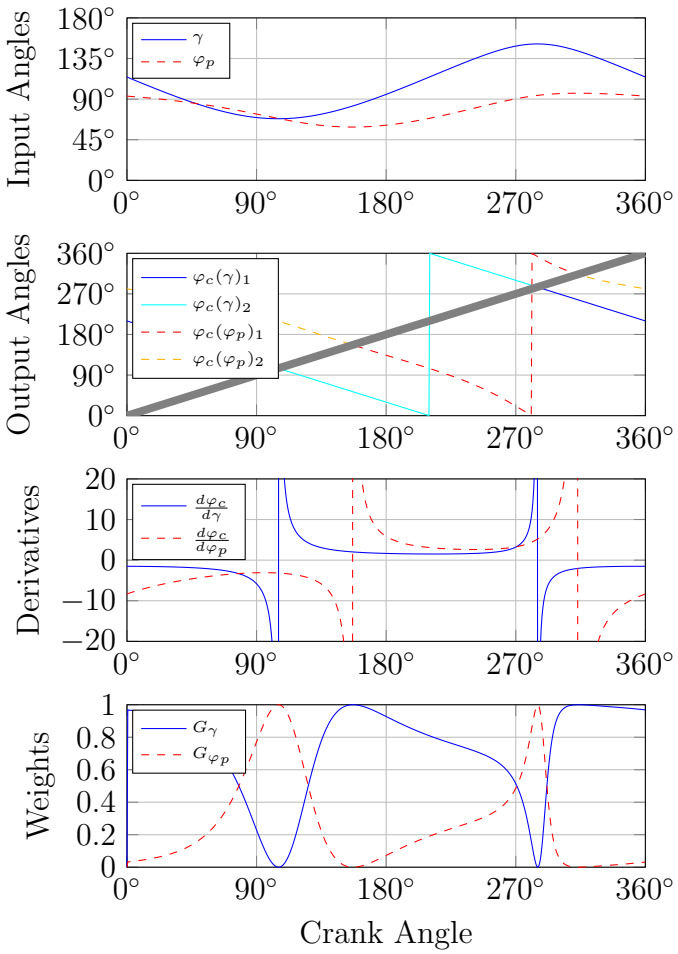

Figure 6.2: Theoretical plots of ideal four bar behavior. The input angles were generated from the inverses of (6.3) and (6.4) as φ_c was swept from 0 to 360°. The second plot shows both possible values of φ_c from (6.3) and (6.4), along with the true value of φ_c. The third plot shows how $d\varphi_c/d\gamma$ and $d\varphi_c/d\varphi_p$ evolve as functions of φ_c, indicating the two singularities in the inverse mappings. The fourth plot shows the weights G_γ and G_{φ_p} used to combine the matching outputs of (6.3) and (6.4) to generate the estimate of φ_c.

The internal signals of the prosthesis (knee angle and shank orientation) were logged simultaneously with external motion capture. The data from the prosthesis were streamed to MATLAB Simulink (running Real-time Windows Target) via a Controller Area Network (CAN) interface at a rate of 250 Hz. In the motion capture software environment, five rigid bodies were defined with reflective markers corresponding to the bicycle frame, crank arm, prosthetic foot, prosthetic shank, and artificial thigh. The markers were tracked with a 12 camera motion capture package from Natural Point at 120 fps. These data were then exported to MATLAB for post processing. Principle component analysis was performed on the set of all marker locations for each joint axis. The mean direction of the third principle components of all the axes was used to reduce the data to 2 dimensions. The resulting data were then used to compute the link lengths and angles of the mechanism. A photograph of the setup, along with the motion capture model determined by the markers, is shown in Fig. 6.3.

1.4.1 Parameter Estimation

Upon startup, the algorithm must first obtain sufficient data from the prosthesis in order to converge on the Freudenstein coefficients. A plot of the coefficient estimates is shown in Fig. 6.4. A comparison of the link lengths as determined by both the motion capture system and the prosthesis is provided in Table 11.

Table 11: Determination of four-bar link lengths

Link	Motion Capture		Prosthesis	
	μ (m)	σ (m)	μ (m)	σ (m)
r_0	0.751	0.002	0.732	0.006
r_t	0.335	0.003	0.319	0.005
r_p	0.611	0.001	0.610	0.000
r_c	0.167	0.008	0.163	0.003

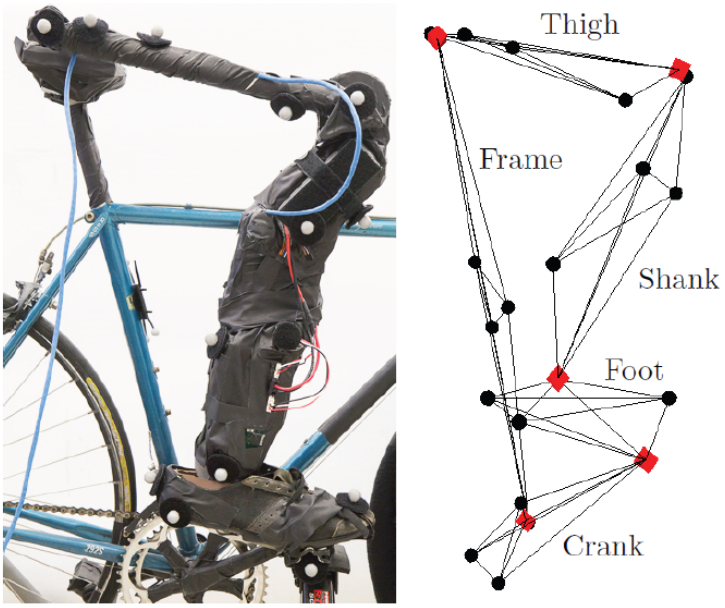

(a) photograph (b) motion capture model

Figure 6.3: The powered prosthesis configured on the bicycle (a) and the motion capture model (b). The red squares in (b) denote the joint axes.

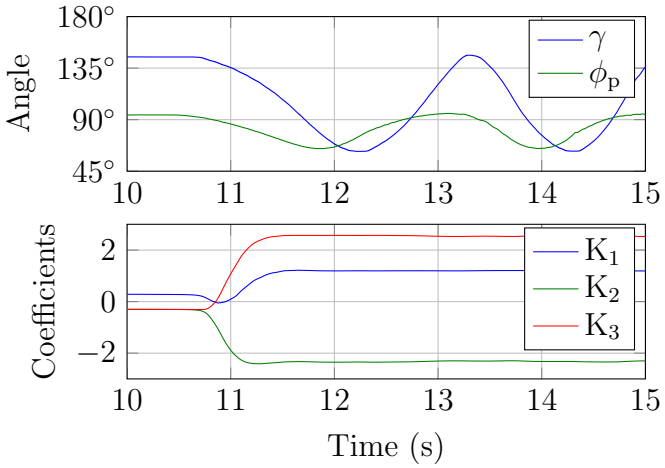

Figure 6.4: Convergence of Freudenstein coefficients using RLS.

1.4.2 Crank Angle Estimation

The error in the crank angle measure over three cycles after parameter convergence is shown in Fig. 6.5. Also included in Fig. 6.5 are the angular errors for each independent estimate of the crank angle before their linear combination using the gains calculated in the previous section. Note that the effect of the singularities is clearly present in each signal, and also that these errors are effectively minimized using the fusion technique described. The measured and estimated crank angles from an entire trial including forward and backward rotation are plotted as functions of time in Fig. 6.6. In this trial the crank was moved in both directions and held in place at several locations. The maximum error after parameter convergence in this trial was approximately 20° (around 19 seconds, when the crank changes direction).

1.5 Conclusion

The presented algorithm robustly avoids singularities from both measurements for the geometry used in the experiment, and estimates the crank angle within 15° when the hip joint is constrained and the bicycle is driven in the forward direction by the contralateral crank arm. Future work will include assessing the estimator with an amputee subject, and, subsequently, using the estimate to time the delivery of knee torque during the power stroke in order to supplement the subject's effort during steady-state cycling.

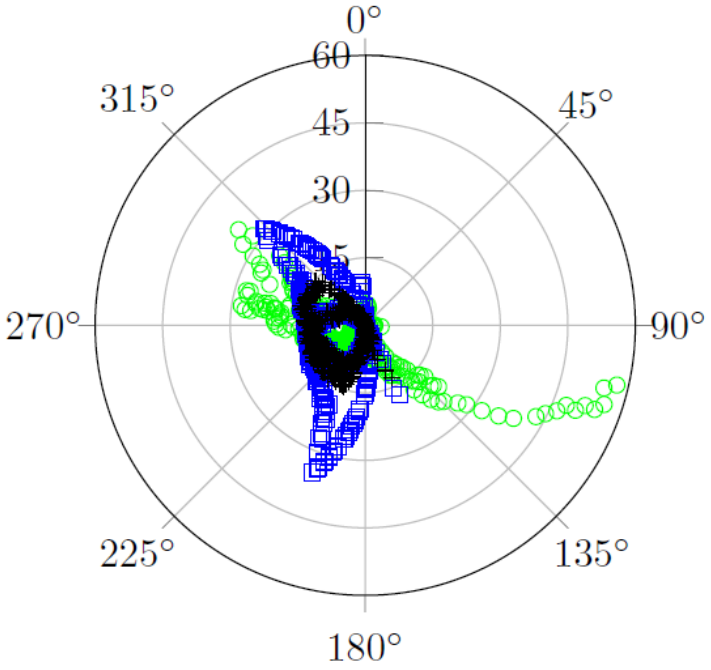

Figure 6.5: Error as a function of crank angle. The error from the γ-based estimate is denoted by blue squares, the error from the φ_p-based estimate by green circles, and the combined estimate by black crosses.

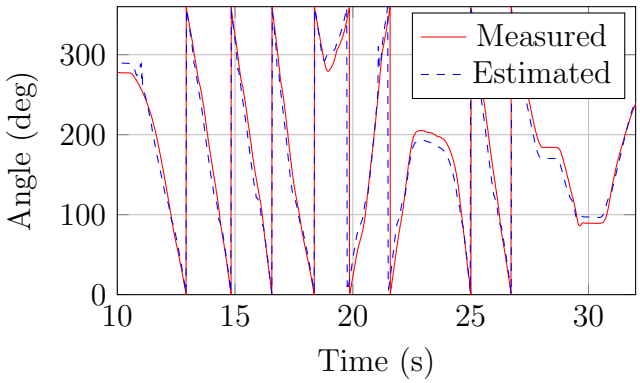

Figure 6.6: Crank angle as measured by the motion capture system and estimated by the prosthesis for the trial showing forward and backward rotation.

1.6 Acknowledgment

The motion capture data used in the experiment were saved as a C3D file type. The data were imported to MATLAB using a script written by Q. Youn Hong, which uses code written by Alan Morris and Jaap Harlaar. The files used were downloaded from: http://mocap.cs.cmu.edu/tools.php on January 11, 2014.

2. Addendum to Manuscript 5: Equation Derivations

Derivations for the equations used in Manuscript 5 are now provided. The derivation of Freudenstein's equation, [111], is performed for the conventions shown in Fig. 6.1. The equation is then solved explicitly by following the form demonstrated in [112].

2.1 Equations 6.1 and 6.2: Freudenstein's Equation ($\varphi_t \leftrightarrow \varphi_p$)

The absolute angles can be found from the loop closure equation. The equation that is generated is Freudenstein's equation, and it can be written for the relationship between any two absolute link angles.

$$\vec{r_c} + \vec{r_p} = \vec{r_0} + \vec{r_t} \tag{6.9}$$

For planar systems, it is convenient to cast this vector equation into a scalar, complex equation.

$$r_c e^{i\varphi_c} + r_p e^{i\varphi_p} = r_0 e^{i\varphi_0} + r_t e^{i\varphi_t} \tag{6.10}$$

At this point we must decide which variable to eliminate (φ_t, φ_p, or φ_c) in order to derive a relationship between the other two. In this case, we want to eliminate φ_c. In order to do so, we rearrange (6.10).

$$r_c e^{i\varphi_c} = r_0 e^{i\varphi_0} + r_t e^{i\varphi_t} - r_p e^{i\varphi_p} \tag{6.11}$$

Now we can multiply (6.11) by its complex conjugate, which will drop φ_c from the expression.

$$r_c^2 = (r_0 e^{i\varphi_0} + r_t e^{i\varphi_t} - r_p e^{i\varphi_p})(r_0 e^{-i\varphi_0} + r_t e^{-i\varphi_t} - r_p e^{-i\varphi_p}) \tag{6.12}$$

Now simplify (6.12).

$$\begin{aligned} r_c^2 =& r_0^2 + r_0 r_t e^{i(\varphi_0-\varphi_t)} - r_0 r_p e^{i(\varphi_0-\varphi_p)} \\ &+ r_t^2 + r_t r_0 e^{i(\varphi_t-\varphi_0)} - r_t r_p e^{i(\varphi_t-\varphi_p)} \\ &+ r_p^2 - r_p r_0 e^{i(\varphi_p-\varphi_0)} - r_p r_t e^{i(\varphi_p-\varphi_t)} \end{aligned} \tag{6.13}$$

Now group the exponential terms with similar arguments.

$$\begin{aligned} r_c^2 =& r_0^2 + r_t^2 + r_p^2 \\ &+ r_0 r_t [e^{i(\varphi_t-\varphi_0)} + e^{-i(\varphi_t-\varphi_0)}] \\ &- r_0 r_p [e^{i(\varphi_p-\varphi_0)} + e^{-i(\varphi_p-\varphi_0)}] \\ &- r_t r_p [e^{i(\varphi_t-\varphi_p)} + e^{-i(\varphi_t-\varphi_p)}] \end{aligned} \tag{6.14}$$

The exponentials can be replaced using the relation $2\cos\theta = e^{i\theta} + e^{-i\theta}$.

$$\begin{aligned} r_c^2 =& r_0^2 + r_t^2 + r_p^2 \\ &+2r_0 r_t \cos(\varphi_t - \varphi_0) \\ &-2r_0 r_p \cos(\varphi_p - \varphi_0) \\ &-2r_t r_p \cos(\varphi_t - \varphi_p) \end{aligned} \tag{6.15}$$

Some rearranging is in order.

$$\frac{r_0}{r_p}\cos(\varphi_t - \varphi_0) - \frac{r_0}{r_t}\cos(\varphi_p - \varphi_0) + \frac{r_0^2 + r_t^2 + r_p^2 - r_c^2}{2r_t r_p} = \cos(\varphi_t - \varphi_p) \tag{6.16}$$

At this point it is customary to collect the constants into three coefficients.

$$\boxed{K_1\cos(\varphi_t - \varphi_0) + K_2\cos(\varphi_p - \varphi_0) + K_3 = \cos(\varphi_t - \varphi_p)} \tag{6.17}$$

where

$$\boxed{\begin{aligned} K_1 &= \tfrac{r_0}{r_p} \\ K_2 &= -\tfrac{r_0}{r_c} \\ K_3 &= \tfrac{r_0^2 + r_t^2 + r_p^2 - r_c^2}{2r_t r_p} \end{aligned}} \tag{6.18}$$

Eq. (6.17) is the implicit formulation of Freudenstein's equation for the relationship between φ_t and φ_p. It is often written with the assumption that $\varphi_0 = 0$. The Freudenstein coefficients, K_{1-3}, will differ depending on the two angles of interest, but the form of (6.17) will remain consistent.

2.2 Equation 6.3: $\varphi_c(\gamma)$ - Law of Cosines

The knee angle is typically defined to be positive in flexion and zero at full knee extension. This value is denoted by θ_k in Fig. 6.1. The supplementary angle, γ, will be a simpler value to use for crank estimation, however, so the following derivation will be in terms of γ instead of θ_k. The relationship between γ and φ_c can be found using the law of cosines.

$$\|\overline{HP}\|^2 = r_p^2 + r_t^2 - 2r_p r_t \cos\gamma \tag{6.19}$$

Similarly,

$$\|\overline{HP}\|^2 = r_c^2 + r_0^2 - 2r_c r_0 \cos\left(\varphi_0 - \varphi_c\right) \tag{6.20}$$

Eqns. (6.19) and (6.20) can be combined to eliminate $\overline{HP}$, yielding an expression relating γ and φ_c.

$$r_p^2 + r_t^2 - 2r_p r_t \cos\gamma = r_c^2 + r_0^2 - 2r_c r_0 \cos\left(\varphi_0 - \varphi_c\right) \tag{6.21}$$

Eq. (6.21) can be solved explicitly for both the forward and inverse problems.

$$\boxed{\gamma = \arccos\left(\frac{-r_c^2 - r_0^2 + r_p^2 + r_t^2 + 2r_c r_0 \cos\left(\varphi_0 - \varphi_c\right)}{2r_p r_t}\right)} \tag{6.22}$$

$$\boxed{\varphi_c = \varphi_0 - \arccos\left(\frac{r_c^2 + r_0^2 - r_p^2 - r_t^2 + 2r_p r_t \cos\gamma}{2r_c r_0}\right)} \tag{6.23}$$

2.3 Equation 6.4: $\varphi_c(\varphi_p)$ - Explicit Solution of Freudenstein

Freudenstein's equation can be explicitly solved in closed form for either the input or the output angles. In this section we will solve for φ_c as a function of φ_p.

We will start first with Freudenstein's equation reformulated for $\varphi_c \leftrightarrow \varphi_p$.

$$K_1 \cos(\varphi_c - \varphi_0) + K_2 \cos(\varphi_p - \varphi_0) + K_3 = \cos(\varphi_c - \varphi_p) \tag{6.24}$$

where

$$\begin{aligned} K_1 &= \tfrac{r_0}{r_p} \\ K_2 &= \tfrac{r_0}{r_c} \\ K_3 &= \tfrac{r_t^2 - r_c^2 - r_p^2 - r_0^2}{2 r_c r_p} \end{aligned} \tag{6.25}$$

The terms containing φ_c on both sides of (6.24) can be expanded with the sum-difference formula for cosine ($\cos(u \pm v) = \cos u \cos v \mp \sin u \sin v$).

$$K_1 \left(\cos\varphi_c \cos\varphi_0 + \sin\varphi_c \sin\varphi_0\right) + K_2 \cos\left(\varphi_p - \varphi_0\right) + K_3 = \cos\varphi_c \cos\varphi_p + \sin\varphi_c \sin\varphi_p \tag{6.26}$$

All sine and cosine functions containing φ_c can be replaced using the following relations.

$$\sin\theta = \frac{2\tan(\frac{1}{2}\theta)}{1 + \tan^2(\frac{1}{2}\theta)} \tag{6.27}$$

and

$$\cos\theta = \frac{1 - \tan^2(\frac{1}{2}\theta)}{1 + \tan^2(\frac{1}{2}\theta)} \tag{6.28}$$

such that

$$K_1\left(\frac{1-\tan^2\left(\frac{1}{2}\varphi_c\right)}{1+\tan^2\left(\frac{1}{2}\varphi_c\right)}\cos\varphi_0+\frac{2\tan\left(\frac{1}{2}\varphi_c\right)}{1+\tan^2\left(\frac{1}{2}\varphi_c\right)}\sin\varphi_0\right)+K_2\cos(\varphi_p-\varphi_0)+K_3 = \frac{1-\tan^2\left(\frac{1}{2}\varphi_c\right)}{1+\tan^2\left(\frac{1}{2}\varphi_c\right)}\cos\varphi_p+\frac{2\tan\left(\frac{1}{2}\varphi_c\right)}{1+\tan^2\left(\frac{1}{2}\varphi_c\right)}\sin\varphi_p \tag{6.29}$$

Now multiply through by the denominator.

$$\begin{aligned} K_1\left(\cos\varphi_0-\tan^2\left(\frac{1}{2}\varphi_c\right)\cos\varphi_0+2\tan\left(\frac{1}{2}\varphi_c\right)\sin\varphi_0\right) \\ +K_2\cos(\varphi_p-\varphi_0)\left(1+\tan^2\left(\frac{1}{2}\varphi_c\right)\right) \\ +K_3\left(1+\tan^2\left(\frac{1}{2}\varphi_c\right)\right) \\ =\left(1-\tan^2\left(\frac{1}{2}\varphi_c\right)\right)\cos\varphi_p+\left(2\tan\left(\frac{1}{2}\varphi_c\right)\right)\sin\varphi_p \end{aligned} \tag{6.30}$$

Rearrange.

$$\begin{aligned} (-K_1\cos\varphi_0+K_2\cos(\varphi_p-\varphi_0)+K_3+\cos\varphi_p)\tan^2\left(\frac{1}{2}\varphi_c\right) \\ +(2K_1\sin\varphi_0-2\sin\varphi_p)\tan\left(\frac{1}{2}\varphi_c\right) \\ +(K_1\cos\varphi_0+K_2\cos(\varphi_p-\varphi_0)+K_3-\cos\varphi_p)=0 \end{aligned} \tag{6.31}$$

Define the following terms to simplify (6.32).

$$A=-K_1\cos\varphi_0+K_2\cos(\varphi_p-\varphi_0)+K_3+\cos\varphi_p \tag{6.32}$$

$$B=2K_1\sin\varphi_0-2\sin\varphi_p \tag{6.33}$$

$$C=K_1\cos\varphi_0+K_2\cos(\varphi_p-\varphi_0)+K_3-\cos\varphi_p \tag{6.34}$$

Substituting in these relations yields a quadratic equation in $\tan\left(\frac{1}{2}\varphi_c\right)$.

$$A\tan^2\left(\frac{1}{2}\varphi_c\right) + B\tan\left(\frac{1}{2}\varphi_c\right) + C = 0 \tag{6.35}$$

for which the explicit solution is given by

$$\boxed{\varphi_c = 2\arctan\left(\frac{-B \pm \sqrt{B^2 - 4AC}}{2A}\right)} \tag{6.36}$$

In general, eq. 6.36 will have different A, B, and C depending on the input and output defined. We will call the mapping from φ_c to φ_p and φ_t the forward mapping, and the mapping from φ_p and φ_t to φ_c the inverse mapping. The coefficients for both cases are listed below. The input angle is denoted by φ_x to indicate that either φ_p or φ_t can be used. The selection of Freudenstein coefficients will determine whether the forward mapping applies to φ_p or φ_t. The definitions of the K's are restated below.

$$\boxed{\begin{aligned} A = &\quad K_1\cos(\varphi_c - \varphi_0) - K_2\cos\varphi_0 + K_3 + \cos\varphi_c \\ \varphi_x = f(\varphi_c) : B = &\quad 2K_2\sin\varphi_0 - 2\sin\varphi_c \\ C = &\quad K_1\cos(\varphi_c - \varphi_0) + K_2\cos\varphi_0 + K_3 - \cos\varphi_c \end{aligned}} \tag{6.37}$$

$$\boxed{\begin{aligned} A_{inv} = &\quad -K_1\cos\varphi_0 + K_2\cos(\varphi_x - \varphi_0) + K_3 + \cos\varphi_x \\ \varphi_c = f(\varphi_x) : B_{inv} = &\quad 2K_1\sin\varphi_0 - 2\sin\varphi_x \\ C_{inv} = &\quad K_1\cos\varphi_0 + K_2\cos(\varphi_x - \varphi_0) + K_3 - \cos\varphi_x \end{aligned}} \tag{6.38}$$

$$\boxed{\begin{aligned} K_{p1} = &\quad \tfrac{r_0}{r_p} \\ K_{p2} = &\quad \tfrac{r_0}{r_c} \\ K_{p3} = &\quad \tfrac{r_t^2 - r_c^2 - r_p^2 - r_0^2}{2r_c r_p} \end{aligned}} \tag{6.39}$$

$$\boxed{\begin{aligned} K_{t1} &= -\frac{r_0}{r_t} \\ K_{t2} &= \frac{r_0}{r_c} \\ K_{t3} &= \frac{-r_p^2+r_c^2+r_t^2+r_0^2}{2r_c r_t} \end{aligned}} \tag{6.40}$$

2.4 Equation 6.5: Implicit Derivative of $\varphi_c(\gamma)$

Since we have expressions relating all the angles of the mechanism, we do not need to explicitly solve for derivatives as functions of a single parameter. Instead, we can formulate an implicit relation to easily calculate $d\varphi_c/d\gamma$.

To start, we can differentiate (6.21) with respect to time.

$$\frac{d}{dt}\left(r_p^2 + r_t^2 - 2r_p r_t \cos\gamma\right) = \frac{d}{dt}\left(r_c^2 + r_0^2 - 2r_c r_0 \cos\left(\varphi_0 - \varphi_c\right)\right) \tag{6.41}$$

The only variables that will change in time are γ and φ_c, such that

$$2r_p r_t \sin\gamma \frac{d\gamma}{dt} = -2r_c r_0 \sin\left(\varphi_0 - \varphi_c\right) \frac{d\varphi_c}{dt} \tag{6.42}$$

which yields

$$\boxed{\frac{d\varphi_c}{d\gamma} = -\frac{r_p r_t \sin\gamma}{r_c r_0 \sin\left(\varphi_0 - \varphi_c\right)}} \tag{6.43}$$

2.5 Equation 6.6: Implicit Derivative of $\varphi_c(\varphi_p)$

In a manner similar to the derivation of $d\varphi_c/d\gamma$, the derivative of $\varphi_c(\varphi_p)$ can be expressed implicitly. The original loop closure expression can be differentiated with respect to time, and then the result can be used to determine changes in the output relative to changes in the input. The rate of change of the loop closure equation with respect to time is

$$\frac{d}{dt}\left(r_c e^{i\varphi_c}\right) + \frac{d}{dt}\left(r_p e^{i\varphi_p}\right) = \frac{d}{dt}\left(r_0 e^{i\varphi_0}\right) + \frac{d}{dt}\left(r_t e^{i\varphi_t}\right) \tag{6.44}$$

Which simplifies since the link lengths and the orientation of the base link do not change with time.

$$r_c \frac{d}{dt}\left(e^{i\varphi_c}\right) + r_p \frac{d}{dt}\left(e^{i\varphi_p}\right) = r_t \frac{d}{dt}\left(e^{i\varphi_t}\right) \tag{6.45}$$

Evaluating the derivatives yields

$$\frac{d\varphi_c}{dt} r_c e^{i\varphi_c} + \frac{d\varphi_p}{dt} r_p e^{i\varphi_p} = \frac{d\varphi_t}{dt} r_t e^{i\varphi_t} \tag{6.46}$$

And now any one of the derivatives can be eliminated by multiplying the equation by $e^{-i\varphi}$. We will eliminate $\frac{d\varphi_t}{dt}$ in order to obtain an expression for $\frac{d\varphi_c}{d\varphi_p}$.

$$\frac{d\varphi_c}{dt} r_c e^{i\varphi_c} e^{-i\varphi_t} + \frac{d\varphi_p}{dt} r_p e^{i\varphi_p} e^{-i\varphi_t} = \frac{d\varphi_t}{dt} r_t e^{i\varphi_t} e^{-i\varphi_t} \tag{6.47}$$

which simplifies to

$$\frac{d\varphi_c}{dt} r_c e^{i(\varphi_c - \varphi_t)} + \frac{d\varphi_p}{dt} r_p e^{i(\varphi_p - \varphi_t)} = \frac{d\varphi_t}{dt} r_t \tag{6.48}$$

Since the right hand side of (6.48) is only real, then the imaginary portion of the equation will not contain $\frac{d\varphi_t}{dt}$.

$$\frac{d\varphi_c}{dt} r_c \sin\left(\varphi_c - \varphi_t\right) + \frac{d\varphi_p}{dt} r_p \sin\left(\varphi_p - \varphi_t\right) = 0 \tag{6.49}$$

This expression can be rearranged to express $\frac{d\varphi_c}{d\varphi_p}$.

$$\boxed{\frac{d\varphi_c}{d\varphi_p} = -\frac{r_p \sin\left(\varphi_p - \varphi_t\right)}{r_c \sin\left(\varphi_c - \varphi_t\right)}} \tag{6.50}$$

CHAPTER VII

CONCLUSION

This dissertation has presented a variety of control systems for various applications in a powered knee and ankle prosthesis. Beginning with the finite state-based impedance control framework previously presented, this technique was applied to two new problems: that of active stumble recovery and the navigation of stairs. Subsequently, a new approach, consisting of a combination of impedance-based control and trajectory control, was applied to the original problem of variable cadence level ground walking. The approach was shown to achieve a continuously variable cadence with significantly fewer tuned parameters than finite state-based impedance control alone. A similar hybrid approach was implemented for a bilateral intervention, which additionally leveraged communication between the prostheses for enhanced safety and stability. Finally, an algorithm to adaptively estimate the angle of the crankshaft of a bicycle was presented and tested on a prosthesis prototype.

The eclectic nature of the presented work in this dissertation should emphasize the extreme versatility of a powered transfemoral prosthesis. This versatility stems from the fact that all the prototypes used in this work were designed to include as few passive components as possible to achieve the desired behavior. With full software control of the torque supplied to the knee and ankle joints, the limitations of the prosthesis are defined solely by the sophistication of the control system and the sensor signals available.

1. Clinical Assessment and Statistical Significance

This work is interdisciplinary by nature, and an important aim has been to develop a device that has the potential to provide a clinical benefit to the amputee population. The scope of such a project must have its limits, however, and the process of designing and carrying out a clinical trial on a statistically significant portion of the amputee population lies outside of these limits. Furthermore, such a large scale study is not an effective use of resources for a laboratory prototype that is likely to undergo significant revisions before approval from the Food and Drug Administration (FDA) or its appearance as a commercially available medical device. Consequently, the assessments achieved in this work have been the verification of the effectiveness of the design and control methodologies, as determined by the biomechanical comparisons of a limited number of amputee subjects using both the prototype devices and their daily-use prostheses.

2. Commercialization and Competing Interests

The prostheses used in this work were laboratory prototypes, although they were designed with practical considerations in mind. The control systems presented in this work have also been developed with a concern for practical implementation. A specific goal through this effort has been to design and build devices that have the potential to commercially translate. Along with the publications this work has produced, several provisional patent applications have been filed by the Vanderbilt University Office of Technology Transfer. Some of these applications have been licensed by Freedom Innovations, LLC, a US-based manufacturer of prosthetic devices. I am a co-inventor of the intellectual property licensed by Vanderbilt University to Freedom Innovations, and, as such, have a limited financial interest in the successful translation of this technology to the commercial market.

3. Future Work

Especially in the field of engineering, it is never clear when a system, project, or effort is complete. In my mind, there are two major directions for this project: further biomechanical assessment and further hardware and control development. The Center for Intelligent Mechatronics is primarily a mechanical engineering laboratory, although its focus as of late has moved firmly into the realm of rehabilitation robotics, which necessarily includes biomedical and biomechanical engineering. With mature prototypes, it is now feasible to fit more subjects and take more clinically oriented measurements, such as heart rate, oxygen consumption, carbon dioxide production, etc. As stated earlier, statistically significant trials on large sample sizes will most likely remain outside of the abilities of the lab for the near term, but incorporating smaller assessments into the development cycle has the potential to speed iterations and improve feedback. These sorts of studies move slightly outside the traditional realm of mechanical engineering, and they may attract students and researchers with more clinical mindsets. All the better, if this is the case, though, as working directly with amputee subjects provides invaluable insights as to what the real issues are for the target population.

With regard to hardware and control development, a key feature of the prototypes described herein is their versatility with respect to programmable behaviors, as mentioned at the beginning of this chapter. With minimal open loop passive components, an extremely wide variety of lower limb activities can be explored with these devices. Cycling is a perfect example, and future work should necessarily include building a full control system based upon the crank angle estimator presented in Chapter 6. All lower limb activities are fair game, though power limitations will generally prevent high-intensity activities such as many forms of rigorous exercise.

Simplicity is also key for the translation of these devices. The hybrid control

scheme presented in Chapter 4 significantly reduces the parameterization of the level walking controller, though more simplification is surely possible and would reduce the effort required by prosthetists when fitting new patients. With more experience on a wider variety of subjects (and also with a wider variety of researchers and prosthetists fitting the devices), there will be a clearer picture of what the core parameter set is for the majority of users. It is my hope and belief that this set is actually quite small and tractable.

For a more thorough discussion concerning the state of the art and future directions for this work, the interested reader is directed to an article that appeared in the 210th issue of the 5th volume of Science Translational Medicine entitled "Realizing the promise of robotic leg prostheses" [113]. This article highlights the fundamental challenges to the design and control of lower limb prostheses, and describes some presumed biomechanical benefits which provide some guidelines for assessments yet to come.

The supporting technologies for self-contained robotic devices continue to evolve. Few could have predicted that MEMS-based gyroscopes and accelerometers would be as cheap and pervasive as they are now. Research efforts in alternative energy are also likely to continue to have a significant impact on the micro level as well as the macro. It will be exciting to follow, contribute, and share in the progress that will surely continue to be made.

REFERENCES

[1] K. Fite, J. Mitchell, F. Sup, and M. Goldfarb, "Design and control of an electrically powered knee prosthesis," in *Proc. IEEE Int. Conf. Rehabil. Robot.*, 2007, pp. 902–905.

[2] K. H. Ha, H. A. Varol, and M. Goldfarb, "Volitional control of a prosthetic knee using surface electromyography," *IEEE Trans. Biomed. Eng.*, vol. 58, no. 1, pp. 144–51, 2011.

[3] B. E. Lawson, H. A. Varol, and M. Goldfarb, "Standing stability enhancement with an intelligent powered transfemoral prosthesis," *IEEE Trans. Biomed. Eng.*, vol. 58, no. 9, pp. 2617–24, 2011.

[4] F. Sup, H. A. Varol, and M. Goldfarb, "Upslope walking with a powered knee and ankle prosthesis: Initial results with an amputee subject," *IEEE Trans. Neural Syst. Rehabil. Eng.*, vol. 19, no. 1, pp. 71–8, 2011.

[5] F. Sup, H. A. Varol, J. Mitchell, T. J. Withrow, and M. Goldfarb, "Preliminary evaluations of a self-contained anthropomorphic transfemoral prosthesis," *IEEE ASME Trans. Mechatron.*, vol. 14, no. 6, pp. 667–676, 2009.

[6] H. A. Varol, F. Sup, and M. Goldfarb, "Multiclass real-time intent recognition of a powered lower limb prosthesis," *IEEE Trans. Biomed. Eng.*, vol. 57, no. 3, pp. 542–51, 2010.

[7] K. Ziegler-Graham, E. J. MacKenzie, P. L. Ephraim, T. G. Travison, and R. Brookmeyer, "Estimating the prevalence of limb loss in the United States: 2005 to 2050," *Arch. Phys. Med. Rehabil.*, vol. 89, no. 3, pp. 422–9, 2008.

[8] M. F. Owings and L. J. Kozak, "Ambulatory and inpatient procedures in the

United States, 1996," *National Center for Health Statistics. Vital Health Stat 13*, no. 139, 1998.

[9] P. F. Adams, G. E. Hendershot, and M. A. Marano, "Current estimates from the National Health Interview Survey, 1996," *National Center for Health Statistics. Vital Health Stat 10*, no. 200, 1999.

[10] C. Gauthier-Gagnon, M. C. Grise, and D. Potvin, "Enabling factors related to prosthetic use by people with transtibial and transfemoral amputation," *Arch. Phys. Med. Rehabil.*, vol. 80, no. 6, pp. 706–13, 1999.

[11] B. J. Hafner and D. G. Smith, "Differences in function and safety between medicare functional classification level-2 and -3 transfemoral amputees and influence of prosthetic knee joint control," *J. Rehabil. Res. Dev.*, vol. 46, no. 3, pp. 417–33, 2009.

[12] S. K. Au, J. Weber, and H. Herr, "Powered ankle-foot prosthesis improves walking metabolic economy," *IEEE Trans. Robot.*, vol. 25, no. 1, pp. 51–66, 2009.

[13] S. K. Au, H. Herr, J. Weber, and E. C. Martinez-Villalpando, "Powered ankle-foot prosthesis for the improvement of amputee ambulation," in *Conf. Proc. IEEE Eng. Med. Biol. Soc.*, 2007, pp. 3020–6.

[14] S. Au, M. Berniker, and H. Herr, "Powered ankle-foot prosthesis to assist level-ground and stair-descent gaits," *IEEE Trans. Neural Networks*, vol. 21, no. 4, pp. 654–66, 2008.

[15] S. Au and H. Herr, "Powered ankle-foot prosthesis," *IEEE Robot. Automat. Mag.*, vol. 15, no. 3, pp. 52–59, 2008.

[16] E. C. Martinez-Villalpando, H. Herr, and M. Farrell, "Estimation of ground reaction force and zero moment point on a powered ankle-foot prosthesis," in *Conf. Proc. IEEE Eng. Med. Biol. Soc.*, 2007, pp. 4687–92.

[17] M. A. Holgate, J. K. Hitt, R. D. Bellman, T. G. Sugar, and K. W. Hollander, "The SPARKy (Spring Ankle with Regenerative Kinetics) project: Choosing a DC motor based actuation method," in *Conf. Proc. IEEE/RAS-EMBS Biomed. Robot. Biomechatron.*, 2008, pp. 163–168.

[18] R. D. Bellman, M. A. Holgate, and T. G. Sugar, "Sparky 3: Design of an active robotic ankle prosthesis with two actuated degrees of freedom using regenerative kinetics," in *Conf. Proc. IEEE/RAS-EMBS Biomed. Robot. Biomechatron.*, 2008, pp. 511–516.

[19] J. Joseph G. Wells, P. A. Voglewede, and D. N. Rocheleau, "Design for improved trans-tibial prosthetic devices using four bar mechanisms," in *ASME 2005 International Design Engineering Technical Conferences and Computers and Information in Engineering Conference*, 2005, pp. 467–473.

[20] M. R. Tucker and K. B. Fite, "Mechanical damping with electrical regeneration for a powered transfemoral prosthesis," in *IEEE/ASME Int. Conf. Advanced Intelligent Mechatronics*, 2010, pp. 13–18.

[21] S.-K. Wu, G. Waycaster, and X. Shen, "Active knee prosthesis control with electromyography," in *ASME Int. Conf. Dynamic Systems and Control*, 2010, pp. 785–791.

[22] C. D. Hoover and K. B. Fite, "A configuration dependent muscle model for the myoelectric control of a transfemoral prosthesis," in *Proc. IEEE Int. Conf. Rehabil. Robot.*, 2011, pp. 1–6.

[23] O. T. Altinoz and A. Yilmaz, "Prediction of knee angle from accelerometer data for microcontroller implementation of semi-active knee prosthesis," in *Biomedical Engineering Meeting (BIYOMUT), 2010 15th National*, 2010, pp. 1–4.

[24] B. J. Bergelin, J. O. Mattos, J. G. Wells Jr, and P. A. Voglewede, "Concept through preliminary bench testing of a powered lower limb prosthetic device," *ASME J. Mech. Robot.*, vol. 2, no. 4, pp. 41 005–41 013, 2010.

[25] B. J. Bergelin and P. A. Voglewede, "Design of an active ankle-foot prosthesis utilizing a four-bar mechanism," *J. Mech. Design*, vol. 134, no. 6, p. 061004, 2012.

[26] B. G. A. Lambrecht and H. Kazerooni, "Design of a semi-active knee prosthesis," in *IEEE Int. Conf. Robot. Autom.*, 2009, Conference Proceedings, pp. 639–645.

[27] R. Suzuki, T. Sawada, N. Kobayashi, and E. P. Hofer, "Control method for powered ankle prosthesis via internal model control design," in *IEEE Int. Conf. Mechatronics Automat.*, 2011, pp. 237–242.

[28] R. Versluys, A. Desomer, G. Lenaerts, M. Van Damme, P. Beyl, G. Van der Perre, L. Peeraer, and D. Lefeber, "A pneumatically powered below-knee prosthesis: Design specifications and first experiments with an amputee," in *Conf. Proc. IEEE/RAS-EMBS Biomed. Robot. Biomechatron.*, 2008, pp. 372–377.

[29] F. Sup, A. Bohara, and M. Goldfarb, "Design and control of a powered transfemoral prosthesis," *Int. J. Robot. Res.*, vol. 27, no. 2, pp. 263–273, 2008.

[30] F. Sup, "A powered self-contained knee and ankle prosthesis for near normal gait in transfemoral amputees," Dissertation, Vanderbilt University, 2009.

[31] H. A. Varol, "Progress towards the intelligent control of a powered transfemoral prosthesis," Dissertation, Vanderbilt University, 2009.

[32] H. A. Varol, F. Sup, and M. Goldfarb, "Powered sit-to-stand and assistive stand-to-sit framework for a powered transfemoral prosthesis," 2009, pp. 645–651.

[33] B. E. Lawson, H. Atakan Varol, F. Sup, and M. Goldfarb, "Stumble detection and classification for an intelligent transfemoral prosthesis," in *Conf. Proc. IEEE Eng. Med. Biol. Soc.*, 2010, pp. 511–4.

[34] B. Lawson, H. A. Varol, A. Huff, E. Erdemir, and M. Goldfarb, "Control of stair ascent and descent with a powered transfemoral prosthesis," *IEEE Trans. Neural Syst. Rehabil. Eng.*, vol. 21, no. 3, pp. 466–473, 2013.

[35] L. Hargrove, A. Simon, R. Lipschutz, S. Finucane, and T. Kuiken, "Non-weight-bearing neural control of a powered transfemoral prosthesis," *J. Neuroeng. Rehabil.*, vol. 10, no. 1, p. 62, 2013.

[36] L. J. Hargrove, A. M. Simon, A. J. Young, R. D. Lipschutz, S. B. Finucane, D. G. Smith, and T. A. Kuiken, "Robotic leg control with EMG decoding in an amputee with nerve transfers," *N. Engl. J. Med.*, vol. 369, no. 13, pp. 1237–42, 2013.

[37] N. Hogan, "Impedance control - An approach to manipulation: 1. Theory," *J. Dyn. Syst-T ASME*, vol. 107, no. 1, pp. 1–7, 1985.

[38] ——, "Impedance control - An approach to manipulation: 2. Implementation," *J. Dyn. Syst-T ASME*, vol. 107, no. 1, pp. 8–16, 1985.

[39] ——, "Impedance control - An approach to manipulation: 3. Applications," *J. Dyn. Syst-T ASME*, vol. 107, no. 1, pp. 17–24, 1985.

[40] A. H. Hansen, D. S. Childress, S. C. Miff, S. A. Gard, and K. P. Mesplay, "The human ankle during walking: Implications for design of biomimetic ankle prostheses," *J. Biomech.*, vol. 37, no. 10, pp. 1467–74, 2004.

[41] D. A. Winter, A. E. Patla, S. Rietdyk, and M. G. Ishac, "Ankle muscle stiffness in the control of balance during quiet standing," *J. Neurophysiol.*, vol. 85, no. 6, pp. 2630–3, 2001.

[42] M. S. Branicky, "Multiple Lyapunov functions and other analysis tools for switched and hybrid systems," *IEEE Trans. Autom. Control*, vol. 43, no. 4, pp. 475–482, 1998.

[43] S. Mastellone, D. M. Stipanovic, and M. W. Spong, "Stability and convergence for systems with switching equilibria," in *Conf. Proc. IEEE Decision and Control*, 2007, pp. 4013–4020.

[44] D. Liberzon and A. S. Morse, "Basic problems in stability and design of switched systems," *IEEE Control Systems Magazine*, vol. 19, no. 5, pp. 59–70, 1999.

[45] R. A. DeCarlo, M. S. Branicky, S. Pettersson, and B. Lennartson, "Perspectives and results on the stability and stabilizability of hybrid systems," *Proceedings of the IEEE*, vol. 88, no. 7, pp. 1069–1082, 2000.

[46] E. Martinez-Villalpando, J. Weber, G. Elliott, and H. Herr, "Design of an agonist-antagonist active knee prosthesis," in *Conf. Proc. IEEE/RAS-EMBS Biomed. Robot. Biomechatron.*, 2008, pp. 529 – 534.

[47] W. C. Miller, M. Speechley, and B. Deathe, "The prevalence and risk factors of falling and fear of falling among lower extremity amputees," *Arch. Phys. Med. Rehabil.*, vol. 82, no. 8, pp. 1031–7, 2001.

[48] A. M. Schillings, B. M. Van Wezel, and J. Duysens, "Mechanically induced stumbling during human treadmill walking," *J. Neurosci. Methods*, vol. 67, no. 1, pp. 11–7, 1996.

[49] A. M. Schillings, B. M. Van Wezel, T. Mulder, and J. Duysens, "Widespread short-latency stretch reflexes and their modulation during stumbling over obstacles," *Brain Res.*, vol. 816, no. 2, pp. 480–6, 1999.

[50] M. Pijnappels, M. F. Bobbert, and J. H. van Dieën, "Contribution of the support limb in control of angular momentum after tripping," *J. Biomech.*, vol. 37, no. 12, pp. 1811–1818, 2004.

[51] ——, "Control of support limb muscles in recovery after tripping in young and older subjects," *Exp. Brain Res.*, vol. 160, no. 3, pp. 326–333, 2005.

[52] ——, "How early reactions in the support limb contribute to balance recovery after tripping," *J. Biomech.*, vol. 38, no. 3, pp. 627–634, 2005.

[53] M. J. Pavol, T. M. Owings, K. T. Foley, and M. D. Grabiner, "Mechanisms leading to a fall from an induced trip in healthy older adults," *The Journals of Gerontology Series A: Biological Sciences and Medical Sciences*, vol. 56, no. 7, pp. M428–M437, 2001.

[54] ——, "Influence of lower extremity strength of healthy older adults on the outcome of an induced trip," *Journal of the American Geriatrics Society*, vol. 50, no. 2, pp. 256–262, 2002.

[55] J. J. Eng, D. A. Winter, and A. E. Patla, "Strategies for recovery from a trip in early and late swing during human walking," *Exp. Brain Res.*, vol. 102, no. 2, pp. 339–49, 1994.

[56] ——, "Intralimb dynamics simplify reactive control strategies during locomotion," *J. Biomech.*, vol. 30, no. 6, pp. 581–8, 1997.

[57] A. M. Schillings, B. M. van Wezel, T. Mulder, and J. Duysens, "Muscular responses and movement strategies during stumbling over obstacles," *J. Neurophysiol.*, vol. 83, no. 4, pp. 2093–102, 2000.

[58] A. M. Schillings, T. Mulder, and J. Duysens, "Stumbling over obstacles in older adults compared to young adults," *J. Neurophysiol.*, vol. 94, no. 2, pp. 1158–68, 2005.

[59] A. Forner Cordero, H. F. Koopman, and F. C. van der Helm, "Multiple-step strategies to recover from stumbling perturbations," *Gait Posture*, vol. 18, no. 1, pp. 47–59, 2003.

[60] A. F. Cordero, H. J. Koopman, and F. C. van der Helm, "Mechanical model of the recovery from stumbling," *Biol. Cybern.*, vol. 91, no. 4, pp. 212–20, 2004.

[61] S. T. Blumentritt, T. Schmals, and R. Jarasch, "Safety of C-Leg: Biomechanical tests," *J. Prosthet. Orthot.*, vol. 21, pp. 2–17, 2009.

[62] D. A. Winter, *The biomechanics and motor control of human gait: Normal, elderly and pathological.* Waterloo, Ontario, Canada: University of Waterloo Press, 1991.

[63] R. Riener, M. Rabuffetti, and C. Frigo, "Stair ascent and descent at different inclinations," *Gait Posture*, vol. 15, no. 1, pp. 32–44, 2002.

[64] S. M. Reid, S. K. Lynn, R. P. Musselman, and P. A. Costigan, "Knee biomechanics of alternate stair ambulation patterns," *Med. Sci. Sports Exerc.*, vol. 39, no. 11, pp. 2005–11, 2007.

[65] B. J. McFadyen and D. A. Winter, "An integrated biomechanical analysis of normal stair ascent and descent," *J. Biomech.*, vol. 21, no. 9, pp. 733–44, 1988.

[66] J. K. Hitt, T. G. Sugar, M. Holgate, and R. Bellman, "An active foot-ankle prosthesis with biomechanical energy regeneration," *J. Med. Devices*, vol. 4, no. 1, 2010.

[67] K. Koganezawa, H. Fujimoto, and I. Kato, "Multifunctional above-knee prosthesis for stairs' walking," *Prosthet. Orthot. Int.*, vol. 11, no. 3, pp. 139–45, 1987.

[68] T. Schmalz, S. Blumentritt, and B. Marx, "Biomechanical analysis of stair ambulation in lower limb amputees," *Gait and Posture*, vol. 25, no. 2, pp. 267–278, 2007.

[69] I. P. Pappas, M. R. Popovic, T. Keller, V. Dietz, and M. Morari, "A reliable gait phase detection system," *IEEE Trans. Neural Syst. Rehabil. Eng.*, vol. 9, no. 2, pp. 113–25, 2001.

[70] J. E. Zachazewski, P. O. Riley, and D. E. Krebs, "Biomechanical analysis of body mass transfer during stair ascent and descent of healthy subjects," *J. Rehabil. Res. Dev.*, vol. 30, no. 4, pp. 412–22, 1993.

[71] J. J. Genin, G. J. Bastien, B. Franck, C. Detrembleur, and P. A. Willems, "Effect of speed on the energy cost of walking in unilateral traumatic lower limb amputees," *Eur. J. Appl. Physiol.*, vol. 103, no. 6, pp. 655–63, 2008.

[72] R. L. Waters, J. Perry, D. Antonelli, and H. Hislop, "Energy cost of walking of amputees: the influence of level of amputation," *J. Bone Joint Surg. Am.*, vol. 58, no. 1, pp. 42–6, 1976.

[73] S. M. Jaegers, J. H. Arendzen, and H. J. de Jongh, "Prosthetic gait of unilateral transfemoral amputees: A kinematic study," *Arch. Phys. Med. Rehabil.*, vol. 76, no. 8, pp. 736–43, 1995.

[74] M. Schmid, G. Beltrami, D. Zambarbieri, and G. Verni, "Centre of pressure displacements in trans-femoral amputees during gait," *Gait Posture*, vol. 21, no. 3, pp. 255–62, 2005.

[75] R. E. Seroussi, A. Gitter, J. M. Czerniecki, and K. Weaver, "Mechanical work adaptations of above-knee amputee ambulation," *Arch. Phys. Med. Rehabil.*, vol. 77, no. 11, pp. 1209–14, 1996.

[76] A. H. Vrieling, H. G. van Keeken, T. Schoppen, E. Otten, J. P. Halbertsma, A. L. Hof, and K. Postema, "Uphill and downhill walking in unilateral lower limb amputees," *Gait Posture*, vol. 28, no. 2, pp. 235–42, 2008.

[77] W. C. Miller, A. B. Deathe, M. Speechley, and J. Koval, "The influence of falling, fear of falling, and balance confidence on prosthetic mobility and social activity among individuals with a lower extremity amputation," *Arch. Phys. Med. Rehabil.*, vol. 82, no. 9, pp. 1238–44, 2001.

[78] R. Tomovic and R. B. McGhee, "A finite state approach to the synthesis of bioengineering control systems," *IEEE Trans. Hum. Factors Electron.*, no. 2, pp. 65–69, 1966.

[79] W. C. Flowers, "Use of an amputee-computer interactive facility in above-knee prosthesis research," in *ACM*, 1974, pp. 335–339.

[80] Z. L. Justin and G. Robert, "Advances in lower-limb prosthetic technology," *Physical medicine and rehabilitation clinics of North America*, vol. 21, no. 1, pp. 87–110, 2010.

[81] R. Jimenez-Fabian and O. Verlinden, "Review of control algorithms for robotic ankle systems in lower-limb orthoses, prostheses, and exoskeletons," *Med. Eng. Phys.*, vol. 34, no. 4, pp. 397–408, 2012.

[82] E. C. Martinez-Villalpando, L. Mooney, G. Elliott, and H. Herr, "Antagonistic active knee prosthesis. A metabolic cost of walking comparison with a variable-damping prosthetic knee," in *Conf. Proc. IEEE Eng. Med. Biol. Soc.*, 2011, pp. 8519–22.

[83] J. E. Colgate and J. M. Brown, "Factors affecting the Z-width of a haptic display," in *IEEE Int. Conf. Robot. Autom.*, 1994, pp. 3205–3210.

[84] S. D. Eppinger and W. P. Seering, "Understanding bandwidth limitations in robot force control," in *IEEE Int. Conf. Robot. Autom.*, vol. 4, 1987, Conference Proceedings, pp. 904–909.

[85] J. E. Colgate and G. G. Schenkel, "Passivity of a class of sampled-data systems: Application to haptic interfaces," *J. Robot. Sys.*, vol. 14, no. 1, pp. 37–47, 1997.

[86] C. C. Gordon, T. Churchill, C. E. Clauser, B. Bradtmiller, and J. T. McConville, "Anthropometric survey of US army personnel: Methods and summary statistics, 1988," DTIC, Report, 1989.

[87] B. E. Lawson, A. H. Shultz, and M. Goldfarb, "Evaluation of a coordinated control system for a pair of powered transfemoral prostheses," in *IEEE Int. Conf. Robot. Autom.*, 2013, pp. 3888–93.

[88] "The amputee statistical database for the United Kingdom: 2006/07 report." *Information Services Division NHS Scotland*, 2009.

[89] C. P. U. Stewart and A. S. Jain, "Dundee revisited—25 years of a total amputee service," *Prosthet. Orthot. Int.*, vol. 17, no. 1, pp. 14–20, 1993.

[90] M. M. Torres and A. Esquenazi, "Bilateral lower limb amputee rehabilitation: A retrospective review," *West. J. Med.*, vol. 154, no. 5, pp. 583–6, 1991.

[91] J. Z. Laferrier, L. V. McFarland, M. L. Boninger, R. A. Cooper, and G. E. Reiber, "Wheeled mobility: Factors influencing mobility and assistive technology in veterans and servicemembers with major traumatic limb loss from Vietnam war and OIF/OEF conflicts," *J. Rehabil. Res. Dev.*, vol. 47, no. 4, pp. 349–60, 2010.

[92] D. Datta, P. N. Nair, and J. Payne, "Outcome of prosthetic management of bilateral lower-limb amputees," *Disabil. Rehabil.*, vol. 14, no. 2, pp. 98–102, 1992.

[93] M. B. Taylor, E. Clark, E. A. Offord, and C. Baxter, "A comparison of energy expenditure by a high level trans-femoral amputee using the Intelligent Prosthesis and conventionally damped prosthetic limbs," *Prosthet. Orthot. Int.*, vol. 20, no. 2, pp. 116–21, 1996.

[94] R. S. Gailey, M. A. Wenger, M. Raya, N. Kirk, K. Erbs, P. Spyropoulos, and M. S. Nash, "Energy expenditure of trans-tibial amputees during ambulation at self-selected pace," *Prosthet. Orthot. Int.*, vol. 18, no. 2, pp. 84–91, 1994.

[95] G. H. Traugh, P. J. Corcoran, and R. L. Reyes, "Energy expenditure of ambulation in patients with above-knee amputations," *Arch. Phys. Med. Rehabil.*, vol. 56, no. 2, pp. 67–71, 1975.

[96] C. T. Huang, J. R. Jackson, N. B. Moore, P. R. Fine, K. V. Kuhlemeier, G. H. Traugh, and P. T. Saunders, "Amputation: Energy cost of ambulation," *Arch. Phys. Med. Rehabil.*, vol. 60, no. 1, pp. 18–24, 1979.

[97] S. F. Crouse, C. S. Lessard, J. Rhodes, and R. C. Lowe, "Oxygen consumption and cardiac response of short-leg and long-leg prosthetic ambulation in a patient

with bilateral above-knee amputation: Comparisons with able-bodied men," *Arch. Phys. Med. Rehabil.*, vol. 71, no. 5, pp. 313–7, 1990.

[98] L. L. McNealy and S. A. Gard, "Effect of prosthetic ankle units on the gait of persons with bilateral trans-femoral amputations," *Prosthet. Orthot. Int.*, vol. 32, no. 1, pp. 111–26, 2008.

[99] P. Cherelle, V. Grosu, A. Matthys, B. Vanderborght, and D. Lefeber, "Design and validation of the ankle mimicking prosthetic (AMP-) foot 2.0," *IEEE Trans. Neural Syst. Rehabil. Eng.*, vol. 22, no. 1, pp. 138–148, 2014.

[100] J. A. Dawley, K. B. Fite, and G. D. Fulk, "EMG control of a bionic knee prosthesis: Exploiting muscle co-contractions for improved locomotor function," in *Proc. IEEE Int. Conf. Rehabil. Robot.*, 2013, pp. 1–6.

[101] M. Gorsic, R. Kamnik, L. Ambrozic, N. Vitiello, D. Lefeber, G. Pasquini, and M. Munih, "Online phase detection using wearable sensors for walking with a robotic prosthesis," *Sensors*, vol. 14, no. 2, pp. 2776–94, 2014.

[102] R. Unal, R. Carloni, S. M. Behrens, E. E. G. Hekman, S. Stramigioli, and H. F. J. M. Koopman, "Towards a fully passive transfemoral prosthesis for normal walking," in *Conf. Proc. IEEE/RAS-EMBS Biomed. Robot. Biomechatron.*, 2012, pp. 1949–1954.

[103] B. E. Lawson, A. Huff, and M. Goldfarb, "A preliminary investigation of powered prostheses for improved walking biomechanics in bilateral transfemoral amputees," in *Conf. Proc. IEEE Eng. Med. Biol. Soc.*, 2012, pp. 4164–7.

[104] E. C. Martinez-Villalpando and H. Herr, "Agonist-antagonist active knee prosthesis: A preliminary study in level-ground walking," *J. Rehabil. Res. Dev.*, vol. 46, no. 3, pp. 361–73, 2009.

[105] B. J. Fregly and F. E. Zajac, "A state-space analysis of mechanical energy generation, absorption, and transfer during pedaling," *J. Biomech.*, vol. 29, no. 1, pp. 81–90, 1996.

[106] R. Redfield and M. L. Hull, "On the relation between joint moments and pedaling rates at constant power in bicycling," *J. Biomech.*, vol. 19, no. 4, pp. 317–329, 1986.

[107] M. L. Hull and M. Jorge, "A method for biomechanical analysis of bicycle pedalling," *J. Biomech.*, vol. 18, no. 9, pp. 631–44, 1985.

[108] J. C. Martin and N. A. Brown, "Joint-specific power production and fatigue during maximal cycling," *J. Biomech.*, vol. 42, no. 4, pp. 474–9, 2009.

[109] W. L. Childers, R. S. Kistenberg, and R. J. Gregor, "The biomechanics of cycling with a transtibial amputation: Recommendations for prosthetic design and direction for future research," *Prosthet. Orthot. Int.*, vol. 33, no. 3, pp. 256–71, 2009.

[110] K. J. Astrom and B. Wittenmark, *Adaptive Control*, 2nd ed. Mineola, New York: Dover Publications, Inc., 2008.

[111] F. Freudenstein, "Approximate synthesis of four-bar linkages," *Trans. ASME*, vol. 77, pp. 853–861, 1955.

[112] R. S. Hartenberg and J. Denavit, *Kinematic synthesis of linkages*. New York,: McGraw-Hill, 1964.

[113] M. Goldfarb, B. E. Lawson, and A. H. Shultz, "Realizing the promise of robotic leg prostheses," *Sci. Transl. Med.*, vol. 5, no. 210, p. 210ps15, 2013.